bulletin 42

state-of-art report

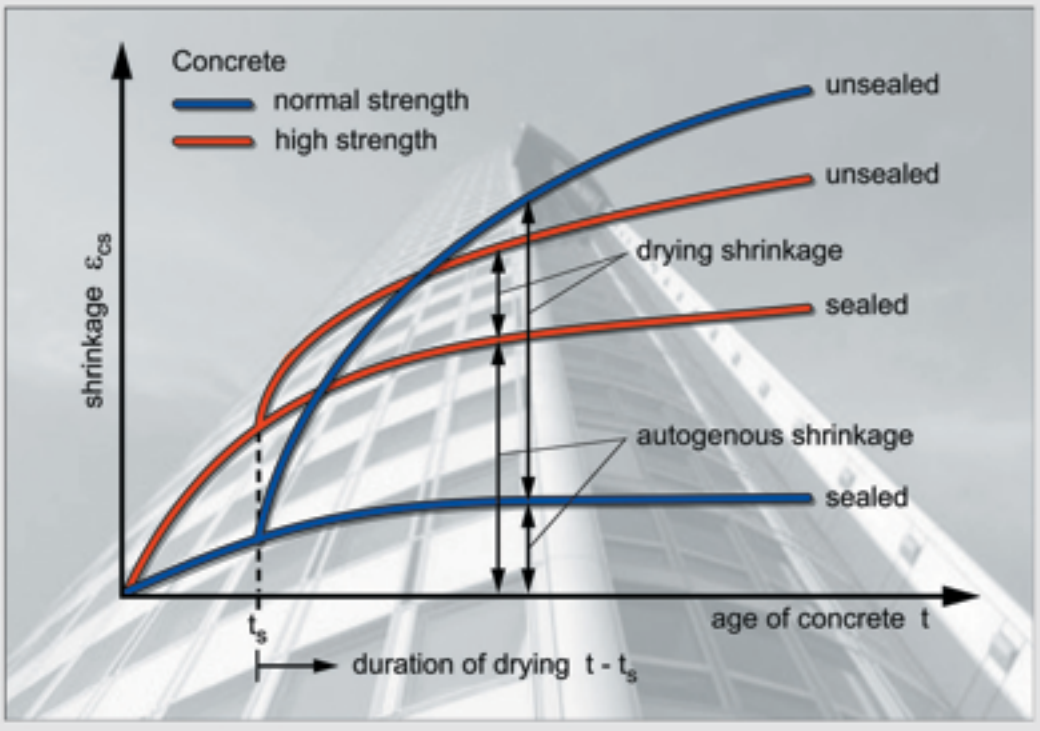

Constitutive modelling of high strength / high performance concrete

Constitutive modelling of high strength / high performance concrete

State-of-art report prepared by

Task Group 8.2

January 2008

Subject to priorities defined by the Technical Council and the Presidium, the results of ***fib***'s work in Commissions and Task Groups are published in a continuously numbered series of technical publications called 'Bulletins'. The following categories are used:

category	minimum approval procedure required prior to publication
Technical Report	approved by a Task Group and the Chairpersons of the Commission
State-of-Art Report	approved by a Commission
Manual, Guide (to good practice) or Recommendation	approved by the Technical Council of ***fib***
Model Code	approved by the General Assembly of ***fib***

Any publication not having met the above requirements will be clearly identified as preliminary draft.

This Bulletin N° 42 was approved as an ***fib*** state-of-art report by Commission 8 in April 2007.

This state-of-art report was drafted by Task Group 8.2, *Constitutive laws for high strength/high performance concrete*, in Commission 8, *Concrete*:

Harald Müller [3; 6; 8] (Convener, Univ. of Karlsruhe, Germany)

Pierre-Claude Aïtcin (Univ. of Sherbrooke, Canada), Arnon Bentur (Israel Institute of Technology, Israel), Mario Alberto Chiorino (Politecnico di Torino, Italy), Jean-Luc Clement (Laboratoire Central des Ponts et Chaussées, France), Manfred Curbach [3.4; 4.4.3; 5] (Technische Univ. Dresden, Germany), Torsten Faust (König, Heunisch und Partner, Frankfurt, Germany), Tor Arne Hammer [1; 2] (SINTEF, Norway), Jean-Paul Jaccoud (Switzerland), Christoph Kessler-Kramer [7] (Deutsche Bahn AG, Germany), Gert König [4] (Univ. of Leipzig, Germany), Jacques Marchand (Univ. Laval, Canada), Viktor Mechtcherine [3; 6; 8] (Secretary, Techn. Universität Dresden, Germany), Bertil Persson [9] (Lund Institute of Technology, Sweden), S. A. Reddi (Gammon India Limited, India), H.-W. Reinhardt [6.2] (Univ. of Stuttgart, Germany), Tassilo Rinder [6.2] (Univ. of Stuttgart, Germany), Keitetsu Rokugo (Gifu Univ., Japan), Luc Taerwe (Univ. of Ghent, Belgium), Tamon Ueda (Hokkaido Univ., Japan), Joost Walraven [4.5] (Delft Univ. of Technology, the Netherlands)

[1; 2; 2.1 ...] Chapter or section for which this TG member was a main author.

Full address details of Task Group members may be found in the ***fib*** Directory or through the online services on ***fib's*** website, www.fib-international.org.

Cover image: Time-development of autogenous and drying shrinkage in normal strength and high strength concrete (see Figure 6-20).

First published in 2008 by the International Federation for Structural Concrete (*fib*)
Postal address: Case Postale 88, CH-1015 Lausanne, Switzerland
Street address: Federal Institute of Technology Lausanne - EPFL, Section Génie Civil
Tel +41 21 693 2747 • Fax +41 21 693 6245
fib@epfl.ch • www.fib-international.org

ISSN 1562-3610
ISBN 978-2-88394-082-6

Printed by Sprint-Digital-Druck, Stuttgart

Foreword

Due to the positive properties of High Strength/High Performance Concrete (HSC/HPC) and to its growing use in the practice of construction, this type of concrete remains the object of great interest and extensive research. In this context, the aim of the ***fib*** Task Group 8.2 was to collect and evaluate the available information on the material behaviour of HSC/HPC and to develop a set of code-type constitutive relations as an extension of CEB-FIP Model Code 1990.

For this purpose, a review of the literature on experimental data for concretes with compressive cylinder strengths up to approximately 150 MPa was carried out. International guidelines, standards and recommendations were also examined, and the already-existing constitutive relations and models were evaluated. In addition to a number of the material laws chosen and adjusted for this report, a few new constitutive relations were developed based on the collected data. The requirements for the choice of the existing relations as well as the development of new constitutive relations involved their simplicity and operationality (code-type mathematical formulations). Furthermore, they should be physically sound and possibly describe the behaviour of both high-performance and normal strength concretes by a unique relation. Finally, the compliance with the features of the relationships given in the CEB-FIP Model Code 1990 was examined.

This state-of-the-art report is written for engineers and represents a summary of the relevant knowledge available to and possessed by the members of the Task Group. Individual chapters and subchapters of this report were drafted by members of the Task Group and subsequently discussed, accomplished and approved by the group. I would like to thank all the members of the Task Group who actively contributed to this report for a fruitful and harmonious collaboration. In particular, I would like to express my warm gratitude to the secretary of TG 8.2, Prof. Mechtcherine, who, apart from his own contributions, realised most of the editorial work concerning this report.

Prof. Harald S. Müller
Convener of Task Group 8.2

Contents

1 Definitions and classification

1.1 Range of applicability

HSC/HPC is basically constituted of the same materials as normal strength, normal weight concretes (NSC). This means that methods and techniques used to increase strength are the same as for NSC and consequently the influence on other material properties follows the same pattern as known for normal strength concrete. Considering the constituent materials of HSC/HPC the definitions, requirements and recommendations given in the CEB-FIP Model Code 1990 (including appendices) remain valid. The range of applicability of the constitutive relations presented in this report is confined up to the concrete grade C120 if there is no different limitation mentioned.

1.2 Classification by strength – concrete grades

Research on HPC has been performed on concrete with compressive cylinder strengths up to approximately 150 MPa. The results are considered sufficient for suggesting rules valid for concrete grades up to C120, referred to cylinder strength. Hence, in addition to the CEB-FIP Model Code 1990 which considers grades from C12 to C80, further concrete grades (C90, C100, C110 and C120) are covered in this report, see Table 3-1.

2 Density

HSC/HPC contains more cement and less water than NSC does. This constitutes a density increase which may reach 150 kg/m^3, see Table 2-1. Also, HSC/HPC structures may contain more reinforcement than NSC structures. The related values may vary within relatively wide limits depending on mix composition and density of part materials (both may vary between countries), reinforcement ratio and air content. When density is an important design parameter, it is recommended that the density values to be used in design calculations should be pre-calculated on the basis of actual input data. If not, the following values may be used for interpolation, assuming 2 % air content (a change of air content by 1 % gives a density change of 1 %):

Reinforcement ratio	C30 (w/b ≈ 0.65)	C80 (w/b ≈ 0.35)	C120 (w/b ≈ 0.25)
0.0 %	2350	2450	2500
1.0 %	2400	2500	2550
2.0 %	2450	2550	2600

Table 2-1: Density of normal strength and high-strength concrete

3 Strength

3.1 Range of applicability

Concerning the mechanical behaviour of concrete addressed in this chapter the same range of applicability as defined in CEB-FIP Model Code 1990 is proposed. Thus, the information given in this section is valid for monotonically increasing compressive stresses or strains at a rate of $\dot{\sigma} \sim 1.0$ MPa/s or $\dot{\varepsilon} \sim 30 \cdot 10^{-6}\ s^{-1}$, respectively. For tensile stresses or strains it is valid for $\dot{\sigma} \sim 0.1$ MPa/s or $\dot{\varepsilon} \sim 3.3 \cdot 10^{-6}\ s^{-1}$, respectively.

3.2. Compressive strength

3.2.1 Parameters affecting compressive strength

As a first approximation, the compressive strength of concrete is proportional to that of the hydrated cement paste. Thus, concrete strength depends primarily on the water/cement or water/binder ratio, on the degree of hydration, i.e. on concrete age and curing as well as on type and strength class of cement. In the case of high strength concrete the type and amount of additions and in some cases the type of admixtures has a pronounced effect on the compressive strength and its development with time. Furthermore, the significance of the strength and stiffness of the aggregates increases with increasing strength of concrete.

The curing conditions are important not only concerning the hydration process but also with regard to other phenomena affecting the compressive strength. Tensile stresses in concrete near the surfaces of specimens and eventually a formation of microcracks due to drying shrinkage has a minor effect on the compressive strength, since they are "pressed over" during the test. However, in the case of curing in water a reduction of the compressive strength can be observed in comparison to the tests on sealed or dry specimens [Popovics 1986], which can probably be tracked back to a reduction of the bonding energy within the hydrated cement paste due to the water saturation [Setzer (1977)]. For high strength concrete, however, the effect of water curing on the compressive strength is less pronounced in comparison to normal strength concrete [Reinhardt and Hilsdorf (2001)].

In addition, effects of testing such as size and shape of a specimen have to be taken into account in order to insure the comparability of the results. It is well known for normal strength concrete, that for a given concrete composition and defined testing procedure the compressive strength measured on specimens with a constant slenderness decrease with increasing specimen size. This tendency holds true also for high strength concrete. E.g. according to Cook (1989) an approx. 4 % lower compressive strength was measured on cylinders, 150 mm in diameter and 300 mm in height, in comparison to the tests on cylinders with a diameter of 100 mm and a height of 200 mm.

Two opposed phenomena are of significance concerning the influence of the concrete composition on the size effect in compression. On the one hand, usually high strength concrete possesses – due to smaller differences in the properties of its constituents – a more homogeneous structure. After the Weibull theory it might lead to a less pronounced size effect in comparison to normal strength concrete, which shows a higher degree of the heterogeneity. On the other hand, with increasing strength concrete becomes more brittle. The increased brittleness of concrete leads to a more pronounced size effect, which can be explained on the basis of fracture mechanics.

Further, the compressive strength measured on specimens with an equal cross-section decrease with increasing slenderness. Here, the same phenomena are to consider as described above for the case of the size effect.

Another parameter affecting the compressive strength is the material of forms. Imam et al. (1995) reported about a decrease of the compressive strength of high strength concrete up to 10 % when plastic forms were used for cubes instead of metal forms. In [Carrasguillo (1981)] a decrease of the f_c-values by 3 % was observed due to the use of plastic forms for cylinders.

3.2.2 Determination of the compressive strength

Equivalent to the prescriptions of the CEB-FIP Model Code 1990 this document is based on the uniaxial compressive strength f_c of cylinders, 150 mm in diameter and 300 mm in height, and tested at the age of 28 days in accordance with ISO 1920, ISO 2736/2 and ISO 4012 or EN 12390-1, EN 12390-2 and EN 12390-3. For curing the cylinders have to be stored in water at 20 ± 2 °C or alternatively in a fog room at 20 ± 2 °C and a relative humidity ≥ 95 %.

The characteristic compressive strength f_{ck} (MPa) is defined as that strength below which 5 % of all possible strength measurements for the specified concrete may be expected to fall.

For some verifications in design or for an estimate of other concrete properties it is necessary to refer to a mean value of compressive strength f_{cm} associated with a specific characteristic compressive strength f_{ck}. In this case f_{cm} may be estimated from Eq. 3-1:

$$f_{cm} = f_{ck} + \Delta f \tag{3-1}$$

where: $\Delta f = 8$ MPa.

For special requirements or in national codes test specimens other than cylinders 150/300 mm and stored in other environments may be used to specify the concrete compressive strength. In such cases conversion factors should either be determined experimentally or taken from national codes for a given category of testing equipment.

In the case when concrete cubes 150/150/150 mm are used, the characteristic strength values given in Table 3-1 shall be obtained for the various concrete grades.

Concrete grade	C12	C20	C30	C40	C50	C60	C70	C80	C90	C100	C110	C120
f_{ck} (MPa)	12	20	30	40	50	60	70	80	90	100	110	120
$f_{ck,cube}$ (MPa)	15	25	37	50	60	75	85	95	105	115	130	140

Table 3-1: Characteristic strength values

According to Ipatti (1992) and Held (1994) the following formula may be used for the compilation of the results obtained from the tests on cubes with different sizes for all strength classes of concrete:

$$f_{c,cube200} = 0.95 \cdot f_{c,cube150} = 0.92 \cdot f_{c,cube100} \tag{3-2}$$

Some national codes prescribe different kinds of curing as defined in EN 12390-2. E.g. in the German Code DIN 1048-5 (1991) after one week of curing in water the specimens are stored at a temperature of approx. 20 °C in a dry environment (RH of approx. 50 % to 65 %). According to Reinhardt and Hilsdorf (2001) for normal strength concrete this kind of storing provides values of compressive strength, which are approx. 8 % higher in comparison with

values obtained on specimens cured in water until testing. For high strength concrete this difference is about 5 %.

3.3 Tensile strength and fracture properties

3.3.1 Tensile strength

3.3.1.1 Parameters affecting tensile strength

The tensile strength of concrete primarily depends on those parameters which also influence the compressive strength of concrete. However, tensile and compressive strength are not proportional to each other, and particularly for higher strength grades an increase of the compressive strength leads only to a small increase of the tensile strength. One of the reasons for this phenomenon results from the increasing brittleness of the cement paste with increasing strength. Due to a finer and denser pore structure of high strength concrete compared to ordinary concrete the crack propagation in the cement paste is less hindered by voids [Remmel (1994)].

Internal stresses e.g. due to drying shrinkage which frequently lead to microcracks prior to loading are of particular significance for the tensile strength of concrete. As a consequence, the tensile strength may decrease for some time after the end of the curing period until it continues to increase again. The extent to which internal stresses lead to a reduction of the tensile strength depends on the particular test method. For high strength concrete the decrease of the tensile strength due to shrinkage cracks seems to be more pronounced than for normal strength concrete, despite of its denser microstructure [Carrasquillo et al. (1981)]. This effect may be traced back to additional internal stresses induced by autogenous shrinkage which develops very pronouncedly in concretes having a low water-cement ratio. Water storage before testing also leads to a reduction of the tensile strength of concrete compared to the tensile strength determined both on dry or sealed specimens. It has been hypothesized that the strength reduction observed in water saturated concrete is due to a reduction of the bonding energy within the hydrated cement paste [Setzer (1977)] and due to a “smearing” effect of the water [Remmel (1994)].

When the strength of the cement mortar matrix increases, an increasing influence of the type of coarse aggregates on the tensile strength of concrete can be observed, whereas the compressive strength is obviously less affected by the aggregate type [Giaccio et al. (1993)]. The reduction of the water-cement ratio and especially the use of silica fume lead to the formation of a significantly denser and stronger interface zone and consequently improve the bond strength between the aggregates and the hardened cement paste. The quality of this bond depends also on the shape, size, surface condition and the mineralogical character of the aggregates [Hansen et al. (1996)]. Depending on the chemical nature of the aggregates, some pozzolanic reactions may lead to an improved bond strength between the aggregates and the cement paste and thus to an increased tensile strength [Skalny (1989)]. As the bond strength increases, a transition from an interfacial fracture, i.e. failure of aggregate-cement paste bond, to a trans-aggregate fracture gradually takes place. Hence, high strength concretes with more heterogeneous aggregates like e.g. granite show lower values of the ratio of the tensile strength to the compressive strength than concretes containing more or less homogeneous coarse aggregates.

The tensile strength strongly depends on the particular test method employed. In this context the tensile strength generally is more size dependent than the compressive strength. However, the size effect becomes less pronounced as the strength of concrete increases [Rossi et al. (1994)].

3.3.1.2 Effect of the test methods on the obtained tensile strength

The *axial tensile strength* of concrete is the most objective material parameter to describe the behaviour of concrete in tension. However, the particular experimental set-up used for uniaxial tension tests exerts a significant effect on the determined material parameters. Recent experimental and numerical investigations showed that the tensile test on unnotched specimens with non-rotatable boundaries is the most reliable method to determine tensile strength of concrete [Mechtcherine and Müller (1998)]. This holds particularly true for high strength concrete.

For high strength concrete being a rather brittle material the reduction of the tensile strength due to notches is more pronounced than for ordinary concrete. Figure 3-1 indicates the relation between the concrete compressive strength f_{cm} measured on cylindrical specimens and the tensile strength of concrete f_{ct} as obtained from uniaxial tension tests on unnotched and notched specimens, respectively. With increasing compressive strength the increase of the net tensile strength measured on notched specimens is significantly smaller than that of the f_{ct}-values obtained from experiments on unnotched specimens. Moreover, if the compressive strength exceeds approx. 80 MPa the values of net tensile strength obviously stagnate on the same level. The best fit for the results obtained from tests on unnotched specimens is provided by a logarithmic equation also shown in Figure 3-1.

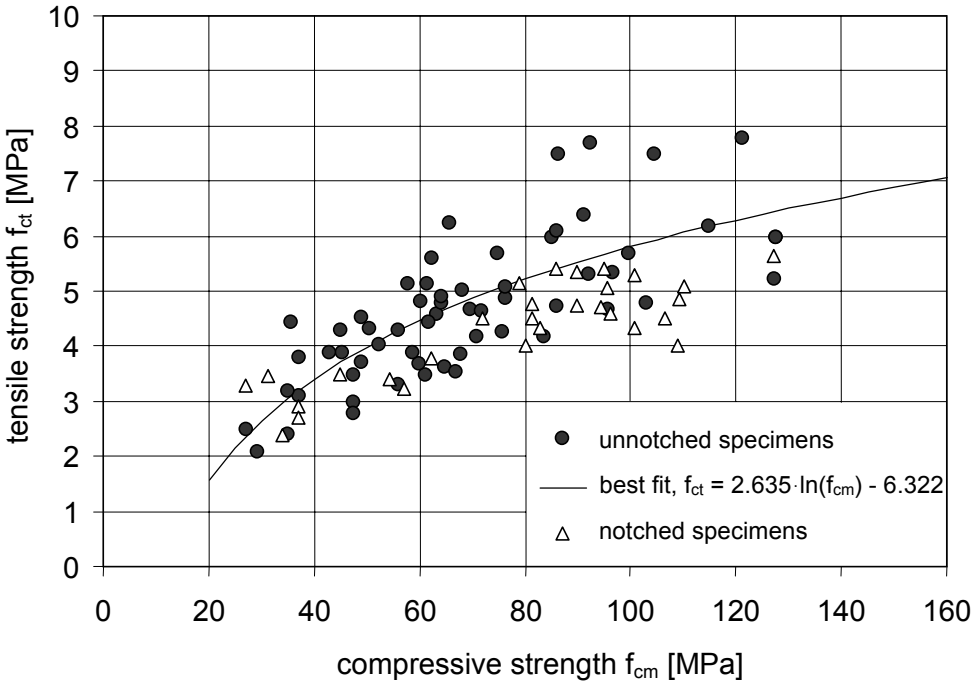

Fig. 3-1: Relation between the compressive strength and the axial tensile strength of concrete

Although the uniaxial tensile testing is the most appropriate method to determine fracture properties of concrete in tension, it is used almost exclusively in research because of the experimental difficulties in performing such experiments. Therefore, in many instances the *tensile splitting strength* is determined. The results obtained from splitting tests depend mainly on the specimen shape [Hansen et al. (1996), Rocco et al. (1999a)], the specimen size [Bazant et al. (1991)] and the width of the bearing strips [Rocco et al. (1999b)]. However, as far as narrow bearing strips are applied, the effect of the specimen shape or size is not significant within the range of sizes of specimens usually used for testing in the laboratory [Rocco et al. (1999b)]. Further, the tensile splitting strength is much less sensitive to curing conditions, because critical stresses act at some distance from the concrete surface [Hilsdorf

(1995)]. For these reasons the values of tensile splitting strength scatter only little compared to the results obtained from other test methods.

In Figure 3-2 experimental results from splitting tests in relation to the compressive strength and the function fitting best these data are presented. It may be seen that the relation between the tensile splitting strength and the compressive strength of concrete is very similar to that observed for the axial tensile strength and the compressive strength.

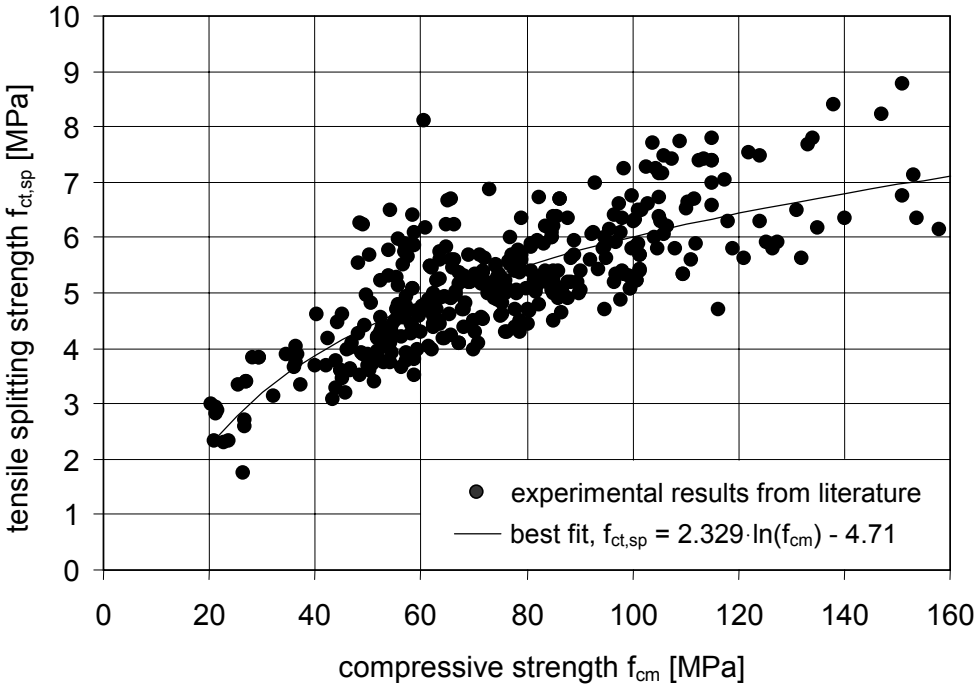

Fig. 3-2: Relation between the compressive strength and the tensile splitting strength of concrete

Since splitting tests are often used as a substitute for uniaxial tension tests, a relation is necessary to estimate the mean value of axial tensile strength f_{ctm} from the tensile splitting strength $f_{ct,sp}$. All known proposed formulas postulate a linear relation between these material parameters being independent of the concrete grade:

$$f_{ctm} = A \cdot f_{ct,sp} \tag{3-3}$$

The differences between the proposed values for the coefficient A are substantial. The Norwegian standard suggests A = 0.667 [NS 3473 (1989)], whereas Jaccoud et al. (1995) derived a coefficient of A = 0.81. The value of A recommended by CEB-FIP MC 1990 (1993) is 0.9. According to Remmel (1994) this coefficient should be about 0.95. In this context, the effect of the compressive strength of concrete on the ratio of the axial tensile strength to the tensile splitting strength is of major interest. Figure 3-3 shows a corresponding relation as obtained by correlating the functions for the experimental results from uniaxial tension tests and splitting tests, respectively (cf. Figures 3-1 and 3-2). This relation indicates a reasonable explanation of the different values for the coefficient A, as the differences are mainly due to the concrete grade under consideration. With increasing compressive strength the values of the tensile strength derived from uniaxial and from splitting tests approach each other. The change of the value of A is pronounced for lower and less pronounced for higher concrete grades.

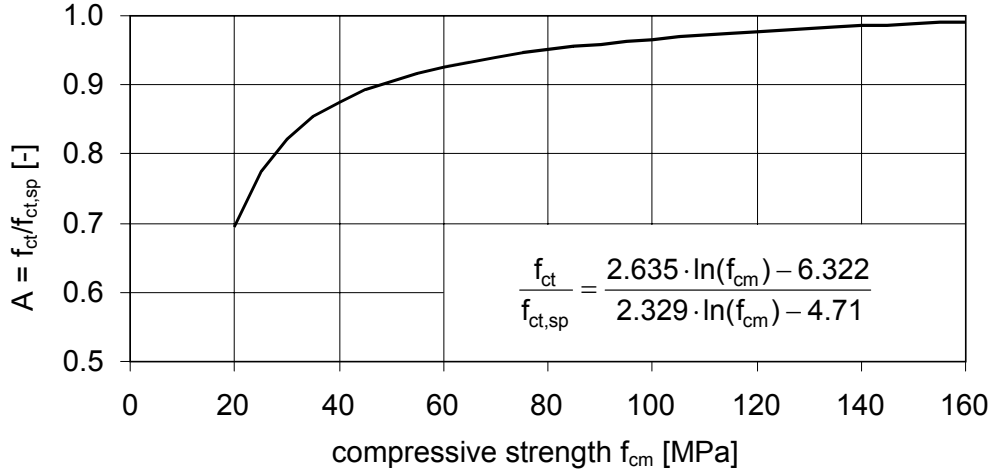

Fig. 3-3: Relation between the compressive strength and the ratio of axial tensile strength to tensile splitting strength of concrete

The interpretation of the obtained $f_{ctm}/f_{ct,sp}$-relation with regard to the decisive failure mechanisms is not straightforward. However, a crucial point is evidently the fundamental difference of the stress fields prevailing in the specimens. In the case of splitting tests, concrete is exposed to multiaxial compression in the area near the bearing strips and to mixed compression-tension stress in the center plane of the specimens. The experiments performed by Kupfer et al. (1969) clearly showed that concretes having a higher compressive strength are more sensitive to compression-tension loading than low strength concretes.

Another simple method to determine the resistance of concrete against tensile stresses is given by testing its *flexural strength*. This strength value is generally higher than the axial tensile strength and strongly depends on the size of the beam, particularly on its depth [Müller and Hilsdorf (1993)]. As the depth of the beam increases, the flexural strength approaches the axial tensile strength. Further, the results obtained from bend tests are affected by notches or the notch size, respectively, as well as by the particular test set-up, e.g. three- or four-point bend tests [Wright (1952)]. The effect of curing conditions on the flexural strength is more pronounced in comparison to the other test methods, i.e. uniaxial or splitting tests.

Figure 3-4 shows experimental results collected by Jaccoud et al. (1995) and more recent data from publications which appeared after the year 1995, respectively. Both data sets show a very large scatter of the flexural strength values which obviously is caused by the pronounced effect of the testing parameters on the obtained $f_{ct,fl}$-values. Besides the experimental data Figure 3-4 also shows the best fits for all data and the more recent data, respectively. It is evident that the more recent data indicate a less pronounced increase of the flexural strength with increasing compressive strength than all collected data. The reasons for this difference which might be traced back to statistical causes still have to be investigated.

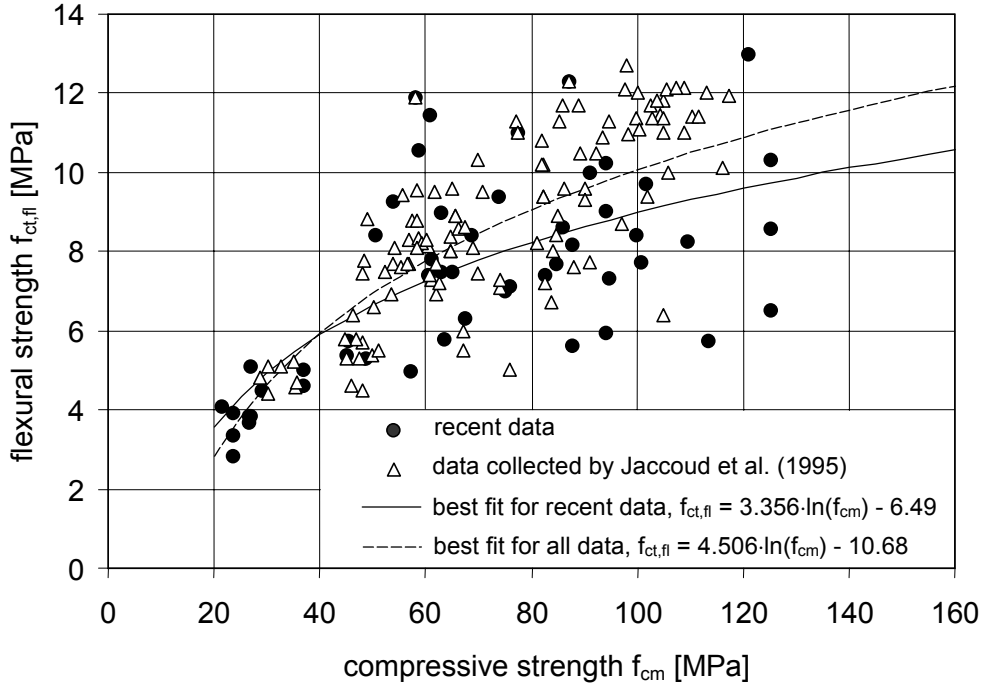

Fig. 3-4: Relation between the compressive strength and the flexural strength of concrete

In order to estimate the axial tensile strength from the flexural strength a relation between these two parameters has to be derived. CEB-FIP MC 90 gives the following formula which has been deduced from fracture mechanics considerations:

$$f_{ct,fl} = f_{ctm} \frac{1 + \alpha_{fl}\left(\frac{h_b}{h_o}\right)^{0.7}}{\alpha_{fl}\left(\frac{h_b}{h_o}\right)^{0.7}} \tag{3-4}$$

where: $f_{ct,fl}$ flexural strength [MPa]
f_{ctm} mean axial tensile strength [MPa]
h_b beam depth [mm]
h_o 100 mm
α_{fl} coefficient which depends on the characteristic length acc. to Eq. 3-13.

In CEB-FIP MC 90 a value α_{fl} = 1.5 has been proposed, though α_{fl} depends on the brittleness of the concrete and decreases as brittleness increases [Müller and Hilsdorf (1993)]. This means that for a given beam depth, the ratio of flexural strength to axial tensile strength of concrete $f_{ct,fl}/f_{ctm}$ decreases as the concrete becomes more brittle. The compilation of the corresponding functions for flexural und axial tensile strengths, taken from Fig. 3-2 and Fig. 3-4 and shown in Figure 3-5 proves the correctness of this approach with regard to the effect of compressive strength on fracture properties of concrete. The $f_{ct,fl}/f_{ctm}$-relation obtained from the more recent data matches very well the values for low strength, normal strength and high strength concretes as estimated by using Eq. 3-2 and an additional formula for α_{fl} given in [Müller and Hilsdorf (1993)]. However, considering all data only a slight decrease of the $f_{ct,fl}/f_{ctm}$-ratio with increasing compressive strength of concrete can be observed.

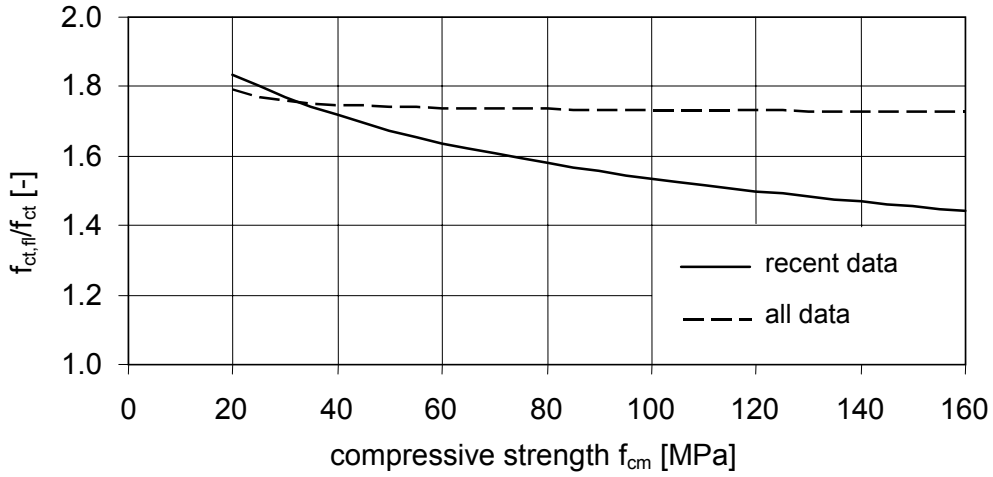

Fig. 3-5: Relation between the compressive strength and the ratio of flexural strength to axial tensile strength of concrete

3.3.1.3 Constitutive relations between tensile strength and compressive strength

As has been shown in the previous section only uniaxial tension tests on unnotched specimens provide reliable data for the derivation of relations between tensile strength and compressive strength for different concrete grades. Figure 3-6 presents two new formulas developed from data on uniaxial tension tests on unnotched specimens.

The CEB-FIP MC 1990 proposal for the estimation of a mean value of the tensile strength f_{ctm} is based on the subsequent power function:

$$f_{ctm} = f_{ctko,m} \cdot \left(\frac{f_{ck}}{f_{cko}} \right)^{\frac{2}{3}} \tag{3-5}$$

where: f_{ck} = characteristic compressive strength [MPa]
$f_{ctko,m}$ = 1.40 MPa
f_{cko} = 10 MPa.

Basically recent evaluation had shown that Eq. 3-5 is valid only up to the concrete grade C50 [CEB-FIP Working Group on HSC/HPC (1995)]. For concrete grades beyond this limit, i.e. for high strength concrete, this equation overestimates the tensile strength of concrete. Alternatively, a relation has been proposed which is valid for both, high strength concrete and normal strength concrete:

$$f_{ctm} = f_{ctko,m} \left(\frac{f_{ck} + \Delta f}{f_{cko} + \Delta f} \right)^{0,6} \tag{3-6}$$

where: $f_{cko,m}$ = 1.8 MPa
f_{cko} = 10 MPa
Δf = 8 MPa.

Besides the different values of the coefficient $f_{cko,m}$ and the applied exponent, the main difference between both approaches given by Eqs. 3-3 and 3-4 is that the proposal of the CEB-FIP Working Group refers to the mean values of the compressive strength $f_{cm} = f_{ck} + \Delta f$, whereas CEB-FIP MC 90 operates with the characteristic compressive strength f_{ck}.

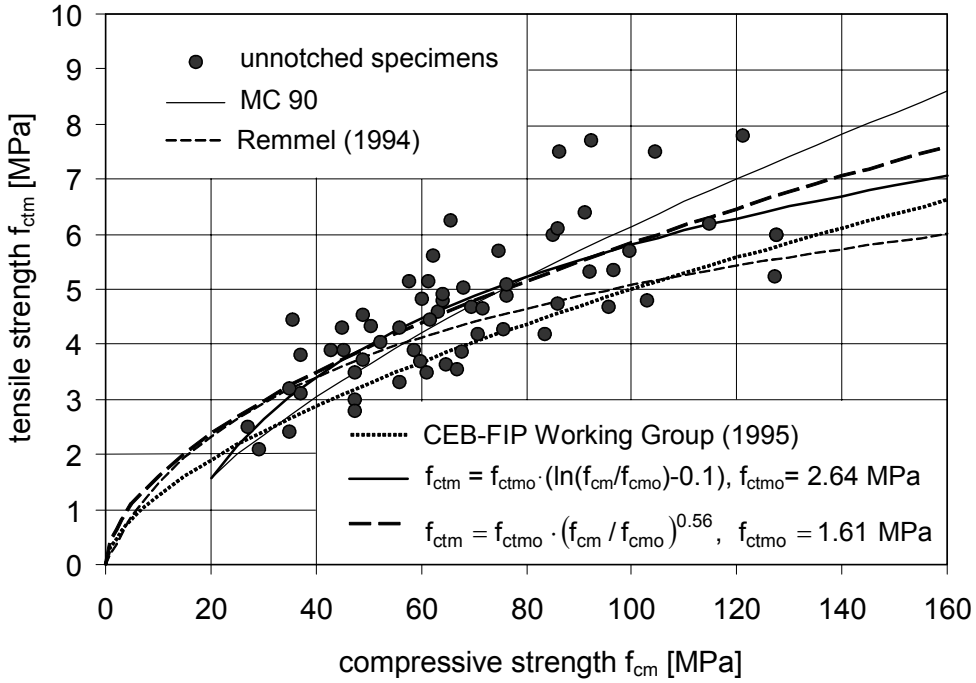

Fig. 3-6: Relations between tensile and compressive strength of concrete

Another formula to describe the relation between mean values of tensile and compressive strength of concrete has been proposed by Remmel (1994):

$$f_{ctm} = f_{ctmo} \cdot ln\left(1 + \frac{f_{cm}}{f_{cmo}}\right) \tag{3-7}$$

where: f_{ctm} mean axial tensile strength [MPa]
f_{cm} mean compressive strength [MPa]
f_{ctmo} = 2.12 MPa
f_{cmo} = 10 MPa.

As it is evident from Figure 3-6 the above given equations do not match sufficiently well the experimental data obtained from uniaxial tests on unnotched specimens. As a consequence a new logarithmic equation has been derived and optimised as shown in Figure 3-6:

$$f_{ctm} = f_{ctmo} \cdot \left(ln\left(\frac{f_{cm}}{f_{cmo}}\right) - 0.1\right) \tag{3-8}$$

where: f_{ctmo} = 2.64 MPa
f_{cmo} = 10 MPa.

The comparison of Eq. 3-5 with the experimental results or with Eq. 3-8 obtained from the best fit shows that the relation given by CEB-FIP MC 90 clearly overestimates the axial

tensile strength for concrete grades higher than C80. However, for normal strength concrete this relation matches the recent data very well.

The relation proposed by CEB-FIP Working Group [CEB-Bulletin 228 (1995)] underestimates significantly the tensile strength for all concrete grades above C20. The corresponding curve marks more or less the lower bound of the test results. One of the reasons might be that during the evaluation of the experimental data no distinction had been made between the tests on notched and unnotched specimens. Further, the data obtained from splitting tests had also been used. There a constant ratio had been assumed ($f_{ctm}/f_{ct,sp} = 0.81$) to calculate the axial tensile strength from the splitting tensile strength [Jaccoud et al. (1995)].

Eq. 3-7 predicts too high values of the tensile strength for concretes with a mean value of the compressive strength f_{cm} below 40 MPa, whereas the predicted f_{ctm}-values for higher concrete grades are apparently too low. The underestimation is significant for high strength concrete. This might be explained by the fact that Remmel (1994) mainly considered own tension tests on notched specimens, which show especially for high strength concrete a considerable reduction of the apparent tensile strength.

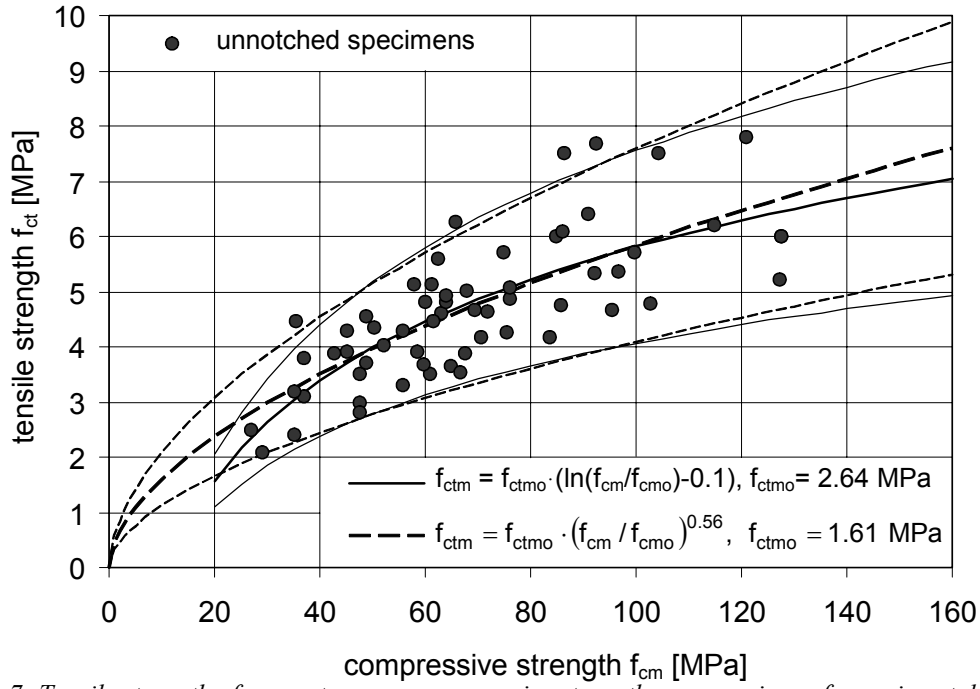

Fig. 3-7: Tensile strength of concrete versus compressive strength – comparison of experimental results and predictions acc. to Eqs. 3-8 and 3-9

The best prediction accuracy for the relation between mean values of the tensile and compressive strength of concrete is obtained when Eq. 3-8 is applied. However, its range of validity starts, analogous to the approach of the MC 90, at the concrete grade C12. For concretes with a very low compressive strength this logarithmic equation gives inconsistent results. Among the "consistent" formulas, a power function matches best the experimental data. Considering the collected data, the following equation represents an optimum fit:

$$f_{ctm} = f_{ctmo} \cdot \left(\frac{f_{cm}}{f_{cmo}} \right)^{0.56} \tag{3-9}$$

where: f_{ctmo} = 1.61 MPa
f_{cmo} = 10 MPa.

Figure 3-7 shows these new approaches based on a logarithmic and a power function, respectively, and the curves, which correspond roughly to the 5 % and 95 % bound limits of the concrete tensile strength. It can be seen from this figure that for the range of the compressive strength between 40 MPa and 110 MPa both relations provide nearly identical results.

3.3.2 Fracture energy

The fracture mode of concrete subjected to tension allows for the application of fracture mechanics concepts, i.e. energy considerations. In those concepts the *fracture energy* of concrete G_F, i.e. the energy required to propagate a tensile crack of unit area, is often used as a materials characteristic to describe the resistance of concrete subjected to tensile stresses.

3.3.2.1 Parameters affecting fracture energy

For normal strength concrete the fracture energy primarily depends on the water-cement ratio, the maximum aggregate size and the age of concrete [Wittmann et al. (1987)]. Curing conditions also have a significant effect on experimentally determined G_F-values [Mechtcherine and Müller (1997)]. Further, G_F is affected by the size of a structural member and in particular by the depth of the ligament above a crack or a notch [Hu and Wittmann (1990)].

The fracture energy of high strength concrete is also influenced by the above-mentioned parameters, however not to the same extent as in the case of normal strength concrete. The aggregate type and content seem to affect the fracture energy of concrete much stronger than the size of aggregates [Hansen et al. (1996)]. This phenomenon is caused by the transition from the interfacial fracture to the trans-aggregate fracture. The utilisation of high strength aggregates like basalt or rather heterogeneous materials like granite leads to an increase of the G_F-values. In both cases the crack propagation leading to concrete failure is impeded, so that breaking tougher aggregates, change of crack orientation or multiplication of cracks, respectively, cause a higher energy consumption. For high strength concrete the effect of curing conditions on G_F is somewhat less pronounced than for normal strength concrete, but it is still significant. König and Remmel (1992) supposed the fracture energy measured on dry specimens to be on average approx. 0.05 N/mm higher than values obtained for wet concrete, independent of the concrete grade.

There are different methods to determine the fracture energy. It has been shown that G_F should be determined best, similar to the tensile strength, from uniaxial tension tests on unnotched specimens with non-rotatable boundaries. However, it is much easier to perform stable experiments on notched specimens. This leads, however, to somewhat lower G_F-values even if uniaxial tension tests with non-rotatable boundaries are carried out [Mechtcherine and Müller (1998)]. The application of bend tests or tension tests with rotatable boundaries causes an additional reduction of the obtained G_F-values [Slowik and Wittmann (1992), Mechtcherine and Müller (1998)]. Often the experiments are stopped before the separation of the specimen in two parts has really been completed, so that the measured fracture energy also depends also on the achieved or given deformation limit. In bend tests additional errors can be caused by the dead weight of the specimen and the friction at the supports.

The pronounced effects of the above-mentioned parameters cause a significant scatter of the G_F-values when the results of investigations of different authors are compiled. Figure 3-8 shows the experimental results obtained from uniaxial and bend tests for different concrete grades. Despite of the scatter of the measured values a clear tendency indicating an increase of the fracture energy with increasing compressive strength can be observed.

However, for concretes having a compressive strength above 100 MPa the G_F-values appear to stay on a constant level.

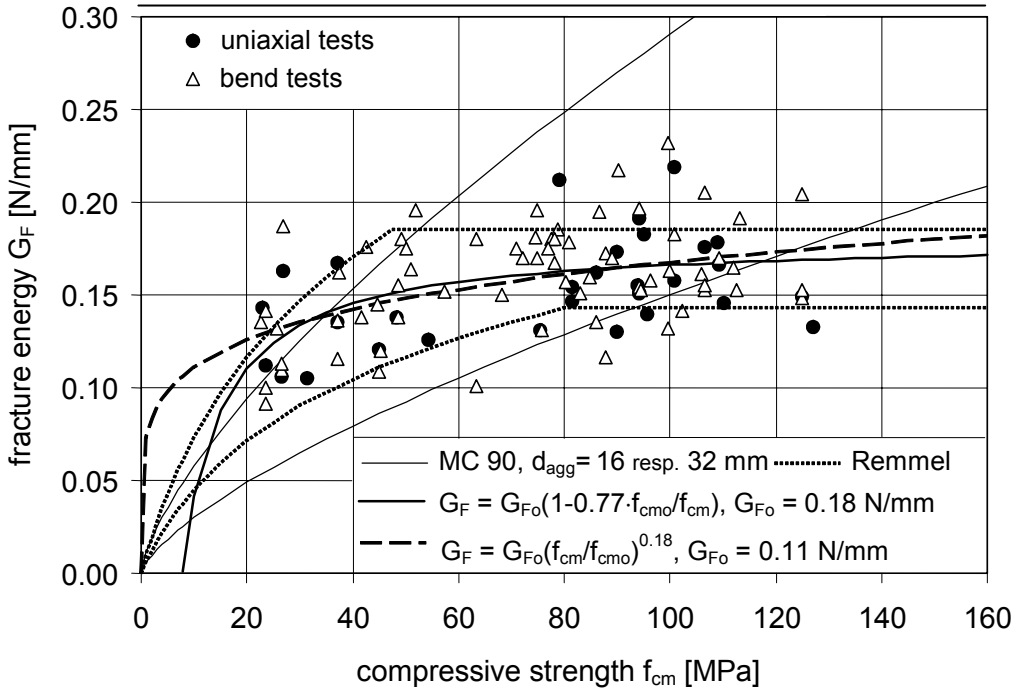

Fig. 3-8: Relation between compressive strength and fracture energy – experimental results and corresponding relations

3.3.2.2 Relations between fracture energy and compressive strength

Figure 3-8 also shows the most important relations for an estimation of the fracture energy from the compressive strength of concrete. CEB-FIP MC 90 gives the following equation:

$$G_F = G_{Fo}\left(\frac{f_{cm}}{f_{cmo}}\right)^{0.7} \tag{3-10}$$

where: G_F fracture energy [N/mm]
G_{Fo} base value of fracture energy which depends on maximum aggregate size d_{max} as given in Table 3-1
f_{cm} mean concrete compressive strength [MPa]
f_{cmo} = 10 MPa.

d_{max}	[mm]	8	16	32
G_{Fo}	[N/mm]	0.025	0.03	0.058

Table 3-2: Effect of maximum aggregate size d_{max} on the base value of fracture energy G_{Fo} [CEB-FIP MC 90 (1993)]

Compared with the experimental data presented in Figure 3-8, Eq. (3-10) predicts a too pronounced effect of the compressive strength on the fracture energy G_F. Further, this relation being applied for concretes with a maximum aggregate size of 16 mm underestimates the values of the fracture energy for all concretes grades with exception of very high strength

concretes (f_{cm} > 120 MPa). The relation obtained for concretes containing coarse aggregates with a maximum size of 32 mm provides, on the contrary, an overestimation of the fracture energy for concretes having a mean value of the compressive strength above 40 MPa.

Remmel (1994) proposed, on the basis of results from own tests with a maximum aggregate size of 16 mm, to use Eq. (3-11) for the estimation of the fracture energy:

$$G_F = G_{Fo} \cdot ln\left(1 + \frac{f_{cm}}{f_{cmo}}\right) \tag{3-11}$$

where: G_{Fo} = 0.065 N/mm for concrete with river gravel aggregate
G_{Fo} = 0.106 N/mm for concrete with crashed basalt aggregate
f_{cmo} = 10 MPa.

For concrete with river gravel aggregates the validity limit of Eq. (3-11) is given by a mean concrete compressive strength of 80 MPa [Remmel (1994)]. The limiting value of the fracture energy for concrete with crushed basalt aggregates is specified at 0.185 N/mm, i.e. starting from the concrete class C40 upwards no further increase of the fracture energy is predicted. The main criticism on this approach may be referred to the sharp bends of the relations at the limiting fracture energy values, which certainly do not reflect the continuous transition from normal strength to high strength concrete behaviour properly. In fact it is desirable for corresponding relations to estimate the fracture energy with respect to the aggregate type. However, the analysis of the collected test data given here does not yet allow for quantifying the influence of different aggregate types on the G_F-values with an accuracy which would satisfy the requirements of a code-type formulation.

Alternatively to the existing formulations two improved relations may be proposed, which have been derived from the available experimental data. The first relation is given by Eq. (3-12):

$$G_F = G_{Fo}\left(1 - 0.77 \cdot \frac{f_{cmo}}{f_{cm}}\right) \tag{3-12}$$

where: G_{Fo} = 0.18 N/mm
f_{cmo} = 10 MPa.

Eq. (3-12) provides the best fit for the experimental data. However, it is not consistent for very low strength concretes, i.e. concrete grades below C12. The second relation (Eq. 3-14) is of the same mathematical type as the one used in CEB-FIP MC 90:

$$G_F = G_{Fo}\left(\frac{f_{cm}}{f_{cmo}}\right)^{0.18} \tag{3-13}$$

where: G_{Fo} = 0.11 N/mm
f_{cmo} = 10 MPa.

This relation is consistent with respect to the concrete grade, but matches the collected data somewhat worse than Eq. (3-12). In addition, it is most likely that Eq. (3-13) overestimates the fracture energy of low strength concrete.

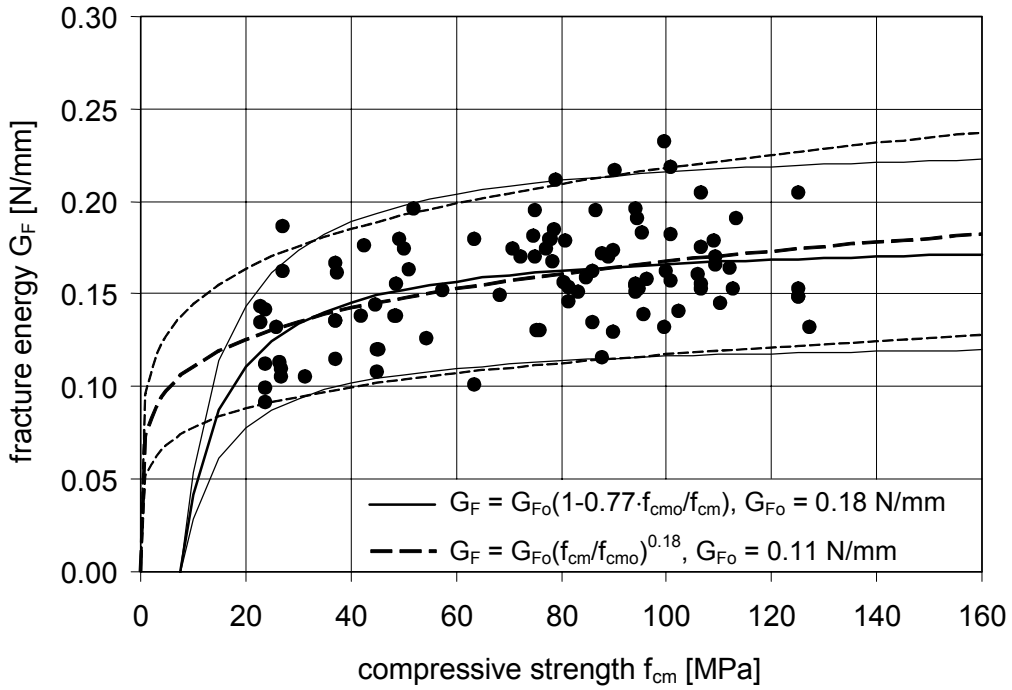

Fig. 3-9: Fracture energy of concrete versus compressive strength – comparison of experimental results and predictions acc. to Eqs. (3-12) and (3-13)

3.3.2.3 Characteristic length

The fracture energy G_F alone is not sufficient to characterise the brittleness of concrete. Therefore, another useful fracture parameter, the *characteristic length* l_{ch} has been deduced. It corresponds to the half of the length of a specimen subjected to axial tension in which just enough elastic strain energy is stored to create one complete fracture surface. The corresponding mathematical expression is given by Eq. (3-14). A decrease of the characteristic length is an indication of an increase of the brittleness.

$$l_{ch} = \frac{E_{ci} \cdot G_F}{f_{ctm}^2} \tag{3-14}$$

where:
- l_{ch} characteristic length [m]
- E_{ci} modulus of elasticity [MPa]
- G_F fracture energy [N/m]
- f_{ctm} axial tensile strength [MPa].

Figure 3-10 shows l_{ch}-values obtained from experimental results. The characteristic length decreases as the compressive strength increases, i.e. the concrete becomes more brittle as its tensile and compressive strength increase. The decrease of the characteristic length becomes less pronounced for concretes with a higher mean value of the compressive strength.

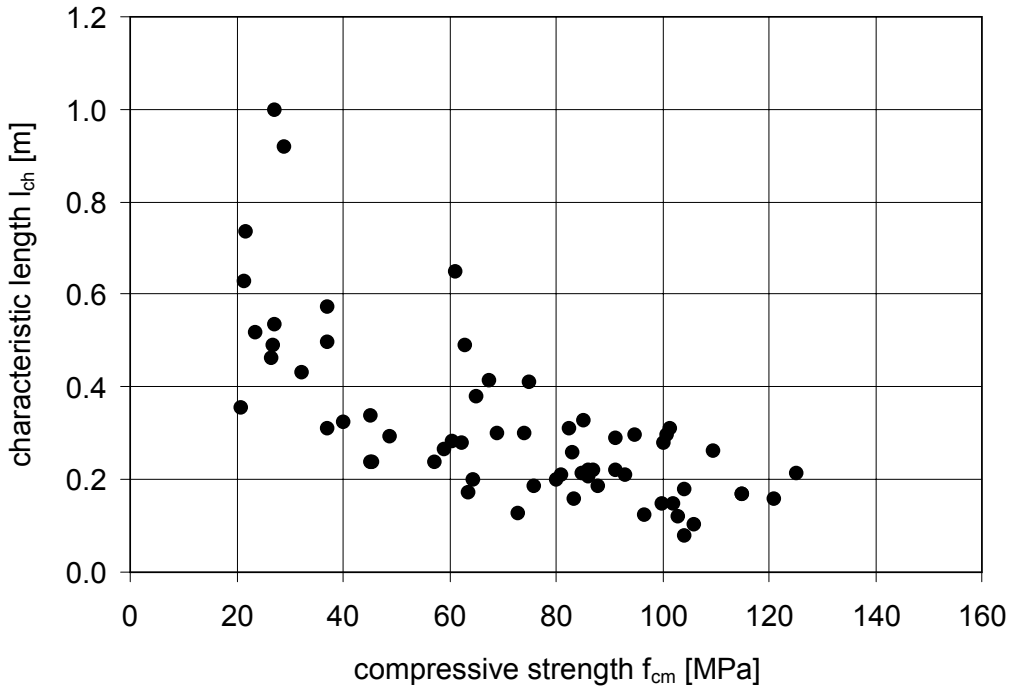

Fig. 3-10: Effect of compressive strength on the characteristic length of concrete

3.4 Strength under multiaxial states of stress

3.4.1 Basic principles

Unfortunately the experimental data of the behaviour of HPC under multiaxial loading are limited. So the following expressions are based on the actual standard of knowledge. All presented functions, with exception of the functions in chapter 3.4.4, are approximations of measured mean values. The formulations are valid for concrete grades from C65 to C105. Compared to uniaxial compression the ultimate strength of high performance concrete is generally higher under multiaxial compression and lower under combined compression-tension. The strength increase or decrease is dependent on the stress ratio and the concrete grade. The higher the concrete grade the smaller is the strength increase under multiaxial compression referring to the uniaxial strength and the higher is the strength decrease under compression-tension.

In order to determine the multiaxial strength of HPC, the knowledge of two principal properties – the uniaxial tensile strength f_{ctm} and compressive strength f_c' – is necessary. The factor between the uniaxial strength measured on standard cylinders f_{cm} and the uniaxial compressive strength f_c' takes into account the different specimen size and loading approach used in the multiaxial tests. The two properties can be calculated as follows.

$$f_{ctm} = 2.12 \cdot ln\left(1 + \frac{f_{cm}}{10}\right) \qquad \text{with } f_{cm} \text{ in } [MPa] \tag{3-15}$$

$$f_c' \approx 0.9 \cdot f_{cm} \tag{3-16}$$

3.4.2 Biaxial stress combinations

For best results it is necessary to use different expressions for each of the three types of stress combinations which are tension-tension, compression-tension and compression-compression. For the biaxial tension region it can be assumed, that the ultimate biaxial tension strength is equal to the uniaxial tension strength, Eq. (3-17).

$$f_{2ct} = f_{ct} \tag{3-17}$$

Referred to the uniaxial strength the ultimate strength of HPC under combined compression-tensile strength is significant lower than for NSC. The failure curve is nearly linear between the uniaxial compressive stress and the failure value at a stress ratio of $\sigma_2/\sigma_1 = 0.5/-1$. A cubic equation [Hampel (2002)] is recommended for the mathematical description, Eq. (3-18).

$$\frac{\sigma_2}{|f_c'|} = a \cdot \sqrt[3]{\frac{\sigma_1}{|f_c'|} + b} + c \cdot \frac{\sigma_1}{|f_c'|} + d \tag{3-18}$$

with: $a = f_1(f_c')$

$b = f_2(f_c')$

$f_i(f_c') = A_i \cdot (f_c') + B_i$ with $i = 1, 2$

A_i, B_i according to Table 3-3

$c = a \cdot \sqrt[3]{b-1} + d$

$d = \frac{f_{ctm}}{|f_c'|} - a \cdot \sqrt[3]{b}$

i	A_i	B_i
1	$-1.3420 \cdot 10^{-4}$	$4.5150 \cdot 10^{-2}$
2	$-4.5351 \cdot 10^{-4}$	$4.0274 \cdot 10^{-2}$

Table 3-3: Parameters for Eq. (3-18)

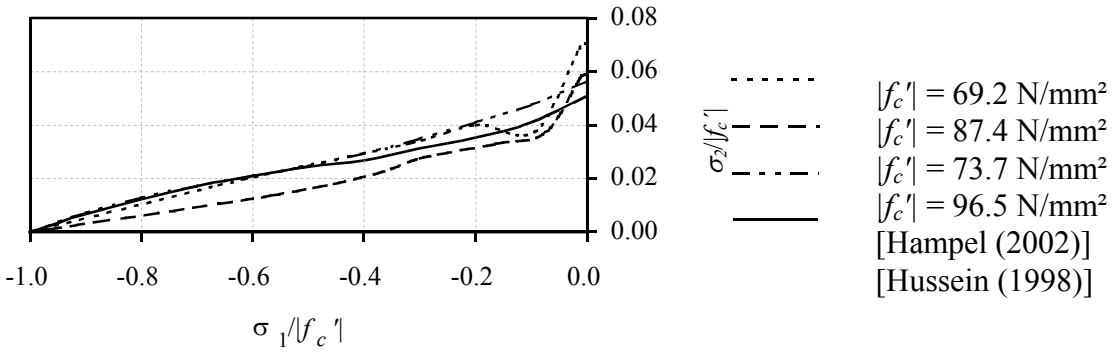

Fig. 3-11: Failure strength of HPC under compression-tension loading

The ultimate strength of HPC under biaxial compression is higher than the uniaxial strength. The magnitude of the biaxial failure value depends on the concrete grade and the stress ratio. The increase of the strength decreases with increasing concrete grade. The maximum increase of the strength is observed on lower stress ratios at higher concrete grades. After this point the failure values decrease until the stress ratio of $\sigma_2 = \sigma_1$ is reached. It is possible to describe the biaxial failure envelope by an ellipse [Hampel (2002)], Eq. (3-19). The function depends on three parameters. The parameters *a* and *b* characterize the radii of the ellipse and the parameter c the center of the ellipse. As the center is situated on the axis $\sigma_2 = \sigma_1$ only one parameter is necessary to describe the center. The functions for *a*, *b* and *c* are dependent on the uniaxial compressive strength as shown below.

$$\frac{(\sigma_1 + \sigma_2 - 2c)^2}{2 \cdot a^2} + \frac{(\sigma_2 - \sigma_1)^2}{2 \cdot b^2} = 1 \tag{3-19}$$

with: $a = f_1(f_c')$

$b = f_2(f_c')$

$c = f_3(f_c')$

$f_i(f_c') = A_i \cdot (f_c')^2 + B_i \cdot (f_c') + C_i$ with $i = 1, 2, 3$

A_i, B_i, C_i according to Table 3-3

i	A_i	B_i	C_i
1	$1.1496 \cdot 10^{-4}$	$1.7305 \cdot 10^{-5}$	$-1.1685 \cdot 10^{-4}$
2	-0.0246	-0.00270	0.01830
3	1.9955	0.80962	-0.23946

Table 3-4: Parameters for Eq. (3-19)

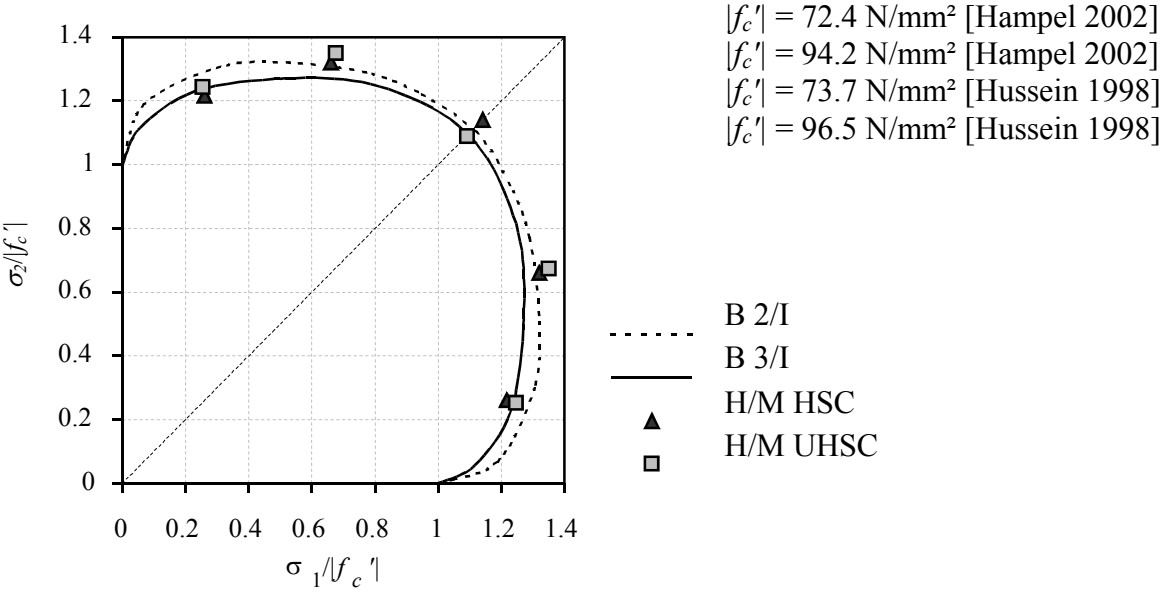

Fig. 3-12: Failure strength of HPC under biaxial compressive stress

3.4.3 Triaxial compression and tension

The ultimate loads form an ultimate strength surface. This ultimate strength envelope is three-fold symmetric in relation to the hydrostatic axis with $\sigma_1 = \sigma_2 = \sigma_3$. The surface is characterized by the compressive meridian with $\sigma_1 < \sigma_2 = \sigma_3$ and the tension meridian with $\sigma_1 = \sigma_2 < \sigma_3$. For a material whose uniaxial compressive strength differs from its tensile strength the meridians distinguish from each other, see Fig. 3-13. Every three dimensional stress vector can be expressed by the octahedral normal stress $\sigma_{0,}$ the shear stress τ_0 and the deviatoric angle Θ. The octahedral normal stress is the vector along the hydrostatic axis. The octahedral shear stress is the vector orthogonal to the normal stress and the deviatoric angle is the angle of rotation. The plain perpendicular to the hydrostatic axis at a defined octahedral normal stress is the so-called Pi-plain. The polar figure marks the ultimate strength within the Pi-plain.

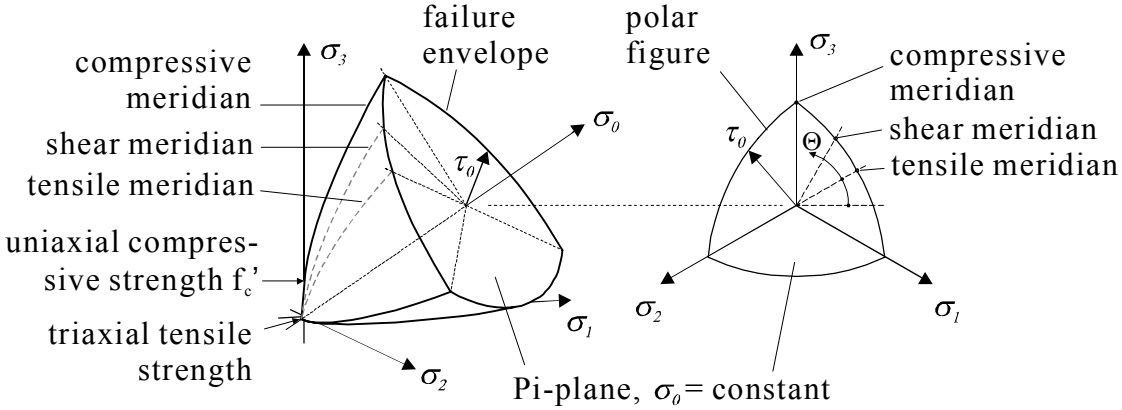

Fig. 3-13: Definitions in the three-dimensional stress space

The failure criterion according to Dahl (1992) is recommended for the calculation of HPC. The criterion was developed from the criterion of Ottosen [Ottosen (1979)] and is given in a simple form in Eq. (3-20).

$$f\left(I_1, J_2, cos\left(3\cdot\Theta\right)\right) = A\cdot\frac{J_{2\sigma}}{\left|f_c\right|^2} + \lambda\cdot\frac{\sqrt{J_{2\sigma}}}{\left|f_c\right|} + B\cdot\frac{I_{1\sigma}}{\left|f_c\right|} - 1 = 0 \tag{3-20}$$

$I_{1\sigma}$ is the first invariant of the stress tensor and $J_{2\sigma}$ is the second invariant of the deviatoric stress tensor.

$$I_{1\sigma} = \sigma_1 + \sigma_2 + \sigma_3 = \sigma_{ii} = 3\cdot\sigma_O = \underline{\sigma}^T \tag{3-21}$$

$$J_{2\sigma} = \frac{1}{2}\left(\tilde{\sigma}_1^{\,2} + \tilde{\sigma}_2^{\,2} + \tilde{\sigma}_3^{\,2}\right) = \frac{1}{6}\left[\left(\sigma_1-\sigma_2\right)^2 + \left(\sigma_2-\sigma_3\right)^2 + \left(\sigma_1-\sigma_3\right)^2\right] = \frac{3}{2}\cdot\tau_O^{\,2} \tag{3-22}$$

The function λ is dependent on the angle Θ.

$$\lambda = K_1\cdot cos\left[\frac{1}{3}\cdot arccos\left(K_2\cdot cos\left(3\cdot\Theta\right)\right)\right] \qquad \text{for } cos\left(3\cdot\Theta\right) \geq 0 \tag{3-23}$$

$$\lambda = K_1\cdot cos\left[\frac{\pi}{3} - \frac{1}{3}\cdot arccos\left(-K_2\cdot cos\left(3\cdot\Theta\right)\right)\right] \qquad \text{for } cos\left(3\cdot\Theta\right) \leq 0 \tag{3-24}$$

A, B, K_1, K_2 and λ are free parameters of the criterion. The parameters of Ottosen's model were calibrated by the concrete properties, which are the uniaxial and the equal biaxial compressive strength and one failure value at the compressive meridian. Dahl calculated the criterion with a fix value of 0.1 for the ratio between the tensile and compressive strength and with 1.16 for the equal biaxial compressive strength referring to the uniaxial strength. The parameters A, B, K_1 and K_2 could be approximated using second degree polynomials. These polynomials are stated in the following equations.

$$A = -1.66 \cdot x^2 + 3.49 \cdot x + 0.73 \tag{3-25}$$

$$B = -0.19 \cdot x^2 + 0.41 \cdot x + 3.13 \tag{3-26}$$

$$K_1 = 0.46 \cdot x^2 - 0.97 \cdot x + 11.89 \tag{3-27}$$

$$K_2 = -0.02 \cdot x^2 + 0.04 \cdot x + 0.974 \tag{3-28}$$

with: $x = \dfrac{f_{cm}}{100\ MPa}$

Because of the fix value of the uniaxial tensile and compressive strength there are larger differences between the known test results and the criterion in the biaxial region. Therefore it is recommended to use the listed biaxial functions to determine the failure strength in the biaxial region.

Unfortunately at this point of time there are no experimental data for the triaxial compression-tension region available. So there is no opportunity to check the usefulness of Dahl's criterion for these stress states.

3.4.4 Partial area loading

Triaxial states of stress are situated in a local area, when a partial area of a very large surface is penetrated with concentrated compressive stress or when a significant confinement is available on the surface. The reason for this multiaxial stress is the restraint on the loading surface. Due to that hydrostatic pressure the ultimate load in this area is significantly higher than the uniaxial strength. The following approach is identical with that enclosed in the European Standard EC 2 [prEN 1992-2(2002)] and other standards. The magnitude of the ultimate load depends on geometrical factors. These geometrical factors are shown in Fig. 3-14. The bearable partial area load F_{Rdu} can be calculated by Eq. (3-29). However, to limit the penetration, the values are not to be taken higher than $3 \cdot f_{\mathrm{cd}}$.

$$f_{cc}^{*} = \frac{F_{Rdu}}{A_{c0}} = f_{cd} \cdot \sqrt{\frac{A_{c1}}{A_{c0}}} \le 3.0 \cdot f_{cd} \tag{3-29}$$

with: A_{c0} loaded area
A_{c1} maximum design distribution area with a similar shape to A_{c0}

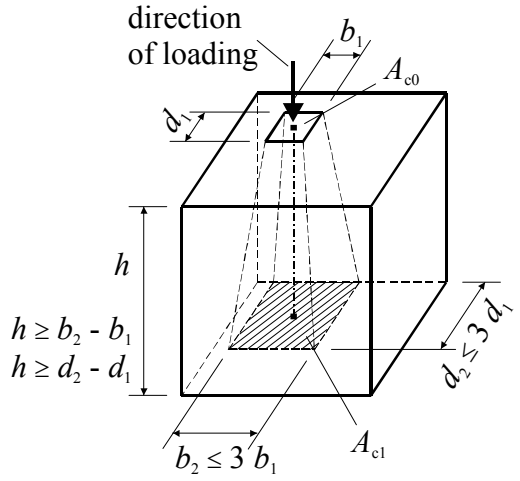

- the centre of the design distribution area A_{c1} should be on the line of action of the centre of the loaded area A_{c0}
- if more than one compressive force acting on the concrete cross section, the design distribution areas should not overlap

Fig. 3-14: Determination of the specific values for the partial area loading

The value of F_{Rdu} is to be decreased, if the load is not regular on the penetrating area or if high lateral forces are situated.

The following proposal for chapter 4 is kept closely to the Model Code 90 [CEB (1993)] and the proposed extensions from bulletin 228 [CEB (1995)]. Changes or new formulations are only introduced where necessary. The general purpose is to find formulations valid for all concrete grades from C12 to C120. Formulations given here should be an aid for a fundamental understanding of the stress strain behaviour of concrete as a material and its impact on the performance of structures. It is addressed to the structural engineer in practice as well as to the code writing engineer.

4 Stress and strain

4.1 Range of application

The information given in this section is valid for monotonically increasing compressive stresses or strains at a rate of $|\dot{\sigma}| \approx 0.6 \pm 0.4$ MPa/s or $|\dot{\varepsilon}| \approx 0.015$ ‰/s, respectively. For tensile stresses or strains it is valid for $\dot{\sigma} \approx 0.06$ MPa/s or $\dot{\varepsilon} \approx 0.0015$ ‰/s, respectively.

4.2 Modulus of elasticity

The modulus of elasticity E_{ci} is defined as the tangent modulus of elasticity at the origin of the stress-strain diagram. It is approximately equal to the slope of the secant of the unloading branch for rapid unloading and does not include initial plastic deformations. It has to be used for the description of the stress-strain diagrams for uniaxial compression, uniaxial tension and multiaxial stress-states, as well as for an estimate of creep.

The modulus of elasticity depends on the stiffness of the aggregates, the cement paste and the contact zone in between. In general aggregates of different sizes and cement paste have different stiffness. Therefore the content each of the different particle sizes, which can be expressed with the grading curves according to appendix 6 [CEB (1993)], has significant influence on the modulus of elasticity. While the cement paste can be described by using the compressive strength, the influence of the type of aggregate has to be considered separately. Compared to quartzitic aggregates with gradings in zone 3 the modulus of elasticity can be increased by 20 % or decreased by 30 % only by changing the type of aggregate. Eq. (4-1) and Table 4-1 give the qualitative changes α_E in the modulus of elasticity for different types of aggregate. To take full account of differences in grading, aggregate stiffness or modulus, direct measurements of E_{ci} are necessary. E_{ci} may then be replaced by E_{cm} from tests. Tests on the modulus of elasticity are necessary where deformations or dynamic behaviour are of interest and where concrete and steel are combined to carry loads in a composite structure.

Values of the modulus of elasticity for normal weight concrete with natural sand and gravel gradings in zone 3 can be estimated from the specified characteristic strength using Eq. (4-1).

$$E_{ci} = E_{c0} \cdot \alpha_E \cdot \left(\frac{f_{ck} + 8\ MPa}{10\ MPa} \right)^{1/3} \tag{4-1}$$

where: E_{ci} is the modulus of elasticity (MPa) at a concrete age of 28 days
f_{ck} is the characteristic strength (MPa) according to section 3.2
$E_{c0} = 20.5 \cdot 10^3$ MPa
α_E is 1.0 for quartzitic aggregates. For different types of aggregate qualitative values for α_E can be found in Table 4-1.

Aggregate type grading in zone 3	α_E	$E_{c0}\cdot\alpha_E$ [MPa]
Basalt, dense limestone aggregates	1.2	24 600
Quartzitic aggregates	1.0	20 500
Limestone aggregates	0.9	18 500
Sandstone aggregates	0.7	14 400

Table 4-1: Effect of type of aggregate on modulus of elasticity

When the actual compressive strength of concrete at an age of 28 days f_{cm} is known, E_{ci} may be estimated from Eq. (4-2).

$$E_{ci} = E_{c0}\cdot\alpha_E\cdot\left(\frac{f_{cm}}{10\ MPa}\right)^{1/3} \tag{4-2}$$

When only an elastic analysis of a concrete structure is carried out, a reduced modulus of elasticity E_c according to Eq. (4-3) should be used in order to account for the initial plastic strain, causing some irreversible deformations. The modulus of elasticity E_{ci} does not include this initial plastic strain due to its definition as the slope of the unloading branch. While the limit for the stress σ_c reached in the serviceability limit state is set to $\sigma_c = -0.4\cdot f_{cm}$ this stress level gives an upper limit for the reduction factor α_i (Fig. 4-1). This factor $\alpha_i = E_{ci}/E_c$ is decreasing with increasing concrete strength. The reduction factor α_i can be found from the stress-strain relation introduced in chapter 4.4 if further initial creep effects are neglected. For concrete grades higher than C80 the difference between first loading up to $\sigma_c = -0.4\cdot f_{cm}$ and the unloading branch is smaller than 3 % and may be neglected. The reduction factor α_i introduced in Eq. 4-3 may be estimated by a bilinear approach (Table 4-2).

$$E_c = \alpha_i\cdot E_{ci} \tag{4-3}$$

where: $\alpha_i = 0.8 + 0.2\cdot\frac{f_{cm}}{88\ N/mm^2} \le 1.0$

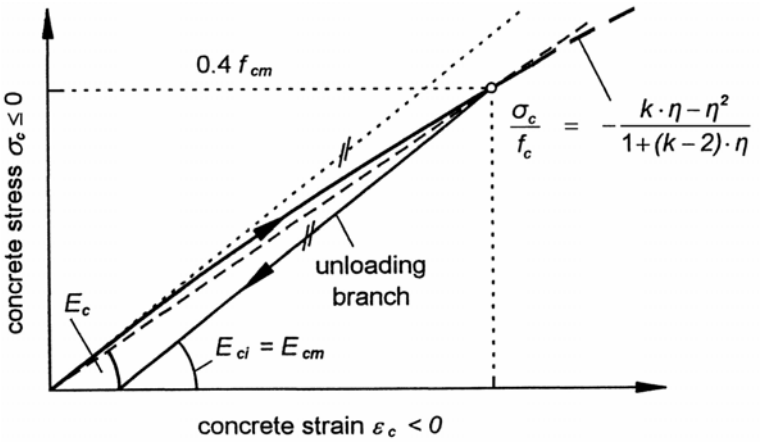

Fig. 4-1: Reduced modulus E_c during first loading

Values of the tangent moduli E_{ci} and the reduced moduli E_c for different concrete grades are given in Table 4-2 (see also Chapter 4.6, Fig. 4.6-1). Quartzitic aggregates with grading in zone 3 are estimated.

Concrete grade	C12	C20	C30	C40	C50	C60	C70	C80	C90	C100	C110	C120
E_{ci} [GPa]	25.8	28.9	32.0	34.6	36.8	38.8	40.7	42.3	43.9	45.3	46.7	48.0
E_c [GPa]	21.8	25.0	28.4	31.4	34.3	37.1	39.7	42.3	43.9	45.3	46.7	48.0
α_i	0.845	0.864	0.886	0.909	0.932	0.955	0.977	1.0				

Table 4-2: Tangent modules and reduced modules of elasticity

4.3 Poisson's ratio

For a range of stresses $-0.6 \cdot f_{ck} < \sigma_c < 0.8 \cdot f_{ctk}$ the Poisson's ratio of concrete ν_c ranges between 0.14 and 0.26. Regarding the significance of ν_c for the design of members especially with the influence of crack formation at the ultimate limit state, the estimation of $\nu_c = 0.20$ meets the required accuracy.

4.4 Stress-strain relations for short term-loading

4.4.1 Compression

The stress-strain diagrams for concrete are generally of the form schematically shown in Fig. 4-2. The strength f_c should be related to the uniaxial compressive strength described in section 4.4.3.

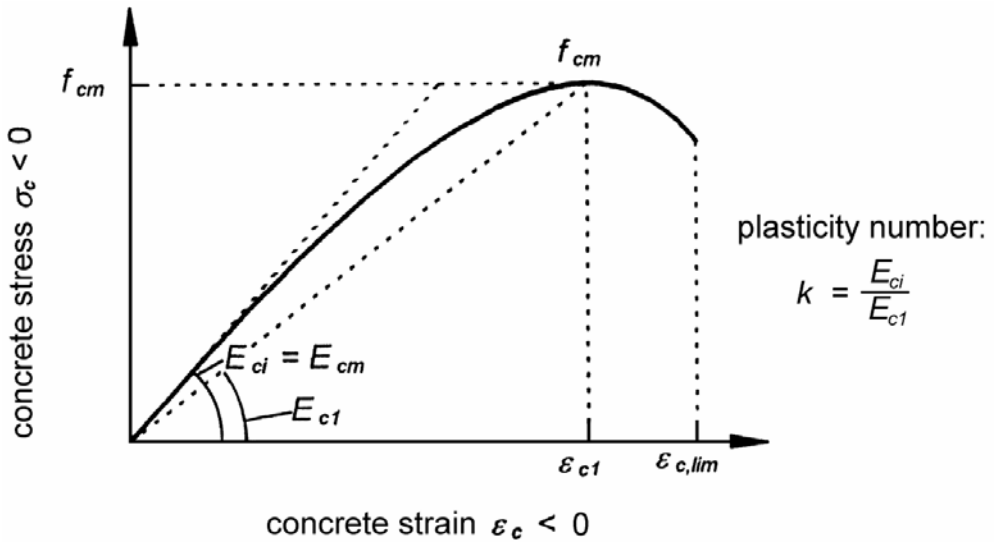

Fig. 4-2: Stress-strain diagram for uniaxial compression

The stress-strain relationship may be approximated by Eq. (4-4). The strain ε_{c1} at maximum compressive stress is increasing with increasing compressive strength. Values for ε_{c1} under short term loading are given in Table 4-3 following the proposal from Propovic (1973) and Meyer (1998). Fig. 4-3 shows the stress-strain relations for concrete grades C12 up to C120.

$$\frac{\sigma_c}{f_c} = -\frac{k \cdot \eta - \eta^2}{1 + (k-2) \cdot \eta} \quad \text{for } |\varepsilon_c| < |\varepsilon_{c,\lim}| \tag{4-4}$$

where: η $= \varepsilon_c / \varepsilon_{c1}$

ε_{c1} $= -1.60\ (f_{cm} / 10\ \text{MPa})^{0.25} / 1000$ strain at maximum compressive stress [Popovic (1973]

k $= E_{ci} / E_{c1}$ plasticity number

Concrete grade	C12	C20	C30	C40	C50	C60	C70	C80	C90	C100	C110	C120
E_{ci} [GPa]	25.8	28.9	32.0	34.6	36.8	38.8	40.7	42.3	43.9	45.3	46.7	48.0
E_{c1} [GPa]	10.5	13.5	17.0	20.3	23.4	26.3	29.2	31.9	34.6	37.2	39.8	42.7
ε_{c1} [‰]	-1.90	-2.07	-2.23	-2.37	-2.48	-2.58	-2.67	-2.76	-2.83	-2.90	-2.97	-3.0
$\varepsilon_{c,lim}$ [‰]	-3.5	-3.5	-3.5	-3.5	-3.4	-3.3	-3.2	-3.1	-3.0	-3.0	-3.0	-3.0
$k=E_{ci}/E_{c1}$	2.46	2.14	1.88	1.71	1.58	1.48	1.39	1.33	1.27	1.22	1.17	1.12

Table 4-3: Tangent modules E_{ci}, E_{c1}, ε_{c1} and $\varepsilon_{c,lim}$ for various concrete grades

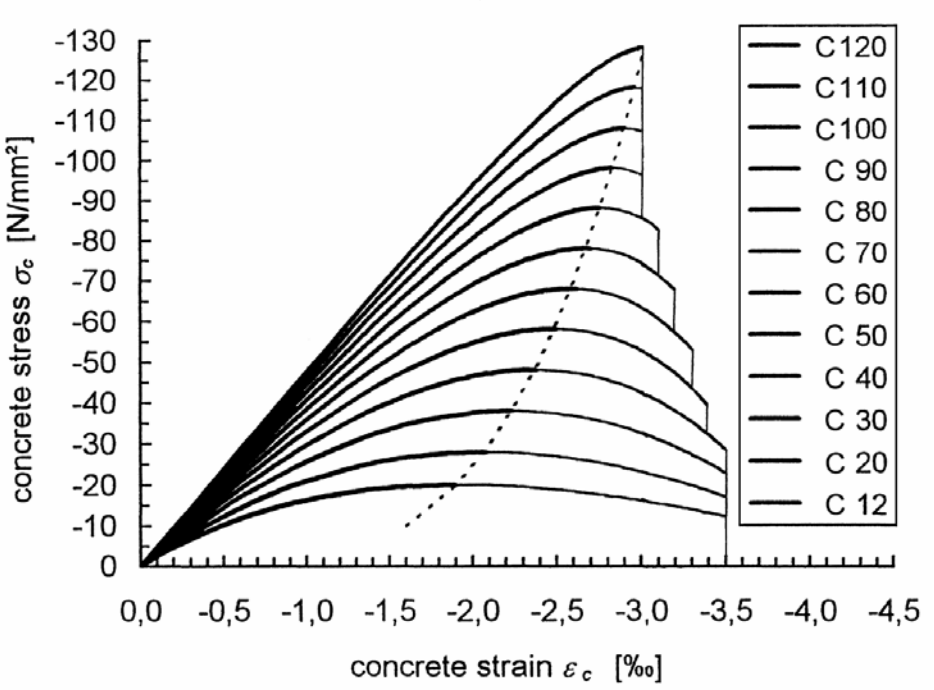

Fig. 4-3: Stress-strain diagrams for different concrete strengths (mean values)

As shown before, the *E*-modulus may be different for some mix designs. If *E*-moduli from tests are used to find the accurate shape of the stress-strain diagram used for design, the modulus E_{c1} should also be taken from tests. An accurate stress-strain diagram can only be found if both modules determining the plasticity number *k* are investigated.

The stress-strain relation for unloading of the uncracked concrete may be described by Eq. (4-5); see also Fig. 4-1.

$$\sigma_c = E_{ci} \cdot \Delta\varepsilon_c \tag{4-5}$$

where: $\Delta\sigma_c$ is the stress reduction
$\Delta\varepsilon_c$ is the strain reduction

The descending part of the stress-strain diagram is strongly depending on the specimen or member geometry, the boundary conditions and possibilities for load redistribution in the structure. In tests a strong influence of the rigidity of the used testing device can be observed. During the softening process microcracking occures in a fracture zone of a limited length l_d and width. One single fracture zone is supposed to be decisive for the failure of a certain member. The stress in the fracture zone drops down with a shear displacement in local shear bands of $w_c \approx 0.5$ mm. The ultimate strain $\varepsilon_{c,lim}$ is caused by this displacement w_c related to a certain length l (Fig. 4-4). Furthermore the possibility for redistribution of stresses in the adjacent uncracked zones is decisive for the deformation capacity in the fracture zone. With a high strain gradient under flexural deformation the ultimate strain is much higher than with a uniform strain distribution across the fracture region. Further the redistribution capacity for stresses is decreasing with increasing strength as the concrete reacts more and more brittle. As a consequence, the descending portion of the stress-strain relation is size dependent and so not only a material property (Fig. 4-5). A general value for $\varepsilon_{c,lim}$ must be applicable for relevant member dimensions in practice. The values for $\varepsilon_{c,lim}$ given in Table 4-3 are in good agreement with tests up to a compressive zone depth of about 500 mm [Meyer (1998), Grimm (1996)]. Under axial compression, the descending part can only be observed with a controlled increase in deformation. For small strain gradients a redistribution of stresses is not possible and the strain should be limited by ε_{c1}. The maximum strains $\varepsilon_{c,lim}$ given in Table 4-3 are valid for small and medium member sizes under a strain gradient. With increasing concrete strength the softening behaviour is less significant and $\varepsilon_{c,lim}$ is getting close to ε_{c1}.

For the analysis of structural deformations under ultimate load the knowledge of the descending branch of the stress-strain diagram is not important. If concrete fails under compression the descending part is usually reached only in local sections including the fracture zone close to the failure load.

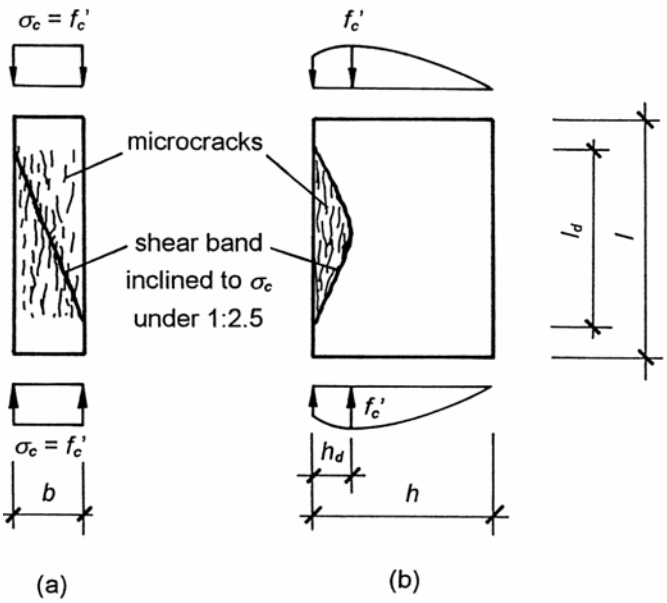

Fig. 4-4: Fracture zone under (a) axial and (b) excentric compression

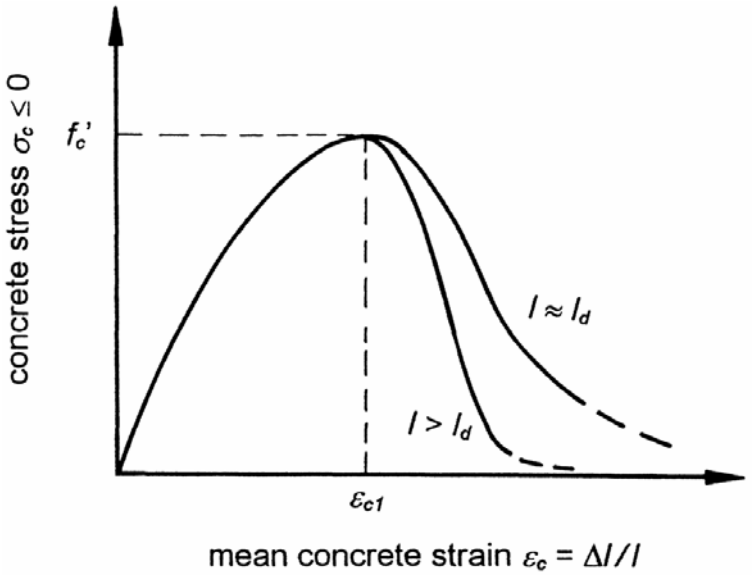

Fig. 4-5: Size dependent descending branch of the stress-strain diagram

To describe the deformations close to a fracture zone including the size dependent softening effect, it is necessary to use a fracture mechanical approach. Grimm (1996) and Meyer (1998) proposed damage zone models which are based on the compression damage zone (CDZ) model by Markeset (1993) (Fig. 4-6). The fracture energy consumption due to microcracking in the fracture zone is used to describe the softening inside the fracture region. The stress-strain relation for increasing strain is divided in three parts. The unloading part from uncracked regions is described with elastic strains ε by Eq. (4-5). The inelastic strains due to the formation of longitudinal cracks and the sliding deformation caused by the formation of a shear band inside the fracture zone are added (Fig. 4-4, Fig. 4-6). The latter parts depend on the absolute size of the fracture zone. As a result size dependent stress-strain relations can be found for each member [Grimm (1996)], [Meyer (1998)]. The influence of lateral reinforcement in the fracture zone can be described as well [Meyer (1998)].

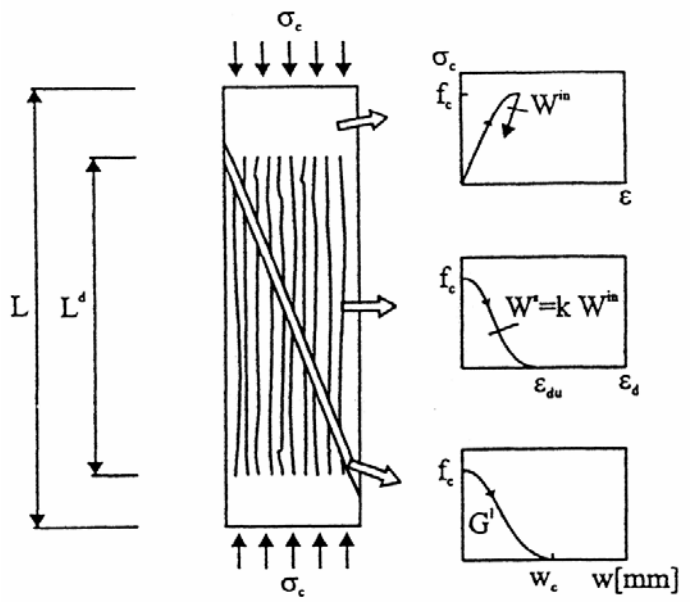

Fig. 4-6: Components of the Compression Damage Zone (CDZ) model [Markeset (1993)]

If the rotation capacity of a single section is of interest, the deformation and stress distribution in the fracture zone can be calculated using the CDZ-model in a numerical analysis [Grimm (1996), Meyer (1998)].

4.4.2 Tension

Tensile failure of concrete is always a discrete phenomenon. Therefore, only the tensile behaviour of the uncracked concrete can be described using a stress-strain diagram. At tensile stresses of about 90 % of the tensile strength f_{ct} microcracking starts to reduce the stiffness in a small damage zone (Eq. 4-6 and 4-7). The microcracks grow and form a discrete crack at stresses around the tensile strength. Stresses and deformations in this local fracture process zone can now be described using a stress-crack opening diagram (Fig. 4-7). All deformations in the fracture process zone can be added to a fictitious crack opening w [Hillerborg (1983)].

$$\sigma_{ct} = E_{ci} \cdot \varepsilon_{ct} \qquad \text{for } \sigma_{ct} \le 0.9 \cdot f_{ctm} \tag{4-6}$$

$$\sigma_{ct} = f_{ctm} \cdot \left(1 - 0{,}1 \cdot \frac{0.00015 - \varepsilon_{ct}}{0.00015 - 0.9 \cdot f_{ctm} / E_{ci}} \right) \qquad \text{for } 0.9 \cdot f_{ctm} < \sigma_{ct} \le f_{ctm} \tag{4-7}$$

where:
- E_{ci} is the tangent modulus of elasticity in MPa from Eq. (4-1)
- f_{ctm} is the tensile strength in MPa from Eq. (3-7)
- σ_{ct} is the tensile stress in MPa
- ε_{ct} is the tensile strain

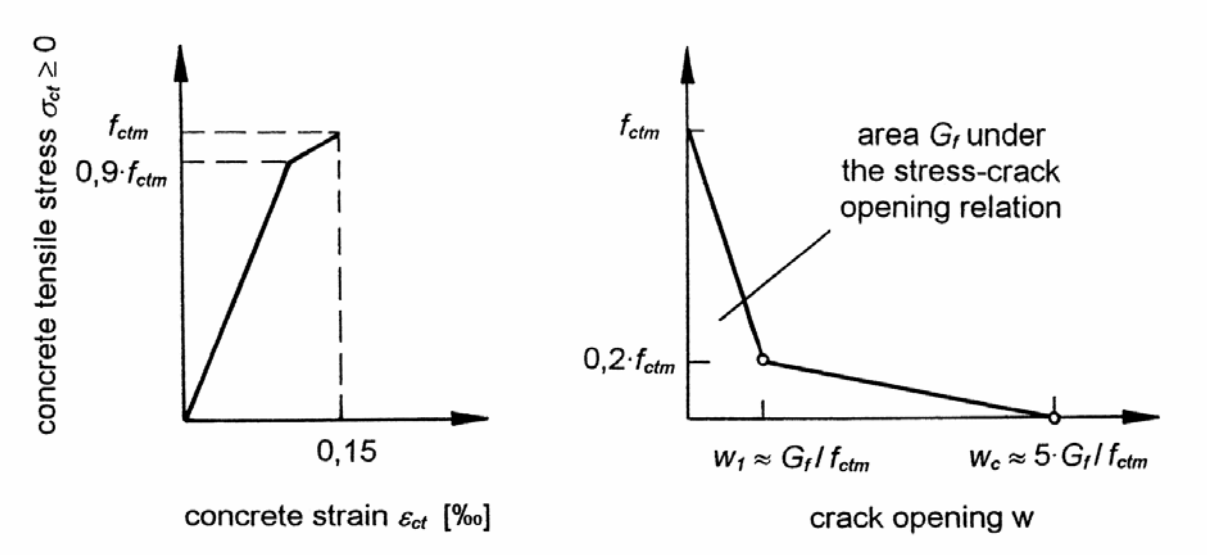

Fig. 4-7: Stress-strain and stress-crack opening diagram for uniaxial tension

Neglecting the small energy consumed by a complete loading cycle in the stress strain diagram, the maximum strain $\varepsilon_{ct,max}$ in the stress-strain diagram can be estimated as $\varepsilon_{ct,max} \approx f_{ctm} / E_{ci}$. For the analysis of the fracture zone a strain $\varepsilon_{ct,max} \approx 0.15$ ‰ can be estimated. Due to the localisation of microcracking in the fracture zone and the large uncracked areas outside the damage zone this strain is only valid inside the fracture zone.

The bilinear approach for the stress-crack opening relation from Fig. 4-5 is given by Eqs. (4-8) and (4-9). This simplified approach can describe the fracture energy consumed by a total crack opening and gives a good estimate for the general shape of the unloading branch in

tension. Where the exact shape is of interest, the fracture energy and the shape of the stress-crack opening curve should be found by a uniaxial tensile test.

$$\sigma_{ct}(w) = f_{ctm} \cdot \left(1.00 - 0.80 \cdot \frac{w}{w_1} \right) \qquad \text{for } w \le w_1 \tag{4-8}$$

$$\sigma_{ct}(w) = f_{ctm} \cdot \left(0.25 - 0.05 \cdot \frac{w}{w_1} \right) \qquad \text{for } w_1 < w \le w_c \tag{4-9}$$

where:
- w is the crack opening in mm
- w_1 = G_f / f_{ctm} where $\sigma_{ct} = 0.20 \cdot f_{ctm}$
- w_c = $5 \cdot G_f / f_{ctm}$ where no stress σ_{ct} is transferred
- G_f is the fracture energy (N/mm) from Eq. (3-11)
- f_{ctm} is the tensile strength in MPa from Eq. (3-7)

In structures the descending branch of the stress-crack opening diagram results in tensile forces carried across cracks close to the crack tips. In small members the forces carried across cracks have significant impact on the tensile capacity of the member. On the other hand, in large members the contribution of the descending branch stresses can be neglected. A significant size effect is caused e. g. in the bending capacity of unreinforced beams and in the flexural shear capacity of members without shear reinforcement as shown in Fig. 4-8. In both cases the capacity of small members ($d \approx 200$ mm) calculated neglecting the descending branch is increased by a factor of 1.6 up to 2.0 by the tensile forces carried in the fracture process zone.

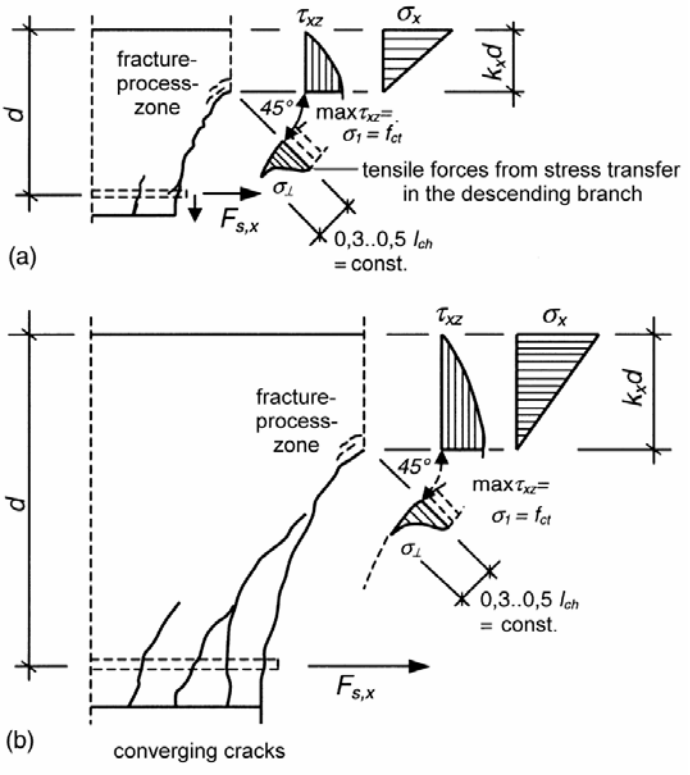

Fig. 4-8: Effect of the tensile stress transfer in the descending branch on the flexural shear capacity of small (a) and large (b) members [Zink (2000)]

4.4.3 Multiaxial states of stress

The available experimental data of the stress-strain relationship of HPC under multiaxial loading scatter in a wide range. The results depend on the used testing equipment and procedure of the respective researcher and differ from each other. The formulation of a constitutive model to describe the deformation behaviour of concrete subjected to any type of loading has proven to be very difficult. Over the years many researchers have proposed different constitutive models for normal strength concrete based on many different theories. Some of the more important ones for high strength concrete are described by Dahl (1992). This model is an improvement of the Ottosen model [Ottosen (1979)].

The proposed model is based on the non-linear elasticity theory, where the secant modulus of elasticity and the Poisson's ratio depend on the actual state and level of stress. The model describes the short term deformations of concrete under monotone increasing compressive loads. The post-failure stress-strain behaviour of concrete under multiaxial states of stress is not covered by the formulae presented here, as sufficient experimental data are not available.

The following parameters are needed to calibrate the model to the specific concrete. All three parameters can be determined from the standard uniaxial compression test:

1) f_{cm} uniaxial compressive strength
2) E_0 initial value of Young's modulus
3) ε_c the strain at the peak stress

The minor principal stress at failure σ_{3f} is determined on the basis of a failure criterion. This stress is used for calculating the non-linearity index β, a measure of the actual level of stress in relation to the failure state (at failure: $\beta = 1$). For the determination of β it is referred to equation (4-10).

$$\beta = \frac{\sigma_3}{\sigma_{3f}} \tag{4-10}$$

The secant value of Young's modulus at failure E_f is determined using equation (4-11). For definitions of E_f see Fig. 4-9.

$$E_f = \frac{\sigma_{3f}}{\varepsilon_{3f}} = \frac{E_c}{1 + 2 \cdot \frac{E_0}{E_c} \cdot \left(\frac{\left(\sqrt{J_2}\right)_f}{f_{cm}} - \frac{1}{\sqrt{3}} \right)} \tag{4-11}$$

with:
- E_0 initial Young's modulus
- E_c uniaxial secant value of Young's modulus at failure
- f_{cm} uniaxial compressive strength
- $\left(\sqrt{J_2}\right)_f$ square-root of the second invariant of the deviatoric stress tensor at failure

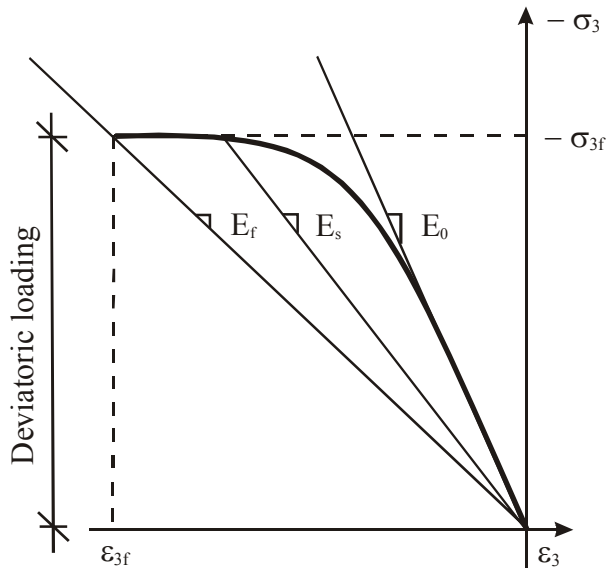

Fig. 4-9: Symbols used in the model according to Dahl (1992)

With E_0, E_f and β the secant value of the Young's modulus E_s at any given stress level can be determined using equation (4-12).

$$E_s = \frac{1}{2}E_0 - \beta \cdot \left(\frac{1}{2}E_0 - E_f\right) \pm \sqrt{\left[\frac{1}{2}E_0 - \beta \cdot \left(\frac{1}{2}E_0 - E_f\right)\right]^2 - \beta \cdot E_f^2} \tag{4-12}$$

The apparent value of Poisson's ratio μ^a can be determined using equations (4-13) and (4-14) and the non-linearity index β.

$$\mu^a = \begin{cases} \mu_i^a & for \;\; \beta \le 0.6 \\ \mu_f^a - \left(\mu_f^a - \mu_i^a\right) \cdot \sqrt{1 - \left(\frac{\beta - \beta_t}{1 - \beta_t}\right)^2} & for \;\; \beta > 0.6 \end{cases} \tag{4-13}$$

Uniaxial and biaxial loading:	Triaxial loading:
$\mu_i^a = 0.20$	$\mu_i^a = 0.15$
$\mu_f^a = 0.36$	$\mu_f^a = 0.50$

(4-14)

Using μ^a and E_s the strains of concrete can be determined using equation (4-15).

$$\varepsilon_3 = \frac{\sigma_3 - \mu^a \cdot (\sigma_1 + \sigma_2)}{E_s}$$
$$\varepsilon_2 = \frac{\sigma_2 - \mu^a \cdot (\sigma_1 + \sigma_3)}{E_s} \tag{4-15}$$
$$\varepsilon_1 = \frac{\sigma_1 - \mu^a \cdot (\sigma_2 + \sigma_3)}{E_s}$$

Another recommendable constitutive model based on an elasto-plastic material law was described by Rogge (2002). This model is sufficiently accurate for modelling the characteristic material behaviour of concrete elements undergoing smeared cracking. By the determination of the plastic, irrecoverable deformation part, the consideration of the load history including unloading is possible.

The stress-strain diagram of concrete under uniaxial or multiaxial loading shows a continuous degradation of the stress-strain ratio in the ascending branch without a significant yield initiation (hardening). This effect is caused by a gradual extension of microcracks already present in the unloaded concrete. Up to a level of about 80 to 90 percent of the maximum stress, the increase is accompanied by a volume reduction due to the closing of microcracks and an ongoing collapse of the pore structure. Close to and behind the maximum stress level the microcracks combine to longer macrocracks resulting in a significant volume increase. Due to the possible redistribution of internal stresses within the inhomogeneous microstructure of concrete, a concrete element also shows a stable material behaviour after passing the maximum stress point in the descending branch of the stress-strain diagram (softening). This model is particularly suitable for numerical analysis. For further details see Rogge (2002).

4.5 Shear friction behaviour in cracks

4.5.1 Introduction

A typical feature of the behaviour of reinforced and prestressed concrete structures is that they show a considerably changed stiffness after cracking. This means that cracking often goes along with a transition to a significantly different bearing mechanism. As a consequence internal forces in a structure can change direction so that shear stresses occur in cracks. A typical example of this is truss action in beams subjected to shear. The first cracks tend to occur under an angle of about 45º with the gravity axis of the member, in accordance with the direction of the principal tensile stresses in the uncracked phase. After the occurrence of the first generation of shear cracks a redistribution of forces occurs, leading to a rotation of the compression struts. Hence, the shear design can be carried out assuming a strut inclination, which is considerably smaller than 45º (EC-2 advises for instance as a lower limit cot θ_{min} = 2,5, which corresponds to θ_{min} = 21,8º. The capacity of cracks in concrete to transmit shear stresses as a contribution to the overall bearing resistance is important in structures which have been precracked due to other combinations of loads as well. In structures which are loaded by a combination of axial tension, bending and shear, cracks can occur which intersect the whole cross-section, and have to carry the ultimate shear load.

4.5.2 The shear friction principle

Mostly the transmission of shear forces across cracks in concrete is described with the so-called shear friction mechanism, Fig. 4-10. Because of the roughness of the cracks a type of wedging action develops if the parts adjacent to the crack are subjected to opposite shear forces. The reinforcement, which intersects the crack, restrains the crack opening and as a consequence counteracts the shear slip. A first evaluation of the shear friction capacity led to the formulation:

$$V_u = A_{vf} \cdot f_y \cdot \tan\theta \qquad (4\text{-}16)$$

or

$$v_u = \rho_v \cdot f_y \cdot \tan\theta \tag{4-17}$$

where V_u = ultimate shear force, A_{vf} = reinforcement intersecting the crack, f_y = yield stress of the reinforcing steel and tan α is a parameter, characterizing the undulation of the crack surface. Moreover v_u = ultimate shear stress and ρ_v = reinforcement ratio of bars, intersecting the crack.

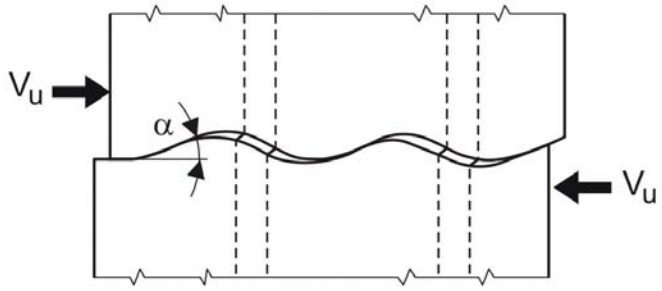

Fig. 4-10: Shear friction mechanism, showing a wedge-type of behaviour at shear sliding

Later on, the equations were modified: since an external compressive stress perpendicular to the crack has the same effect as a yielding reinforcement crossing the crack, the term σ_n was added to $\rho_v \cdot f_y$. Furthermore, in order to achieve a better agreement with regard to test results, the equations were extended with a cohesion term. So Eq. (4-17) changes to the expression of the "modified shear friction equation":

$$v_u = c + (\rho_v \cdot f_y + \sigma_n) \tan\theta \tag{4-18a}$$

On the basis of a statistical evaluation of test, Mattock (1974) proposed values c = 2,8 MPa and tan θ = 0,8 for concretes with moderate strength. Since it was expected that no significant increase of v_u would occur in overreinforced concrete, the restriction

$$v_u \leq 0.3 f_c' \tag{4-18b}$$

was added.

4.5.3 Shear friction across cracks in HPC

The main disadvantage of Eq. (4-18a) is that it does not consider the influence of the concrete strength. In Walraven (1981) and Walraven, Reinhardt (1981) it was shown that there must be an influence, since the shear carrying capacity is actually built up of numerous small forces, exerted through local contact areas between aggregate particles and cement matrix, see Fig. 4-11.

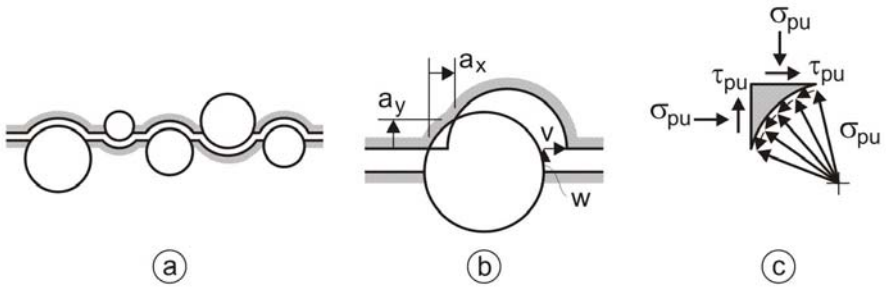

Fig. 4-11: Schematic representation of transmission of forces across a crack
a) Simplified interface representation
b) Origin of a contact area during crack sliding
c) Basis for equilibrium conditions

Indeed, an evaluation of a large number of results, up to a cylinder strength of about 70 MPa, showed the influence of the concrete strength. In a discussion of Walraven, Frenay, Pruijssers (1987) and Mau, Hsu (1988) it was shown that a simple and adequate formulation of the mean shear capacity of cracks intersected by reinforcement is

$$\frac{v_u}{f_c'} = 0.66\sqrt{\omega} \leq 0.3 \tag{4-19}$$

where

$$\omega = \frac{\rho_v \bullet f_y}{f_c'}$$

with

ρ_v = reinforcement ratio of bars, intersecting the crack
f_y = yield stress of the steel
f'_c = concrete cylinder strength

However, a restriction for Eq. (4-19) is that is was based on concretes in which the tensile strength was not high enough to cause fracturing of the aggregate particles. Nowadays a concrete with a strength of 100 MPa and more is easily producable and a common feature of it is that the aggregate particles fracture during the formation of a crack. On the basis of Fig. 4-11 it is clearly imaginable that the shear capacity of a crack will be considerably reduced if the majority of the particles fracture. So, it can therefore be expected that for a concrete strength higher than a certain critical value – which depends on the ratio particle strength to matrix strength – a drop in the shear friction capacity to a much lower level will occur.

In Walraven (1981) it was shown that the shear carrying behaviour of cracks in concrete can be described as a function of the parameters w (crack width), δ (shear displacement between the crack faces), σ (normal compressive stress perpendicular to the crack, counteracting crack widening) and τ (shear stress in crack). A fundamental formulation was derived for cracks with unbroken particles, based on the mechanism described in Fig. 4-11.

The general constitutive equations are:

$$\tau = \sigma_m \cdot (A_y + \mu \cdot A_x) \quad (4\text{-}20a)$$

$$\sigma = \sigma_m \cdot (A_x - \mu \cdot A_y) \quad (4\text{-}20b)$$

where

σ_m = crushing strength of matrix
μ = coefficient of friction for the contact area between particles and matrix

A_x and A_y are projected contact areas which are functions of the crack width, the shear displacement, the relative aggregate volume and the maximum particle diameter [Walraven (1981)]. From tests on concrete with glacial river aggregate it was found that the best agreement with test results was obtained with $\mu = 0.4$ and $\sigma_m = 6.4 \cdot f_{cc}^{0.56}$.

Fig. 4-12 shows a family of curves relating the shear stress τ and the normal stress σ to the shear displacement δ and the crack width w. The curves show the relation τ - δ and σ - δ for a constant crack width.

Fig. 4-12 (left) shows the relations obtained for a concrete with a cube strength of 59 MPa, made with glacial river aggregate. Inspection of the crack faces after the test showed that the aggregate particles were predominantly uncracked. Fig. 4-12 (right) shows the relations for a concrete with a cube strength of 110 MPa. It is seen that there is a considerable reduction of the values τ and σ for the same crack width and shear displacement with regard to the values obtained in Fig. 4-12 (left).

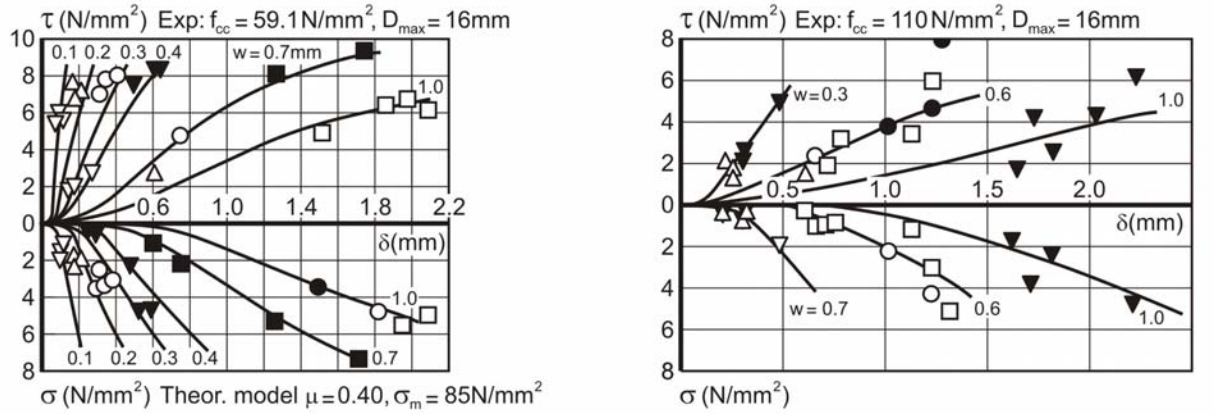

Fig. 4-12: Relation between shear stress τ, normal stress σ, shear displacement δ, crack width w for a concrete with unbroken aggregate particles and a cube strength of 59 MPa(left) and a concrete with broken aggregates and a cube strength of 110 MPa (right)

The basic explanation for the reduction of the shear capacity with an increased concrete strength is the reduction of the contact area due to particle fracturing. It is therefore obvious to reduce the contact areas A_x and A_y by a fracture reduction factor C. The Eqs. (4-20a, 4-20b) are then modified to:

$$\tau = \sigma_m \cdot C \cdot (A_y + \mu \cdot A_x) \quad (4\text{-}21a)$$

$$\sigma = \sigma_m \cdot C \cdot (A_y - \mu \cdot A_y) \quad (4\text{-}21b)$$

For the experiments concerned, a fracture reduction factor C = 0.35 turned out to give the best agreement with the tests.

The fracture factor C can be used as well in combination with curves which approach the theoretical Eqs. (4-21a, 4-21b) and are based on curve fitting of large series of test results, carried out on push-off specimens, Fig. 4-13.

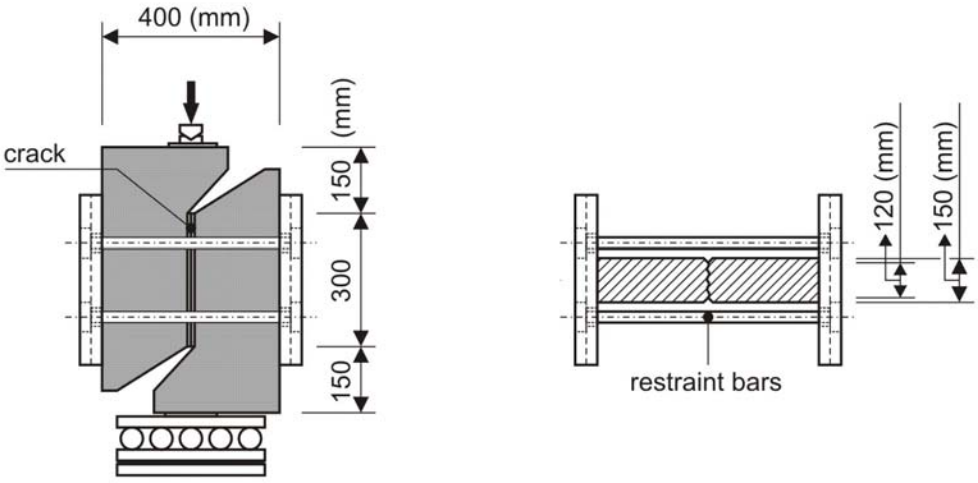

Fig. 4-13: Shear friction tests on push-off specimens with external restraint bars (Walraven [1981])

These relations are:

$$\tau = C\{-\frac{f_{cc}^{'}}{30} + [1.8w^{-0.80} + (0.234w^{-0,707} - 0.20) \cdot f_{cc}^{'}]\delta\} \qquad \text{(4-22a)}$$

with $\tau \geq 0$ (N/mm^2, mm)

$$\sigma = C\{-\frac{f_{cc}^{'}}{20} + [1.35w^{-0.63} + (0.191w^{-0.552} - 0.15) f_{cc}^{'}]\delta\} \qquad \text{(4-22b)}$$

with $\sigma \geq 0$

Fig. 4-14 shows that there is good agreement between Eqs. (4-22a, 4-22b) and the test results.

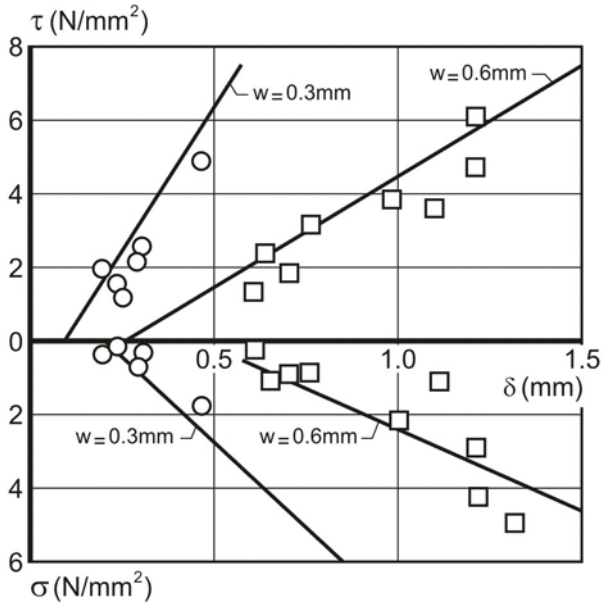

Fig. 4-14: Comparison between test results for concrete with a cube strength of 110 MPa and the linearized relations with a fracture reduction factor C = 0.35 according to Eq. (4-22)

4.5.4 Ultimate shear friction capacity of cracks in reinforced HPC

In the past many tests have been carried out for assessing the shear friction capacity of cracks in reinforced concrete. Most of those tests were carried out on push-off specimens with concrete strengths between 20 and 60 MPa. For those strengths the Eq. (4-19) describes the results with excellent accuracy. For reinforcement ratios for which the yield stress of the steel is reached (which is generally the case if $\tau_u/f_c' < 0.3$) the mean ratio between the shear strength values, found in 60 experiments, was 1.00 and the coefficient of variation was 0.11. For excessive reinforcement ($\tau_u/f_c' < 0.3$) the mean value for 28 tests was 1.06 with a coefficient of variation of 0.13. The 88 specimens used for the evaluation were made of concrete with strong aggregate, so that the percentage of broken particles was very small. The use of Eq. (4-19) for high strength concrete (e.g. $f_{cc}' > 80$ MPa) would however only be valid if the condition of no particle fracturing would be fulfilled. Observation of the crack faces in the specimens made with the high strength concrete in this research program, showed however that a large percentage of the particles was broken. Fig. 4-15 shows a comparison of Eq. (4-19) by [Mao and Hsu (1988)] with the tests on high strength concrete push-off specimens, obtained in this research. The dotted line is hypothetical and is valid for $f_c' = 100$ MPa and unbroken particles. The experimental values are, as expected, considerably smaller: they are in the range of values which would be obtained with a concrete strength of 35-55 MPa. It appears that, due to particle fracturing, the shear capacity was reduced to 55-75 % of the values which would be obtained with unbroken particles: the 55 % applies to low and the 75 % to high reinforcement ratios. Obviously the shear capacity of cracks, intersected by reinforcement, is less reduced by particle fracturing than that of cracks in plain concrete. The reason is twofold:

- the shear capacity of reinforced cracks is partially due to dowel action of the rebars, which is not reduced by particle fracturing

- the bond between the rebars and the concrete is very good, so that the crack width remains relatively small: the relatively larger number of contact points partially compensates for the loss of shear capacity due to particle fracturing.

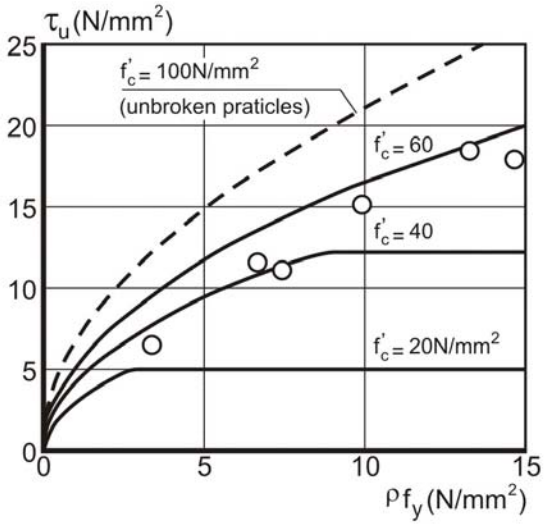

Fig. 4-15: Comparison of test results for high strength concrete with $f_{cc'}$ = 100 MPa, Eq. (4-19) acc. to Mau and Hsu (1988) valid for concretes with unbroken particles

4.6 Rotation and bending capacity

The stress-strain relation for concrete in compression up to grade C120 may be expressed by the subsequent relation (see also Eq. 4-4):

$$F(\eta) = \frac{\sigma_c}{f_c} = -\frac{k \cdot \eta - \eta^2}{1 + (k-2) \cdot \eta} \quad \text{for } |\varepsilon_c| < |\varepsilon_{c,\lim}| \tag{4.6-1}$$

where:
η = $\varepsilon_c / \varepsilon_{c1}$
ε_{c1} = -1,60 · (f_{cm} / 10 MPa)$^{0.25}$ / 1000 strain at maximum compressive stress [Popovic (1973)]
k = E_{ci} / E_{c1} plasticity number
f_c is the compressive strength

For the analysis of the rotation versus the bending moment the following relations are helpful:

$$m = \frac{M_y}{bd^2} = \alpha \cdot k_x \cdot k_z \cdot f_c \tag{4.6-2}$$

where:
m is the bending capacity for a rectangular compression zone in [MPa]
k_x is the relative height of the bending compression zone
k_z is the relative inner lever arm
b is the width of the compression zone
d is the static depth of the bending member
α is the integral factor for the stress-strain relation in the compression zone

$$k_x = \frac{\varepsilon_{c\,\lim}}{\varepsilon_{c,\lim} - \varepsilon_s} \tag{4.6-3}$$

$$\alpha = \frac{1}{\eta_{lim}} \int_0^{\eta_{\lim}} F(\eta)\,\mathrm{d}\eta \tag{4.6-4}$$

$$k_z = 1 - k_x \cdot \frac{\eta_{lim} \quad \eta_R}{\eta_{lim}} \tag{4.6-5}$$

$$\eta_R = \frac{\int_0^{\eta_{lim}} \eta \cdot F(\eta)\,\mathrm{d}\eta}{\int_0^{\eta_{lim}} F(\eta)\,\mathrm{d}\eta} \tag{4.6-6}$$

Helpful integrals used in Eqs. (4.6-4) and (4.6-6) are:

$$\int_0^{\eta_{lim}} F(\eta)\,\mathrm{d}\eta = \frac{1}{a^3} \cdot \left[\frac{(1+a\eta)^2}{2} - 2 \cdot (1+a\eta) - \eta \cdot ka^2 + ln(1+a\eta) \cdot (1+ka) \right]_0^{\eta_{lim}} \tag{4.6-7}$$

$$\int_0^{\eta_{lim}} \eta \cdot F(\eta)\,\mathrm{d}\eta = \tag{4.6-8}$$

$$= \frac{1}{a^4} \cdot \left[\frac{(1+a\eta)^3}{3} - (1+a\eta)^2 \cdot \left(\frac{3}{2} + ka \right) + (1+a\eta) \cdot (3+2ka) - ln(1+a\eta) \cdot (1+ka) \right]_0^{\eta_{lim}}$$

where: $a = k - 2$

The relation $\alpha_i(f_{ck})$ of tangent modulus E_{ci} versus secant modulus $E_{c,sec}$ at $\sigma_c = 0.4 \cdot f_{cm}$ can be calculated from the stress-strain diagrams if initial creep effects are neglected. Fig. 4.6-1 compares the values for α_i from the stress-strain diagrams to the bilinear approach following Eq. (4-3).

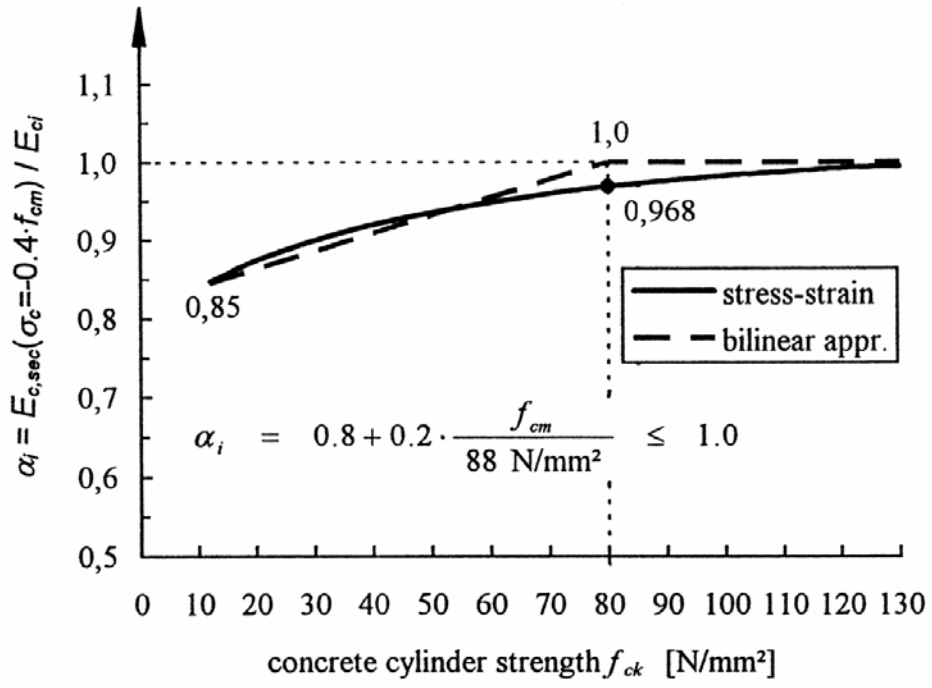

Fig. 4.6-1: Secant versus tangent-stiffness ratio α_i in the stress-strain relation

If the theoretical medium bending capacity is calculated with the stress-strain relation for deformation analysis, an increase of bending capacity should be monotonically with increasing concrete strength. Fig. 4.6-2 shows the results for the characteristic stress-strain relations (index *k*) and design stress-strain relations (index *d*). In the latter relations the concrete stresses at a certain strain are reduced by $\alpha = 0.85$ and $\gamma_c = 1.5/(1.1\text{-}f_{ck}/500) \geq 1.50$. The yielding point of the steel is reduced by a factor $\gamma_s = 1.15$. Both graphs show a sufficient monotone increase with strength. Differences to an ideal curved shape are caused by the approximation of the ultimate strain $\varepsilon_{c,lim}$.

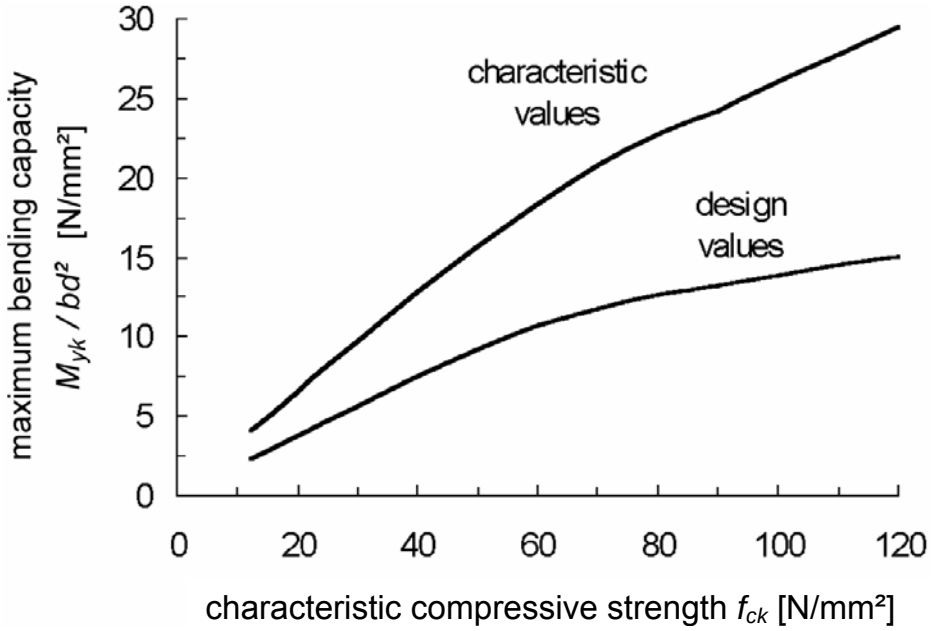

Fig. 4.6-2: Theoretical bending capacity calculated with a steel strain of 2.38 ‰ (k) and 2.07 ‰ (d) respectively

This test proofing the compatibility of stress-strain relations for different concrete strengths should also be applied when approaches to the mean curve are made for design purpose. The bending capacity should be monotone for any other approach like e. g. bilinear relations. Also the factors k_z and α (see Eqs. (4.6-3) and (4.6-4)) have to be equivalent in other approaches to the stress-strain diagram. If safety factors are increased with increasing concrete strength, this must not lead to a decrease in flexural strength.

5 Stress and strain rate effects – impact

5.1 Range of applicability

The petroleum industry as well as military facilities may be subjected to transient loading, such as impacts (missiles, falling off objects), shock waves (explosions, detonations) and earthquakes. Limited information exists on the behaviour of HPC under high loading rate conditions.

It is known, that both the values of tensile and compressive resistance and the Young's modulus in the case of a very short loading application differ from the results under static loads.

Different types of dynamic loading can be differentiated, see Table 5-1.

Type of loading	Strain rate [s^{-1}]
traffic	10^{-6} - 10^{-4}
gas explosions	$5 \cdot 10^{-5}$ - $5 \cdot 10^{-4}$
earthquake	10^{-2} - 10^{0}
pile driving	10^{-2} - 10^{0}
airplane impact	$5 \cdot 10^{-3}$ - $5 \cdot 10^{-2}$
hard impact	10^{0} - 10^{2}
high velocity plate impact	10^{2} - 10^{5}

Table 5-1: Examples of different loading rates according to Reinhardt (1987)

5.2 Compressive strength

In different experiments on HPC it was illustrated, that the compressive resistance increases with increasing loading rate. Fig. 5-1 shows results of Reinhardt (1987) obtained from tests on a C50 and Jensen (1993) obtained from tests on normal strength concrete (C35), on high-performance concrete (C115) and on a specific composite of steel fibres and bauxite aggregate (Cxx2) under different loading rates. The compressive strengths were 46, 109 and 134 MPa, measured on cubes with an edge length of 100 mm. The results of both researchers show similar characteristics regarding the strength increase during shock loading.

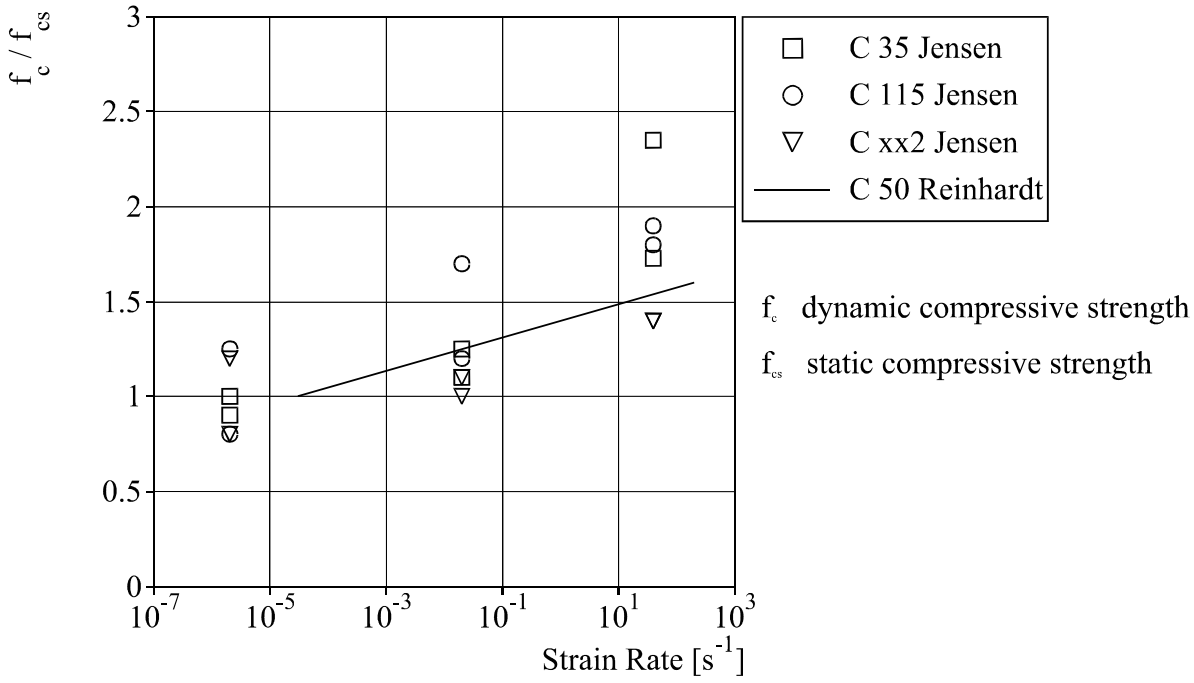

Fig. 5-1: Effects of different strain rates of the compressive strength of concrete according to Jensen (1993) and Reinhardt (1987)

Malvar and Crawfort (1998) determined a so-called dynamic increase factor f_c / f_{cs}. This factor depends on the concrete grade and the strain rate. The factor can exceed 2 under dynamic compression and reaches 6 under dynamic tension. The strain rate was given within the range of 10 s^{-1} to 1000 s^{-1}. The dynamic increase factor f_c / f_{cs} can be determined by Eqs. (5-1) and (5-2).

$$\frac{f_c}{f_{cs}} = \left(\frac{\dot{\varepsilon}}{\dot{\varepsilon}_s}\right)^{1.026\cdot\alpha_s} \qquad \text{for } \dot{\varepsilon} \leq 30\ s^{-1} \tag{5-1}$$

$$\frac{f_c}{f_{cs}} = \gamma_s \left(\frac{\dot{\varepsilon}}{\dot{\varepsilon}_s}\right)^{1/3} \qquad \text{for } \dot{\varepsilon} > 30\ s^{-1} \tag{5-2}$$

with:
- f_c dynamic compressive strength at strain rate ε
- f_{cs} static compressive strength at strain rate ε_s
- f_c / f_{cs} compressive strength dynamic increase factor (DIF)
- $\dot{\varepsilon}$ strain rate in a range between $3 \cdot 10^{-5}$ s^{-1} and 300 s^{-1}
- $\dot{\varepsilon}_s$ static strain rate of $3 \cdot 10^{-5}$ s^{-1}
- log γ_s = 6.156 α_s – 2
- α_s factor to consider the concrete grade, $\alpha_s = 1 / (5 + 9 \cdot f_{cs} / f_{c0})$
- f_{c0} reverence value of 10 N/mm²

5.3 Tensile strength and fracture properties

5.3.1 Tensile strength

In Fig. 5-2 the theoretical tensile strength as a function of the strain rate is represented. If the strain rate increases the viscosity of the matrix increases too because the aggregates crush cumulative. If a static load is applied on a HPC-specimen, the aggregates are destroyed as well as the high-strength matrix and there is no difference in the fracture mechanism in the case of the dynamic load.

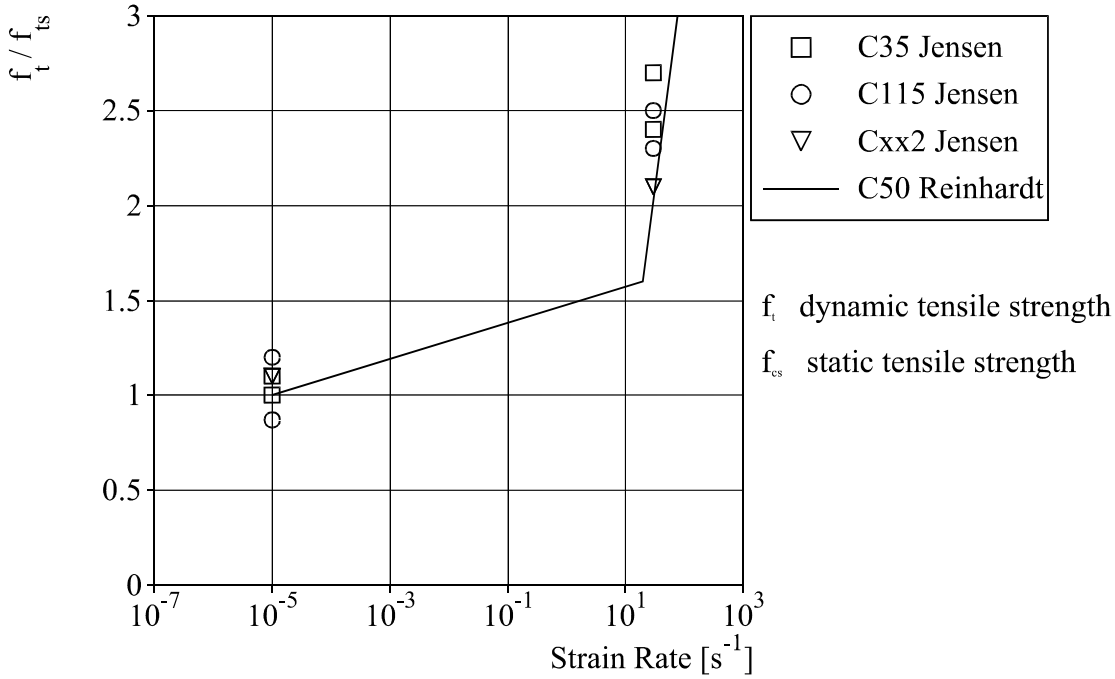

Fig. 5-2: Strain rate effects on tension of concrete according to Jensen (1993) and Reinhardt (1987)

Malvar and Crawfort (1998) also examined the tensile strength of HPC. The tensile tests were executed on cylinders. The dynamic increase factor f_t / f_{ts} is given in Eqs. (5-3) and (5-4).

$$\frac{f_t}{f_{ts}} = \left(\frac{\dot{\varepsilon}}{\dot{\varepsilon}_s}\right)^{1.016\delta} \qquad \text{for } \dot{\varepsilon} \leq 30\ s^{-1} \tag{5-3}$$

$$\frac{f_t}{f_{ts}} = \beta\left(\frac{\dot{\varepsilon}}{\dot{\varepsilon}_s}\right)^{1/3} \qquad \text{for } \dot{\varepsilon} > 30\ s^{-1} \tag{5-4}$$

with:
- f_t dynamic tensile strength
- f_{ts} static tensile strength
- f_t / f_{ts} tensile strength dynamic increase factor (DIF)
- $\dot{\varepsilon}$ strain rate in a range between $3 \cdot 10^{-5}$ s^{-1} and 300 s^{-1}
- $\dot{\varepsilon}_s$ static strain rate of $3 \cdot 10^{-6}$ s^{-1}
- $\log \beta$ $= 7.11 \cdot \alpha - 2.33$
- α factor to consider the concrete grade, $\alpha = 1 / (10 + 6 \cdot f_{cs} / f_{c0})$

f_{c0} reverence value of 10 MPa.

5.3.2 Fracture energy

The fracture energy is defined as the area under the complete displacement curve of the stress-crack opening, see Eq. (5-5) according to MC 90 [CEB (1993)].

$$G_F = \int_0^{\delta_0} \sigma \cdot d\delta \tag{5-5}$$

with: δ crack opening displacement

This energy is dissipated in friction and plastic deformation in the fracture area. Testing results are very scarce. It may be concluded that the fracture energy increases with increasing stress and strain rate.

5.4 Modulus of elasticity

As known, the modulus of elasticity depends on the material properties of the aggregates and the cement. Under dynamic loads the concrete shows a stiffer behaviour which affects the stress-strain curve and thus the elastic modulus. The effect of the stress and strain rate on the modulus of elasticity may be estimated by Eq. (5-6) according to [CEB (1993)]. The concrete grade has no influence in this relation.

$$\frac{E_{c,imp}}{E_{ci}} = \left(\frac{\dot{\sigma}_c}{\dot{\sigma}_{c0}}\right)^{0.025}$$
$$\frac{E_{c,imp}}{E_{ci}} = \left(\frac{\dot{\varepsilon}_c}{\dot{\varepsilon}_{c0}}\right)^{0.026} \tag{5-6}$$

with: $E_{c,imp}$ impact modulus of elasticity
E_{ci} static modulus of elasticity
$\dot{\sigma}_c$ stress rate
$\dot{\varepsilon}_c$ strain rate
$\dot{\sigma}_{c0}$ = - 1.0 MPa/s
$\dot{\varepsilon}_{c0}$ = - $3 \cdot 10^{-5}$ s^{-1} for compression loading

Dargel (1985) found out a typical development of the elastic modulus of ordinary concrete described as a function of the strain rate as represented in Fig. 5-3.

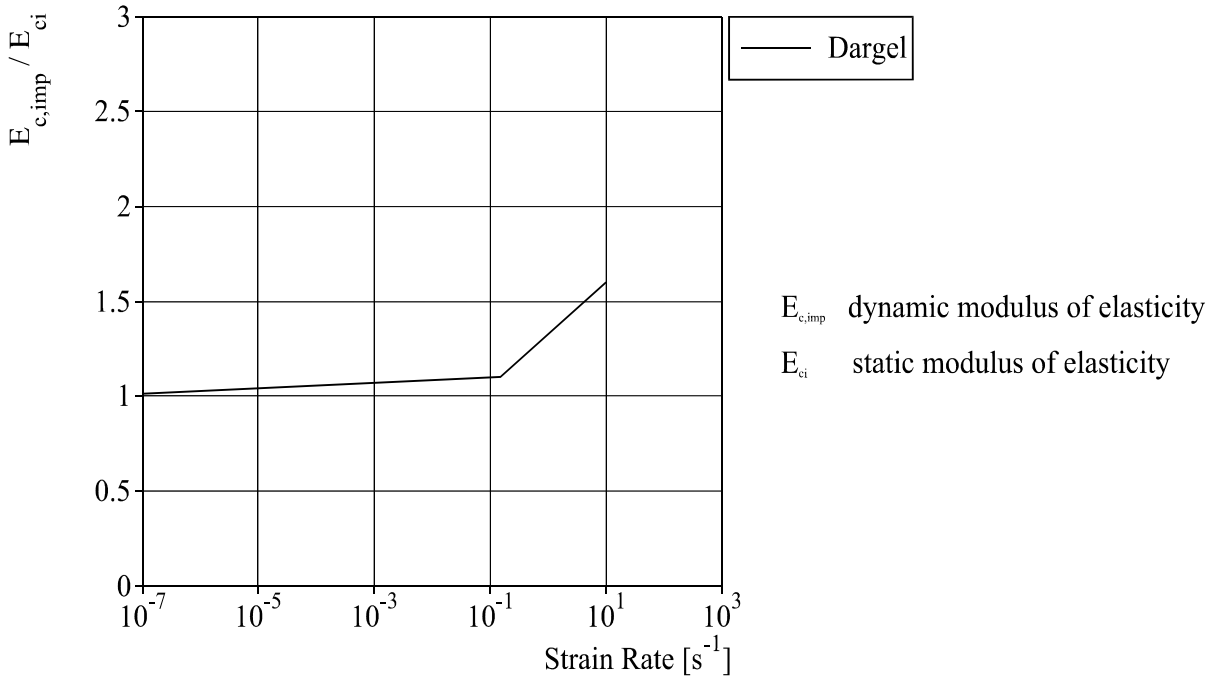

Fig. 5-3: Young's modulus versus to the strain rate according to Dargel (1985)

5.5 Stress-strain relation

There is a lack of information about the stress-strain relations of HPC under dynamic loads.

6 Time effects

6.1 Development of strength with time

6.1.1 Development of the compressive strength

6.1.1.1 General

The rate at which concrete strength increases with time depends on a variety of parameters, in particular type and strength class of cement, type and amount of admixtures and additions, water/cement ratio and environmental conditions. According to CEB-FIP Model Code 1990 for a mean temperature of 20 °C and curing in water the relative compressive strength of concrete at various ages $f_{cm}(t)$ may be estimated from Eqs. (6-1) and (6-2).

$$f_{ctm}(t) = \beta_{cc}(t) \cdot f_{cm} \tag{6-1}$$

with

$$\beta_{cc}(t) = \exp\left\{ s \cdot \left[1 - \left(\frac{28}{t/t_1} \right)^{0.5} \right] \right\} \tag{6-2}$$

where:

$f_{cm}(t)$	mean compressive strength of concrete [MPa] at an age t [days]
f_{cm}	mean compressive strength of concrete [MPa] at an age of 28 days
$\beta_{cc}(t)$	function to describe the development of compressive strength with time
t	concrete age [days]
t_1	= 1 day
s	coefficient which depends on the strength class of cement as given in Table 6-1.

Strength class of cement	32.5	32.5R 42.5	42.5R 52.5
s	0.38	0.25	0.20

Table 6-1: Coefficient s to be used in Eq. (6-2) for different strength classes of cement

In order to take into account the effect of the temperature during curing the actual concrete age should be adjusted according to Eq. (8-2) in section 8.2.

As it will be shown in the following sections Eq. (6-2) is also appropriate for high strength concrete. However, since the composition of the high strength concrete often differs significantly from that of normal strength concrete such parameters as the water/cement ratio or the type of additions have to be considered additionally to the type of cement. It may be done by an appropriate adjustment of the coefficient s.

The evaluation of the experimental data found in literature (the data sources are given in [Lerner (2000)]) by applying different formulas does not provide a better fit of the data than by using Eq. (6-2). Figure 6-1 shows exemplary the development of the relative compressive

strength of high strength concrete containing silica fume. The compressive strength of concrete at an age of 28 days was chosen as a reference value. Besides Eq. (6-2) two other formulas were applied: the relation according to Gardner & Zhao (1993) and a modification of Eq. (6-2), where an additional variable b was introduced instead of the exponent 0.5 (see the corresponding relations in Figure 6-1). For all formulas the determination coefficient B was found to be equal to 0.89. For some other data a minimal improvement of the accuracy (by approx. 1 %) was achieved using the modified formula (Eq. (6-2) with a variable exponent b). However, this does not justify the introduction of an additional coefficient, as making the relation more complex. The relation according to Gardner & Zhao (1993) generally provides the same accuracy as Eq. (6-2). However, it is, in contrast to the relation given in CEB-FIP Model Code 1990, purely empirical. Further, it does not provide the value of the relative compressive strength equal to 1 at an age of 28 days, which means a serious restriction with regard to a desired code type formulation. Further attempts to find a relation alternative to Eq. (6-2) showed that in comparison to this formula a better fitting can only be achieved by rather complex relations with more than 3 variables.

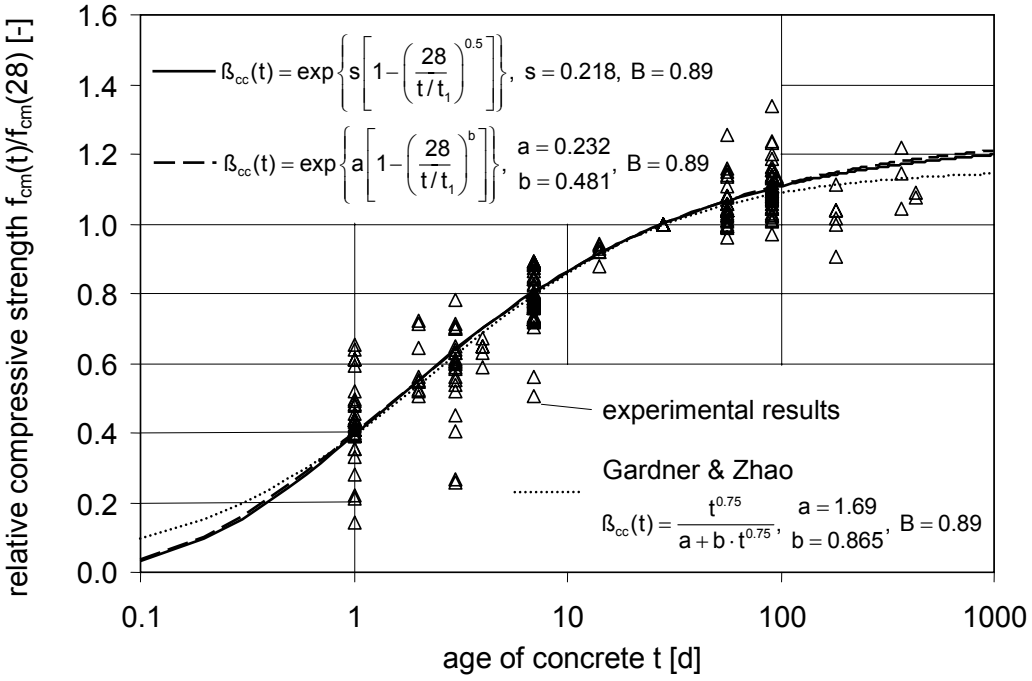

Fig. 6-1: Development of the relative compressive strength of concrete containing silica fume: experimental data and best fit curves obtained using Eq. (6-2), a modified version of it (additional variable b, instead of the exponent 0.5) and the formula by Gardner & Zhao (1993)

Since Eq. (6-2) provides a very good fit with experimental data also for high strength concrete and since this formula is already well established, only this relation will be considered in following contemplations concerning the development of the compressive strength of concrete.

6.1.1.2 Effect of water/cement ratio

The development of the microstructure of hydrated cement paste plays a decisive role in the development of the compressive strength and other mechanical properties of concrete. The process of microstructure formation is strongly affected by the water/cement ratio of concrete. With decreasing water/cement ratio the thickness of the water layer between the unhydrated

cement particles in a concrete mixture decreases. This means on the one hand, that cement particles are positioned closer to each other and less hydration products are needed to fill the voids and to bridge open spaces in the paste matrix. On the other hand, there is generally less water available for the hydration process, so that this process would slow down and finally stop when all mixing water is bound, chemically or physically.

For cases of water/cement ratios below approx. 0.40, which are typical for high strength concrete, the mixing water is not sufficient for the complete hydration of cement. With decreasing water/cement ratio the process of hydration is earlier completed, while an increasing amount of unhydrated cement particles remains within the hydrated cement paste. These cement particles act as a fine filler increasing the strength of the hardened cement paste. Further, with decreasing water/cement ratio and increasing degree of hydration the pore size distribution of the paste is shifted to smaller sizes. As a result, a quicker development of concrete strength can be observed within the first hours and days after mixing, and higher absolute strength values can be measured in comparison to concrete with a higher water/cement ratio.

The experimental data by Bergner (1997), shown in Figure 6-2 by symbols, clearly confirm these considerations. The figure shows the development of the relative compressive strength with time for concretes with different w/c ratios ranging between 0.25 and 0.6. No admixtures were used in these mixtures.

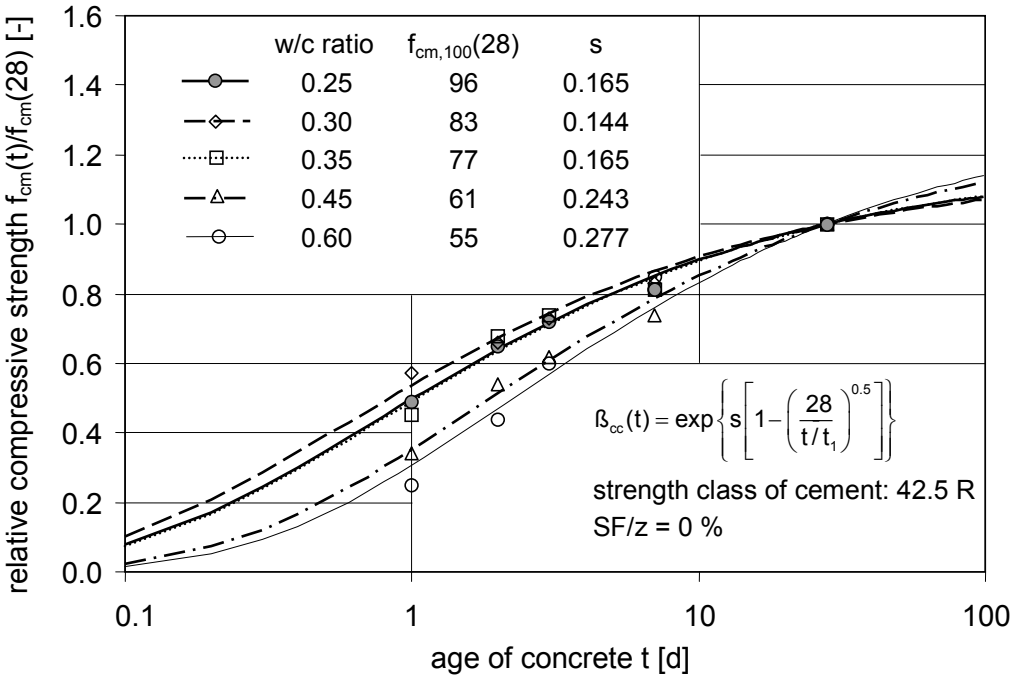

Fig. 6-2: Effect of water/cement ratio on the development of the relative compressive strength of concrete, experimental data acc. to Bergner (1997)

The concretes with lower w/c ratios show a faster strength development within the first hours or days. For instance, the concrete with a w/c ratio of 0.25 attains 50 % of its 28-day-strength in just 24 hours, while the relative compressive strength of the concrete with a w/c ratio of 0.6 at this age amounts to approx. 25 %. However, with further increasing age of concrete the hydration process and, correspondingly, the development of the compressive strength become slower, which is more pronounced in the case of concretes with a lower w/c ratio.

The curves in Figure 6-2 indicate the best fits, which were obtained by applying Eq. (6-2)

on the data for each considered concrete (i.e. for each given w/c ratio), while the coefficient s was the computed variable. The average of all obtained values s is approximately 0.2, i.e. equal to the value given in MC 90 for the strength class of cement used in the experiments (42.5 R). However, when the w/c ratios typical for HSC without admixtures (i.e. w/c = 0.25, 0.30 and 0.35) are considered, the coefficient s is smaller and, in fact for these w/c ratios, the values of this coefficient do not differ very much.

6.1.1.3 Effect of strength class of cement

The type of cement is another important factor affecting the strength development of HSC. Both the mineral composition of the cement clinker and the fineness of cement influence the hydration process. For normal strength concrete the effect of the strength class of cement is considered in MC 90 by the coefficient s, as given in Table 6-1. Applying Eq. (6-2) the analysis of experimental data by Bergner (1997) shows that at least in the case of high strength concrete containing silica fume (SF) as admixture the effect of the strength class of cement is much less pronounced. In the investigation of Bergner (1997) concretes with water/cement ratios between 0.25 and 0.45 were considered containing the same amount of silica fume of 8 % by mass of cement. The calculated value of the coefficient s obtained for slowly hardening cements (strength class 32.5) is close to 0.30. For normal or rapid hardening cements (strength class 42.5) and for rapid hardening high strength cements (strength class 42.5 R) the values s of approx. 0.28 and 0.245, respectively, were obtained.

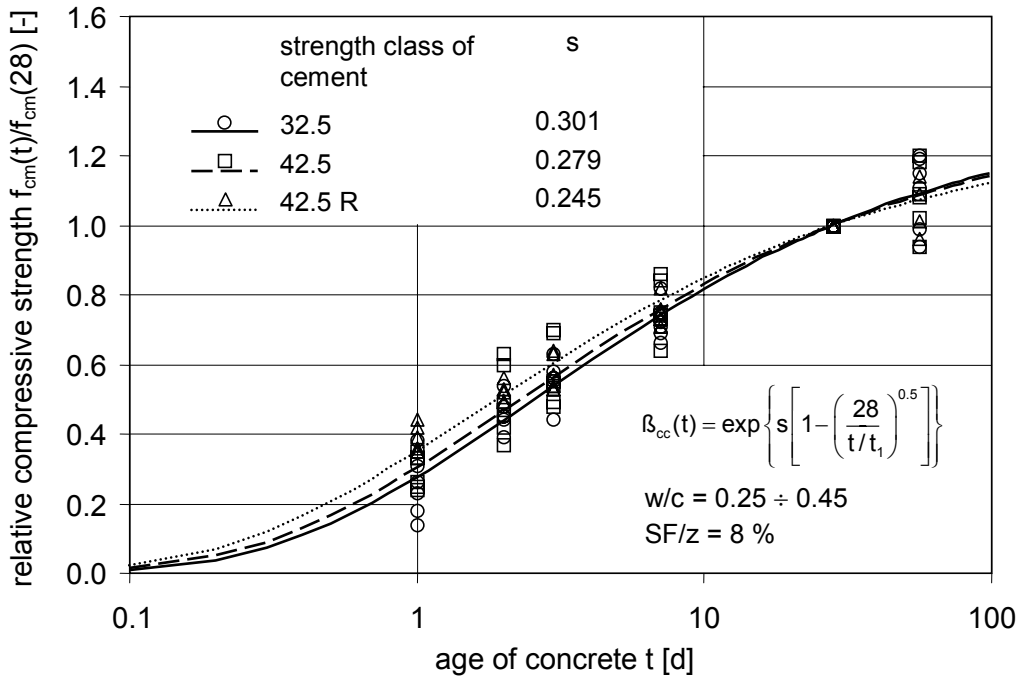

Fig. 6-3: Effect of strength class of cement on the development of the relative compressive strength of concrete, experimental data acc. to Bergner (1997)

The result, that the difference between the values s for individual strength classes is significantly smaller, than the difference of the corresponding values given in MC 90 for normal strength concrete can be, at least partly, traced backto the effects of silica fume on the hydration process of cement [Malhotra, Carette, Sivasundaram].

6.1.1.4 Effect of binding agent

Since high strength concrete often contains besides cement a considerable amount of other binding agents, the effect of such admixtures on the development of the concrete strength should be considered. Two most frequently used additives are silica fume and fly ash, both able to react with $Ca(OH)_2$ in the pore solution building new CSH-phases. The gain of additional strength due to such pozzolanic reactions, which are relatively slow, becomes first remarkable at an advanced concrete age. The rate of the reaction depends on the content of the reactive SiO_2 in the admixture, its particle size as well as on the supply of $Ca(OH)_2$ by the hydration process of cement. Additionally, a certain increase of concrete strength can be explained by the fact, that silica fume particles, which are about 30 to 100 times smaller than cement grains, fill the empty spaces between cement particles increasing the denseness of packing, and with it the density and strength of the hardened binder paste.

Results collected from literature (the data sources are given in [Lerner (2000)]) illustrating the effect of binding agent on the development of the compressive strength with time are presented in Figure 6-4. According to the diagram the relative compressive strength develops slower, when admixtures, especially fly ash, are used. However, at higher ages the increase of the relative strength becomes more pronounced for concretes with additional, pozzolanic binding agents. Again, this is most evident in the case of concretes containing fly ash. These tendencies also find their expression in the coefficient s in Eq. (6-2): HSC containing fly ash provides a maximum value s equal to 0.367, while for high strength concrete without admixtures a minimum value s = 0.161 was calculated. For high strength concrete with silica fume a value s of 0.218 was obtained, which is almost equal to the average value of this coefficient calculated for all tests.

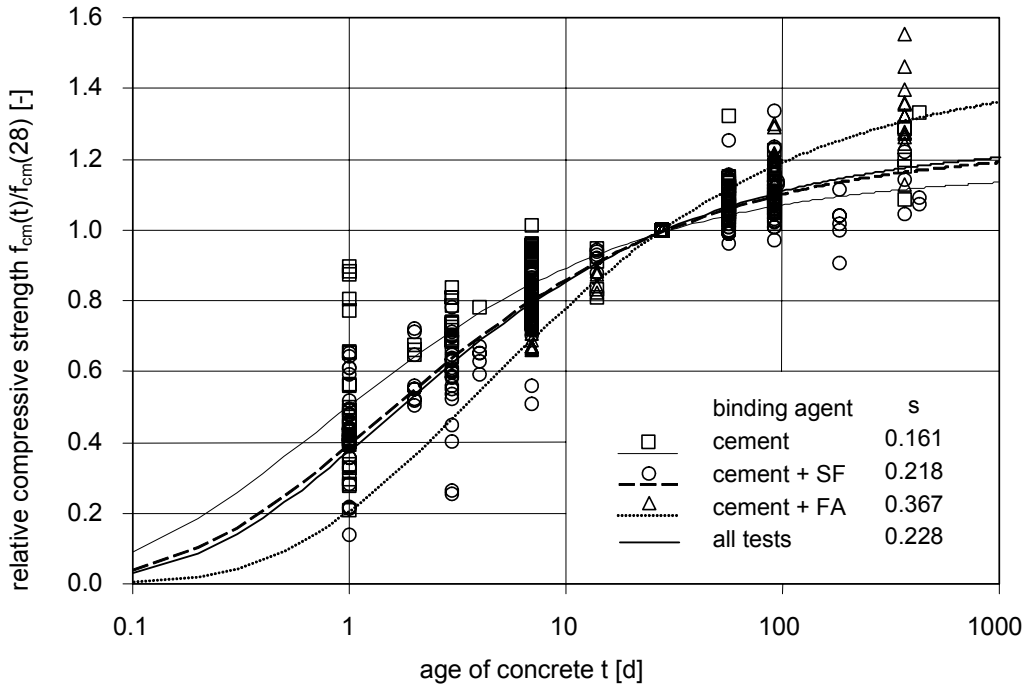

Fig. 6-4: Effect of binding agent on the development of the relative compressive strength of high strength concrete

6.1.2 Development of the tensile strength

It is much more difficult to predict the development of the tensile strength of concrete with time, since it is influenced significantly by the development of shrinkage stresses which in turn depend on the specimen or member size and curing conditions. Since, only very few results on the development of the axial tensile strength for high strength concrete could be found, the tensile strength obtained by means of indirect tests, i.e. spitting or bend tests will be considered in the following.

6.1.2.1 Development of tensile splitting strength

An advantage of the determination of the tensile strength using splitting tests is that the values of the tensile splitting strength are much less sensitive to curing conditions in comparison to other types of tension tests, because critical tensile stresses induced in the test act at some distance from the concrete surface [Hilsdorf (1995)]. However, the data collected from literature (the data sources are given in [Lerner (2000)]) for high strength concrete still show a pronounced scattering, see Figure 6-5. This figure illustrates the development of the relative tensile splitting strength $f_{ct,sp}$ with time, with the $f_{ct,sp}$-value at a concrete age of 28 days serving as reference.

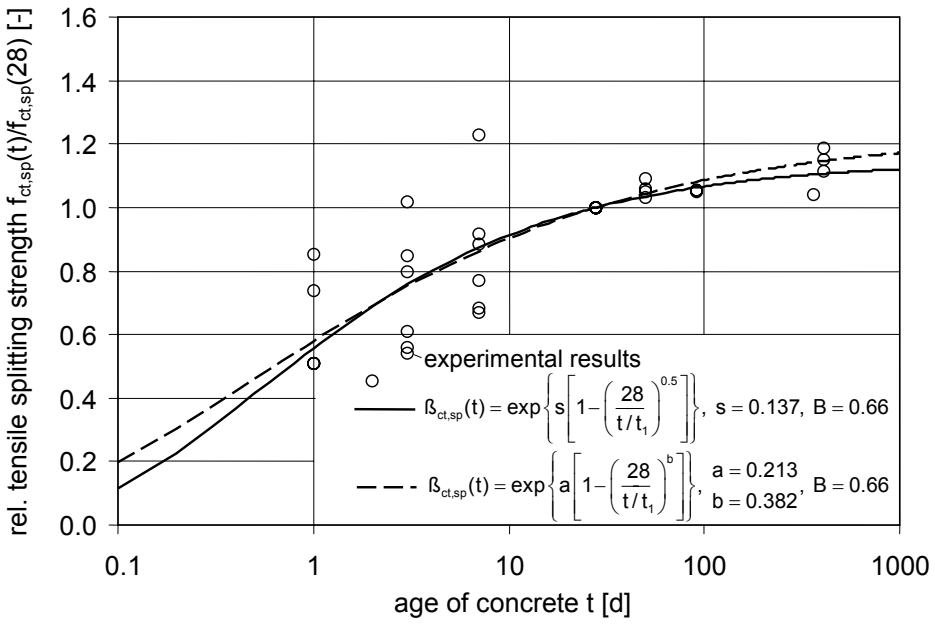

Fig. 6-5: Development of the relative tensile splitting strength of high strength concrete with time

For the mathematical description of this development two formulas were applied: Eq. (6-2) with the coefficient s as variable, and a modification of Eq. (6-2), where an additional variable b was introduced instead of the exponent 0.5 (compare section 6.1.1.1). Both these formulas shown in Figure 6-5 proved to be equally suitable to describe the increase of the tensile splitting strength with time as observed in experiments. This can be recognised by the equal values of the determination coefficient B = 0.66 obtained for both equations. Such relatively low values B were achieved due to scattering of the test results. The parameter s was found to be equal to 0.137 which is clearly below the corresponding values for the compressive strength as shown in section 6.1.1. It means that in comparison to the development of the relative compressive strength of high strength concrete, the development

of the relative tensile strength is faster at early age of concrete and slower for concrete at higher age.

6.1.2.2 Development of tensile flexural strength

In order to determine the resistance of concrete against tensile stresses its flexural strength is often tested as an alternative to the axial tensile strength or tensile splitting strength. The flexural strength is generally higher than the axial tensile strength and strongly depends on the size of the beam, particularly on its depth [Müller and Hilsdorf (1993)] as well as on curing and drying conditions.

The data for high strength concrete available from literature (see [Lerner (2000)] for the sources of the data) are presented in Figure 6-6. Similar to the evaluation of the data for tensile splitting tests two formulas, Eq. (6-2) and the chosen modification of it were applied. Here, the modified formula provided a slightly better fit of the experimental results, than the original Eq. 6-2 (compare the corresponding correlation coefficients B in Figure 6-6). The parameter s for Eq. (6-2) was found to be equal to 0.152, which is slightly higher than the corresponding value for the tensile splitting strength. This indicates, that the flexural strength develops to some extent slower than the tensile splitting strength of high strength concrete.

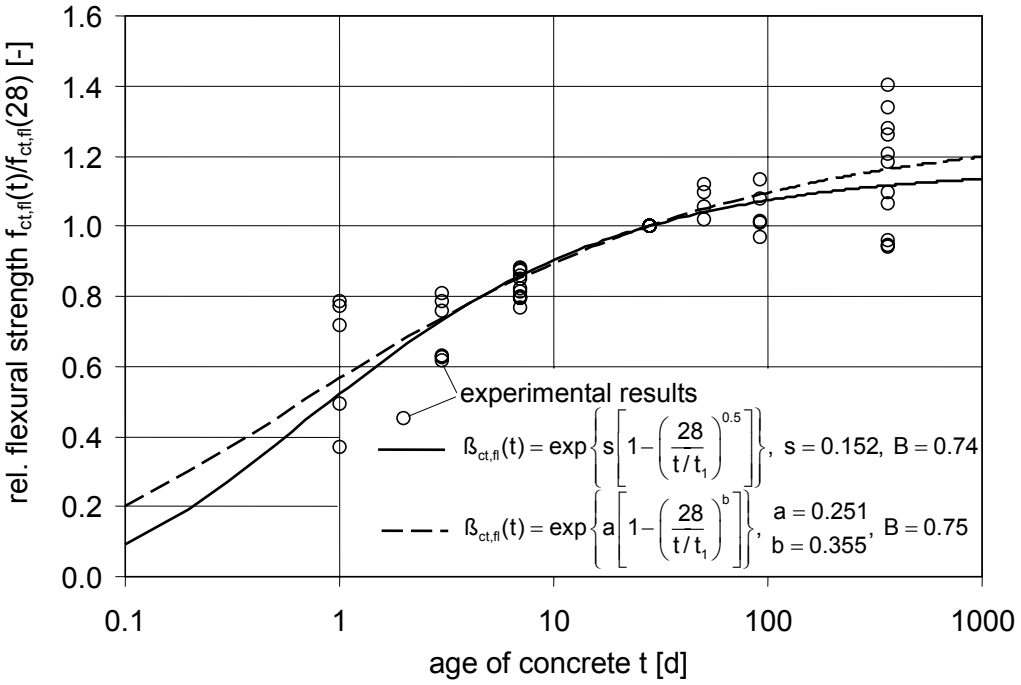

Fig. 6-6: Development of the tensile flexural strength with time

6.2 Strength under sustained loads

Investigations of normal strength concrete show that the tensile strength is reduced by up to 40 % according to loading age and surroundings. The formation of microcracks which are initiated by stress from load, temperature or shrinkage and finally lead to instable crack propagation is responsible for the delayed failure. On the other hand the progressing hydration increases the strength; if there is enough water, microcracks may even be closed.

As the micro structure of normal strength concrete and high strength concrete differs considerably it can be assumed that the findings of the research on normal strength concrete cannot be adapted to high strength concrete without further investigation.

The volume of pores of high strength concrete is, due to the use of silica fume which is a filler as well as a reaction partner, substantial smaller than that of normal strength concrete. It can be assumed that creep is associated with microcracks and their propagation. These microcracks exist in the form of damages before any application of load [Guse, Hilsdorf (1998); Altoubat, Lange (2002)] or they can arise and grow during loading. The stress intensity (*K*-factor) at the crack tips increases and in course of time, with an appropriate load, cracks can propagate and lead to failure. Due to the small volume of pores or the dense structure respectively, HSC have much less damages and cracks before loading and the creep behavior is therefore more restrained.

6.2.1 Long-term compression tests

A summary of results of creep tests under compression load (1971 to 1994) [Setunge (1997)] shows that the creep coefficient generally decreases with an increase of concrete strength. This effect shows up also in connection with an increase of the silica fume content or a decrease of the water/cement ratio. The creep coefficient highly depends on the stress level. Creep coefficients of φ = 1.0 to 1.8 are measured for a compressive strength of f_{cm} = 80 MPa.

Creep tests under high stress levels which lead to failure after a certain time are described in [Han, Walraven (1993)]. Prisms of compressive strengths f_{cm} = 110-120 MPa are herein investigated. The long-term strength under compression and tension is measured. The prisms for the compression tests (100·100·400 mm³) failed after 0.5 to 2.5 hours under a normalized compression load of σ_c / f_{cm} = 85 %. For a compression load of 75 % no failure is observed after 2.5 days. An ultimate long-term compressive strength of 80 % is predicted based on the test results.

6.2.2 Long-term tensile tests

Tensile creep and drying shrinkage tests on concrete partly containing silica fume and steel fibers showed high creep values which can help to reduce restraint stresses in repair layers for example [Bissonnette, Pigeon (1995); Bissonnette, Pigeon (2000)]. The measurements were performed on prisms (50·50·700 mm³ for the creep tests, and 50·50·400 mm³ for the shrinkage tests) up to a compressive strength class C55/67. There was only little influence of the silica fume content on the creep behaviour. Other investigations of dog bone shaped specimens at an age of up to 6 days generally show a larger creep of silica fume containing concrete compared with ordinary concrete [Kovler et al. (1999); Igarashi et al. (2000)]

6.2.2.1 Test set-up

Dog bone shaped specimens have been found most suitable to carry out long-term tensile tests on un-notched specimens. The tensile load is applied by cast-in anchors or glued-on fasteners with hinges. Creep rigs with a lever and an adjustable dead weight are often used to

load the specimens for any duration (Figure 6-7). Shrinkage should be measured on companion specimens of the same shape.

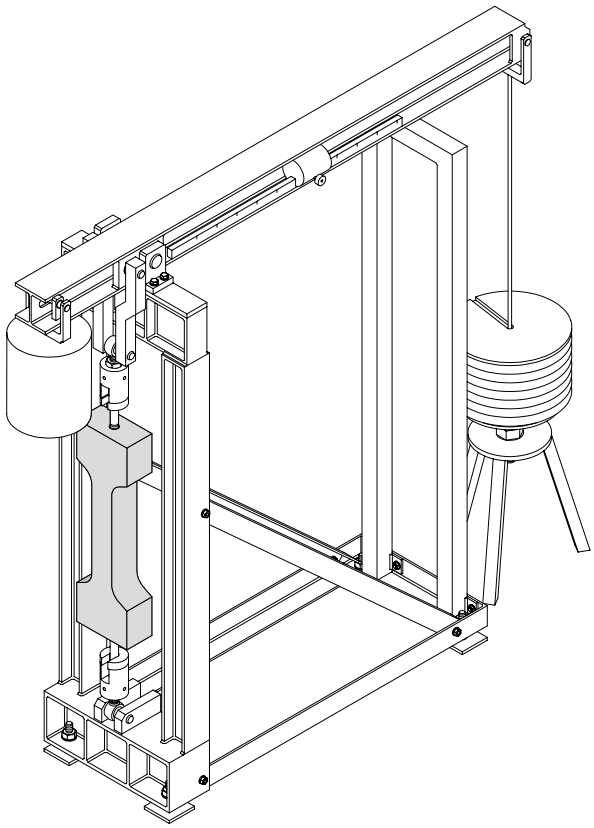

Fig. 6-7: Creep rig (steel construction) with balancing weight and a lever with a leverage of η = 20:1 [Rinder (2003)]

6.2.2.2 Creep under high stress

Applying the load, elastic deformations take place followed by the primary creep. On the basis of already existing microcracks [Heinrich et al. (1999)] and numerous crack nuclei, damages can propagate and expand in the matrix. This process however is stopped due to stress redistribution to zones of higher strength and stiffness. This is the reason for a decreasing course of creep which then, after a few days, becomes the linear secondary creep (Figure 6-8). Generally the measured deformations differ from a linear function. These differences are caused by formation of microcracks and hydration processes which can lead to an additional shrinkage under load [Rinder (2003)]. The long lasting section of secondary creep is determined by stress redistributions which cause sliding motions between gel particles which is measured as a global increase of strain. These processes are stopped by the strength development of concrete if the load is representing a subcritical value. In case of a critical load, local stress concentrations lead to further crack propagation and finally to failure of the specimen. The creep deformations progressively increase just before the delayed failure occurs. This section, the tertiary creep, is influenced by a supercritical accumulation of microcracks in the zone of the later fracture.

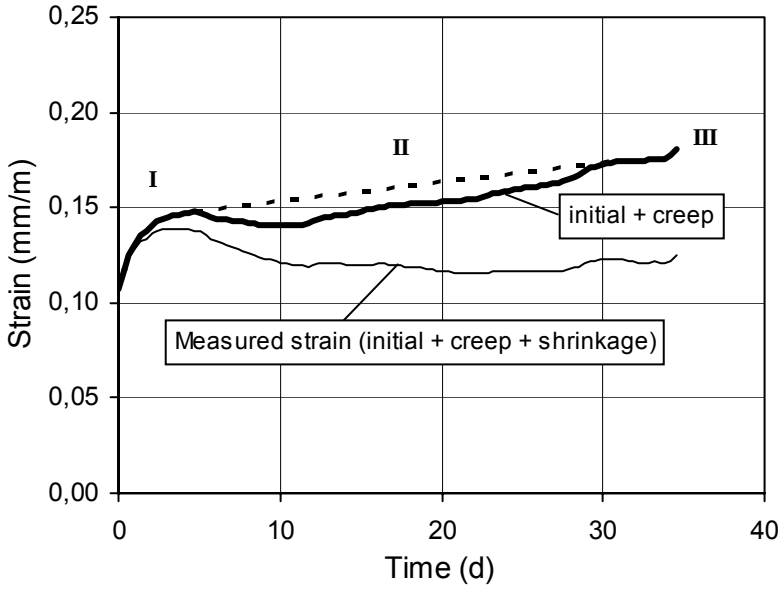

Fig. 6-8: Total strain as function of loading time; concrete C70/85 (σ_{ct} = 4.38 MPa, σ_{ct} / f_{ctm} = 0.90); primary (I), secondary (II), and tertiary creep (III) [Rinder (2003)]

6.2.2.3 Times to failure

Long-term tensile tests with double-sided notched prisms (100·100·250 mm³, f_{cm} = 110-120 MPa) are described in [Han, Walraven (1993)]. The ultimate long-term tensile strength is 75 % of the short-term tensile strength. The test results of long-term tests with dog bone shaped specimens (l = 700 mm) of different concretes (f_{cm} = 76-114 MPa) allow also to predict a strength under sustained loading of about 75 % of the short-term tensile strength. At higher loadings failure can occur even after a short time which is partly explained by the large scatter of the material properties [Rinder (2003)]. On the average the long-term tensile strength of the foil wrapped specimens even amounts to 85 % which is attributed to the eigenstress reducing effect of the foils. Many of the specimens failed unexpectedly early. Only after removing the short times to failure of $t_S \leq 1$ d from the diagram a tendency shows up which goes well with the known results of normal strength concrete (Figure 6-9). The large scatter of the times to failure is caused by the material properties of high strength concrete and essentially comes from the fact that the actual tensile strength of the individual specimen is not known but has to be estimated from the results gained by short-term tests.

The regression calculation leads to for the best relationship between normalized tension and time to failure:

$$\ln\left(t_S\right) = a + b \cdot \frac{\sigma_{ct}}{f_{ctm}} = a + b \cdot r \tag{6-3}$$

with the parameters a = 88.4 und b = -84.0 (t_S in sec). The statistic evaluation of the test results, by assuming a normal distribution, leads to a variation of $\ln t_S = \pm$ 7.4 for the 90 % quantile interval.

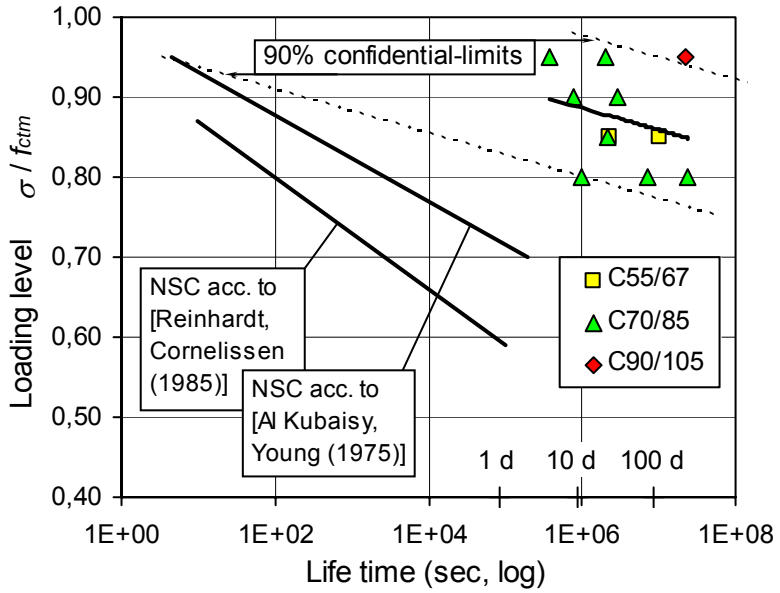

Fig. 6-9: Time to failure of high strength concrete specimens under sustained tensile load [Rinder (2003)]

A substantially better correlation can be reached between the secondary creep rate and the time to failure. The secondary creep is given by the inclination of the creep curves after the shrinkage strain has been subtracted from the total strain. The smaller scatter is due to the fact that creep rate and time to failure has been determined on the same specimen (Figure 6-10).

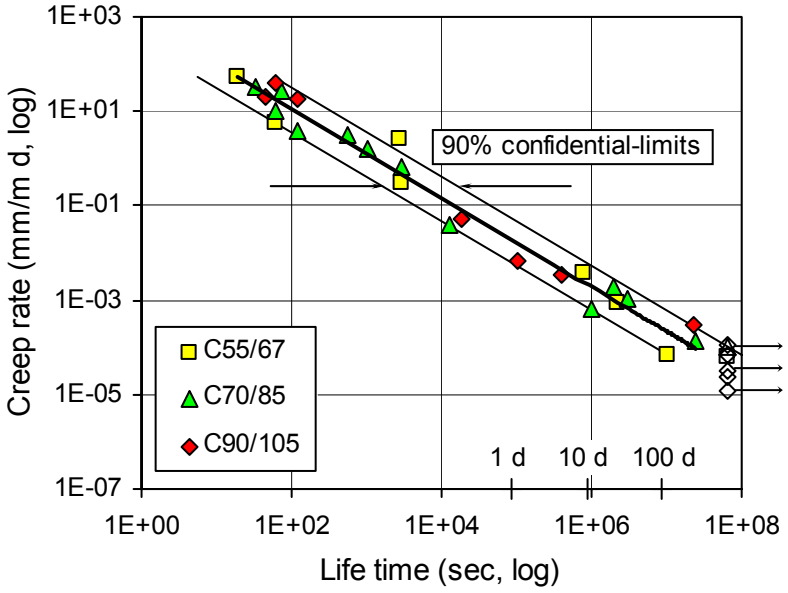

Fig. 6-10: Time to failure as a function of the secondary creep rate $\dot{\varepsilon}_{II}$ (◇ → run out) [Rinder (2003)]

The regression calculation for the equation:

$$\dot{\varepsilon} = c \cdot t_S^d \qquad (6\text{-}4)$$

yields the parameters c = 823 and d = -0.939 for the test results. After inserting these parameters and applying the logarithm

$$\ln t_s = 7.15 - 1.06 \ln \dot{\varepsilon} \tag{6-5}$$

the range for the 90 % quantile interval amounts to $\ln t_S = \pm 1.1$.

6.2.2.4 Development of tensile strength and Young's modulus under stress

The strength and the Young's modulus of high strength concrete are developing considerable fast. After 7 days already 85 % of the compressive strength and 90 % of the Young's modulus of the 28 days values are reached [Yang et al. (1998)]. But with the ongoing hydration of the cement silica fume matrix even in concrete with an extremely low water content a further increase of the strength takes place during long periods of time. So a moderate increase of compressive strength is still measured even after a hardening time of 10 years. In a long-term observation [Maage et al. (1990)] there was a mean compressive strength of 110 % determined after one year and of 120 % of the compressive strength of 28 days after 10 years.

Comparing load free specimens with specimens which were loaded during long periods, a tendency of strength increase as a result of the loading shows up (Figure 6-11). The concrete solidification by a preloading was already found in tensile tests with normal strength concrete. The strength increase can be explained by a reduction of stress concentrations due to creep [Wittmann, Zaitsev (1974)]. Another explanation is, that water can diffuse through widened microcracks under load and so hydration processes can be initiated again [Blaschke et al. (1993)].

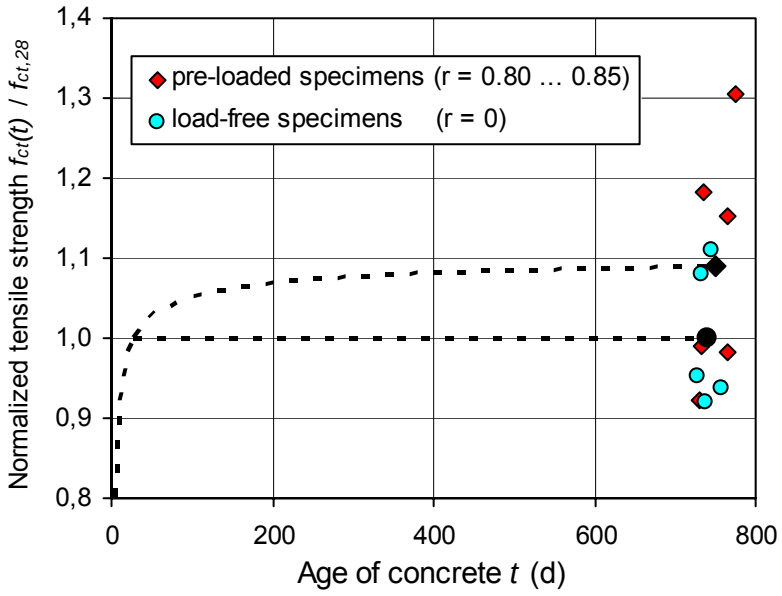

Fig. 6-11: Tensile strength related to the tensile strength at an age of 28 days (silica fume containing concrete C57/65 – C90/105); the bigger symbols represent mean values) [Rinder (2003)]

For the Young's modules the relation between preloaded and not loaded specimens is, as expected, the other way round (Figure 6-12). Load free specimens experience on the average a slight increase of stiffness, whereas the stiffness of loaded specimens obviously decreases in the course of time.

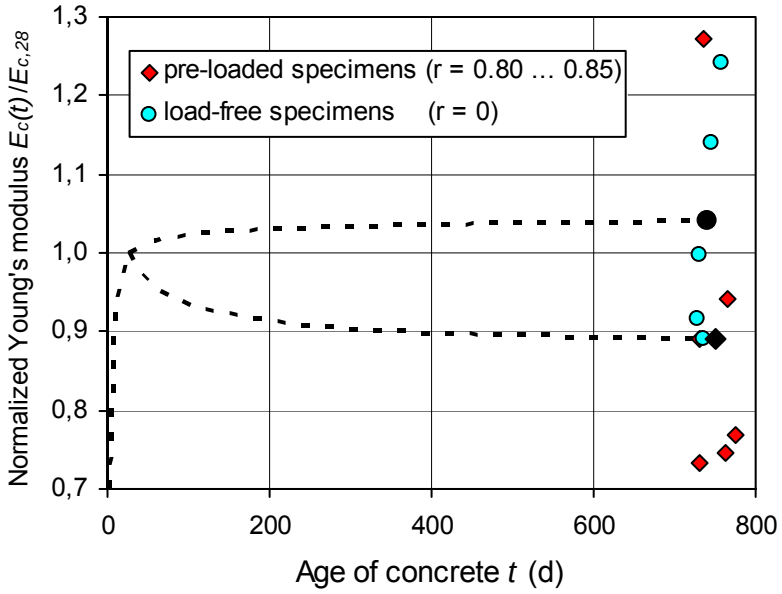

Fig. 6-12: Young's modulus related to the Young's modulus at an age of 28 days (silica fume containing concrete C57/65 – C90/105); the bigger symbols represent mean values) [Rinder (2003)]

6.2.2.5 Tensile creep in comparison with compression creep

For load ratios $r > 0.50$ the creep deformations increase more than proportional compared to the tension which has to be taken into account when different test results are evaluated. The influence of the concrete age at loading on the creep is of particular interest for prestressed concrete.

Test results of compression creep tests on high strength concrete are generally published as creep coefficient:

$$\varphi(t,t_0) = \frac{\varepsilon_\Sigma - \varepsilon_{elastic} - \varepsilon_{shrinkage}}{\varepsilon_{elastic}} = \frac{\varepsilon_{creep}}{\varepsilon_{elastic}} \qquad (6\text{-}6)$$

The observation, that creep under tension is larger than creep under a corresponding compression load [Setunge (1997)] cannot be confirmed, also not for high strength concrete [Rinder (2003)]. Creep coefficients of tensile creep tests are similar to or even smaller than the creep coefficients of compression creep tests (Figure 6-13).

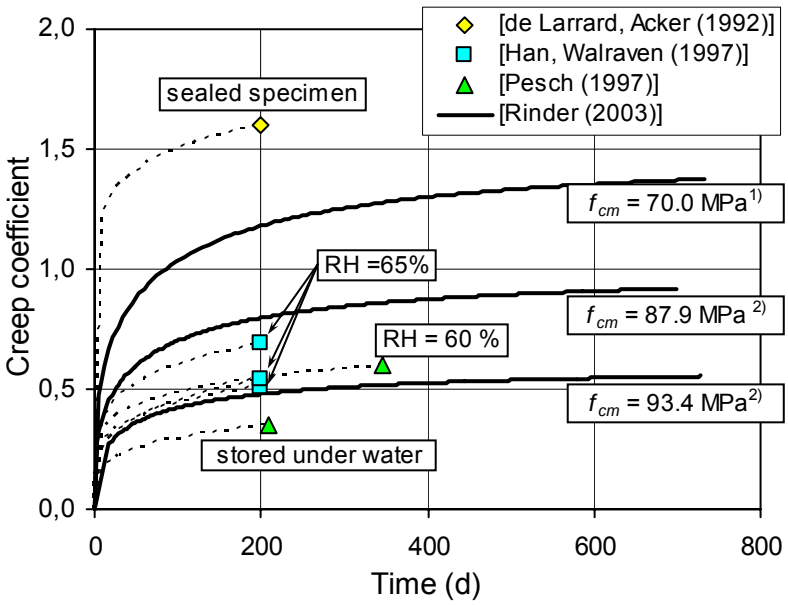

Fig. 6-13: Creep of high strength concrete under compression in comparison with tensile creep of high strength concrete ([1])C55/67, [2])C90/105); no failure within the observation time; for further details see Table 6-2 [Rinder (2003)]

Reference	f_{cm} (MPa)	r
de Larrard, Acker (1992)	83.3	0.26
Han, Walraven (1997)	100.0	0.15-0.50
Pesch (1997)	108.9	0.40
Rinder (2003)	70.0-93.4	0.80-0.85

Table 6-2: Compressive strength and stress level in Figure 6-13

6.2.3 Damage mechanisms and failure under sustained loads

The differences in the structures of high strength and normal strength concrete discussed above are the higher stiffness of the cement matrix, whereby the stiffness difference between cement matrix and aggregates is reduced, the higher tensile strength of the hardened cement paste and the importantly higher bond strength between hardened cement paste and aggregate grains. Cracks which already exist before any loading occurs, are less numerous and on the average smaller than in the case of normal strength concrete. Due to these aspects high strength concrete is more brittle and elastic than normal strength concrete. This means from the view of fracture mechanics for normal strength concrete with its very different crack lengths; since longer cracks reach rather a critical state than shorter cracks, that already in an early stage of load a continuous crack propagation gets started, which shows up in the stress-strain curve. The shorter cracks in the structure of high strength concrete grow only at loadings close to the ultimate load. The stress is approximately evenly distributed to all cracks what leads to a sudden, brittle failure. The effect which is caused by the distribution of the different crack lengths is, in the case of normal strength concrete, restrained by the crack stopping effect of the relative weak and partially separated transition zone between cement matrix and aggregate grain. In this zone a further dissipation of energy besides the fracture surface energy takes place. In the further process the crack is normally diverted from its

original direction and led around the aggregate grain. In high strength concrete the propagating cracks are running directly through the aggregate grains. This contributes again to brittle fracture behaviour [Reinhardt (2000)].

Investigations with X-ray technology on cylinders under long-term compression show differences in the cracking between normal strength and high strength concrete [Smadi, Slate (1989)]. Generally there were, both before and during the load, much less cracks observed in high strength concrete than in normal strength concrete. A considerable crack development was observed only from a level of 80 % of the compressive strength (at normal strength concrete from 75 %). The cracks mainly occur for both types of concretes in the bonding zone between aggregates and cement matrix. Only a short time before failure, more and more increasing cracks in the cement matrix can be observed. This is characteristic for the tertiary creep phase with instable crack growth.

The observation of cracks within the bonding zone between aggregates and matrix seems to stand in contradiction to the fact that especially in high strength concrete this zone has an improved strength. The strength increasing effect becomes dominant with the use of a pozzollanic binding agent such as silica fume. Since in high strength concrete – independent of the storage conditions or other curing methods – shrinkage due to self desiccation takes place and the matrix restrains itself around the not shrinking aggregate grains. Because of that the matrix near the coarse grains is tensioned which can be relaxed by microcracks.

Numerous smallest cracks already exist, as previously mentioned, before a load is applied. Under a high tension load, which does not lead to immediate failure, stress concentrates near the cracks at the crack tips, which can cause crack propagation. In small zones of lower tensile strength caused by inhomogenities of the material, new cracks can be formed as a result of creep procedures of the surrounding matrix. Critical conditions are soon reached due to the high matrix strength. The fast accumulation of microcracks causes a sudden failure. The cracks run around the smaller aggregate grains which means a small change of direction and length of the crack. Coarse grains remain so strongly bonded with the matrix that they crack which is different from normal strength concrete.

6.2.4 Calculation methods

For each specimen there is a load limit, which is much lower than the ultimate short-term load, at whose excess a crack growth begins, which consumes the strength increase caused by hydration. Without any further increase of loading, after a certain time the cracks progressively grow which leads to failure. This means also that lower loads than this load limit can be sustained permanently. Between the load limit and the ultimate short-term load there is the range of long-term tensile strength. A special case of long-term tensile strength is the ultimate long-term tensile strength with a time to failure $t_S \rightarrow \infty$ at which no delayed failure occurs. The critical period however is only the period, during which a high influence of water consumption and transport in the concrete takes place.

6.2.4.1 Empirical approximation method

The calculation formula has to account for the lower limit of the (theoretical) shortest time $t_S = -t_K$ the value $r(-t_K) = \infty$ for the load ratio, since in this case the speed of load application would have to be unrealistically high. For an infinite time to failure the load ratio becomes the ultimate long-term strength: $r\ (t \rightarrow \infty) \rightarrow r_U$. A simple formula, which fulfills these boundary conditions, is [Rinder (2003)]:

$$r(t_S) = r_U + (1 - r_U)\left(\frac{t_K}{t_K + t_S}\right)^n \quad \text{or} \quad t_S(r) = t_K\left(\frac{1 - r_U}{r - r_U}\right)^{\frac{1}{n}} - t_K \tag{6-7}$$

where: r load ratio (loading level) $r = \sigma / f_{ctm}$
r_U load ratio of ultimate long-term tensile strength
t_S time to failure
t_K time to failure in the short-term tensile tests
n parameter to fit the curve to the test results

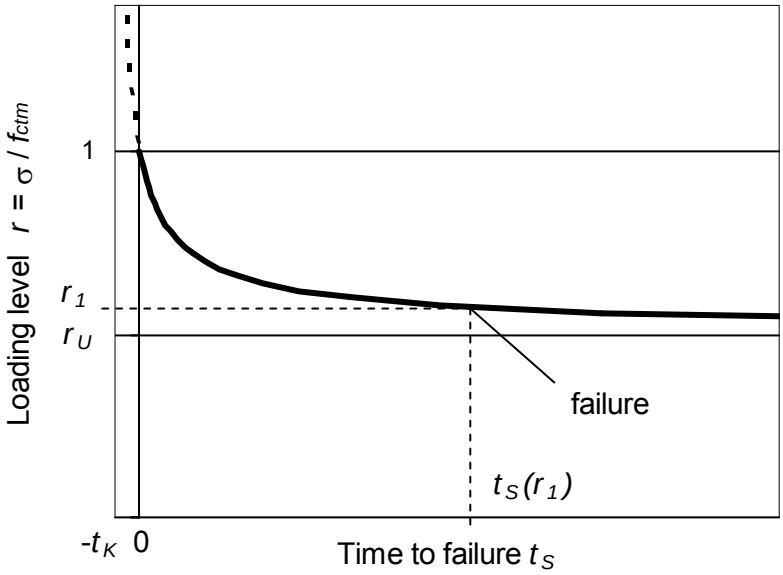

Fig. 6-14: Graphical representation of Eq. 6-7 [Rinder (2003)]

With the empirical method and test results of normal strength and high strength concrete under sustained tensile load, the ultimate long-term tensile load ratio can be shown as a function of the compressive strength (Figure 6-15).

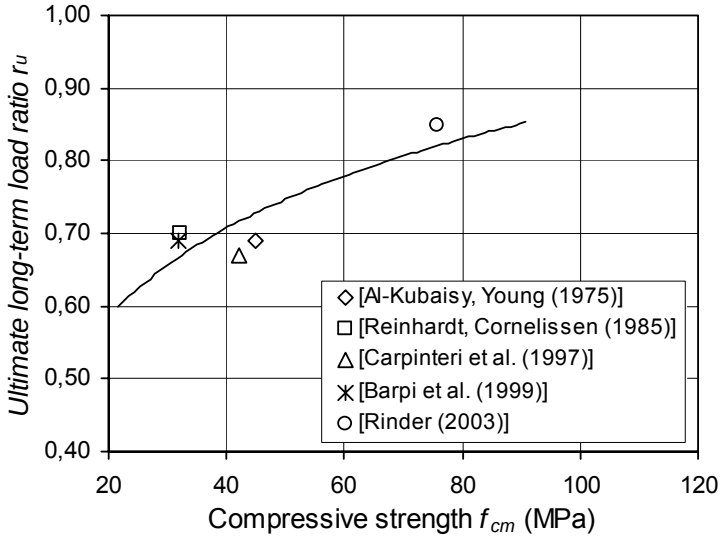

Fig. 6-15: Mean ultimate long-term tensile strength related to the short-term tensile strength as a function of the compressive strength [Rinder (2003)]

6.2.4.2 Energy failure criterion

Based on Griffith's equation

$$\sigma_{ct,cr} = \sqrt{\frac{2E_c \cdot \gamma}{\pi a}} \tag{6-8}$$

where: $\sigma_{ct,cr}$ ultimate tensile stress
E_c Young's modulus
γ specific surface energy; for normal strength concrete $\gamma \approx 0.4$ N/m [Frénaij (1989)]
a half crack length

Wittmann [Wittmann, Zaitsev (1974)] developed an equation for the relationship of long-term to short-term tensile strength, considering the temporal change of the material properties:

$$r(t,t_0) = m(t,t_0) \cdot \frac{f_{ct}(t)}{f_{ct}(t_0)} \sqrt{\frac{E_{ct}(t_0)}{E_{ct}(t)} \cdot \frac{1}{1+\varphi(t,t_0)}} \tag{6-9}$$

where: $m(t,t_0)$ factor for an increase of strength due to preloading; m = 1.00 – 1.35. Here m = 1.00
$f_{ct}(t)$ tensile strength at time t
$f_{ct}(t_0)$ tensile strength at time of load t_0
$E_{ct}(t_0)$ Young's modulus at time of load t_0
$E_{ct}(t)$ Young's modulus at time t
$\varphi(t,t_0)$ Creep coefficient

If the development of strength and Young's modulus and the creep behaviour of a concrete specimen are known, the related times to failure can be determined. Absolute material properties enter only indirectly into the equation.

From this energetic consideration it follows that due to the interaction of creep and strength development, the ultimate long-term strength comes to a minimum after approximately 30 days. If this critical phase is overcome without failure, the strength development exceeds the deterioration caused by load. This means for a structural element of high strength concrete under high constant sustained load that it will fail either within a few weeks or not at all.

6.2.4.3 Crack propagation and damage accumulation

According to the failure criterion of the K-concept of linear elastic fracture mechanics, a material fails, when the stress intensity factor K in the environment of the crack tip of the decisive crack reaches the critical value K_c. This characteristic material property can experimentally be determined. In short-term tests with a monotonic growing load, K_c is usually reached without a substantial elongation of cracks [Franke (1984)]. But under a constant sustained load, not too much below the short-term failure load, crack lengths are growing at an increasing rate. After a certain time the critical stress intensity is reached by the progressive deterioration of the remaining cross section and failure occurs. The crack

propagation rate *da/dt* is described by Paris' equation which was originally developed for fatigue:

$$\frac{da}{dt} = A \cdot K_I(t)^n \tag{6-10}$$

where: A, n factors which depend on the material properties and the load ratio r
K_I stress intensity factor of the decisive defect for crack opening mode I

When the *K*-concept applies:

$$K_I(t) = \sigma_{ct} \cdot y\sqrt{\pi \cdot a(t)} \quad \text{or} \quad K_{Ic} = f_{ct} \cdot y\sqrt{\pi \cdot a_0} \tag{6-11}$$

where: σ_{ct} tensile stress
y factor which depend on the geometry of the specimen and the crack
$a(t)$, a_0 effective crack lengths
f_{ct} tensile strength

This formula, which is valid for the case that the zones of nonlinear material behaviour at the crack tips are small in relation to the crack lengths and the specimen size, can be used for cement-based materials [Alonso Junghanns (1998)]. Using the above equations, after solving the differential equation, to formulate

$$\left(\frac{a_0}{a(t)}\right)^{0,5} \cdot r = \frac{K_I(t)}{K_{Ic}} \tag{6-12}$$

for the time to failure ([Franke (1984)]) it follows:

$$t_S(r) = \frac{1}{B_1 \cdot r^n}\left(1 - r^{n-2}\right) \tag{6-13}$$

where: K_{Ic} fracture toughness $K_{Ic} = K_I(t_S)$
B_1 characteristic value of the material/construction element

The material property B_1 can be determined from long-term tests. For high strength concrete the coefficients become B_1 = 0.01/s and n = 75 [Rinder (2003)]. The different approximation methods are plotted in Figure 6-16.

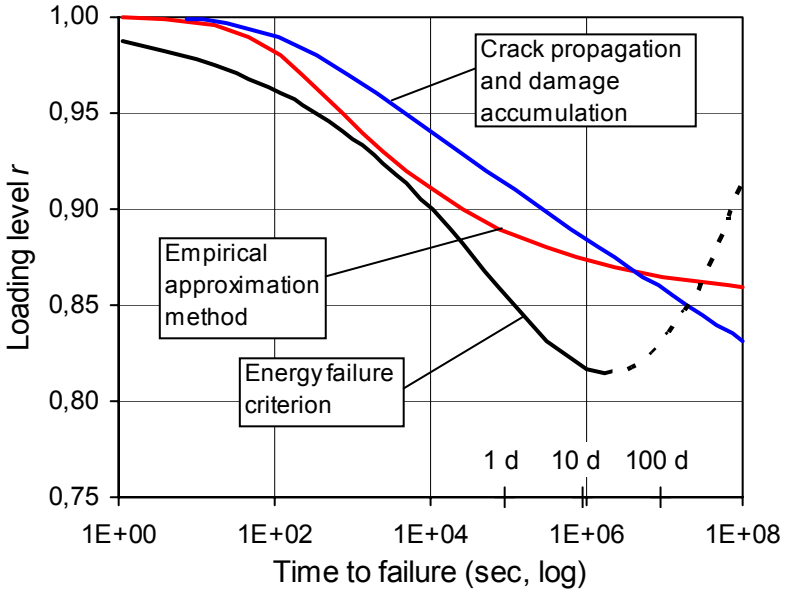

Fig. 6-16: Comparison of the different approximation methods to calculate the time to failure applied to test results [Rinder (2003)]

The approximation methods do not show realistically the so often very small difference between the loads, which lead either to very early failure or to an infinitely long time to failure. A load does not lead to failure if the tensile strength development exceeds the degradation of the specimen at each time. At a slightly higher load however, delayed failure conditions can be approached, since the loss of strength due to load and the loss of strength due to shrinkage are added (Figure 6-17). This loss of strength due to shrinkage (intrinsic damage) depends on the size of the coarse aggregates, the water cement ratio, and the characteristics of the cement silica fume mixture.

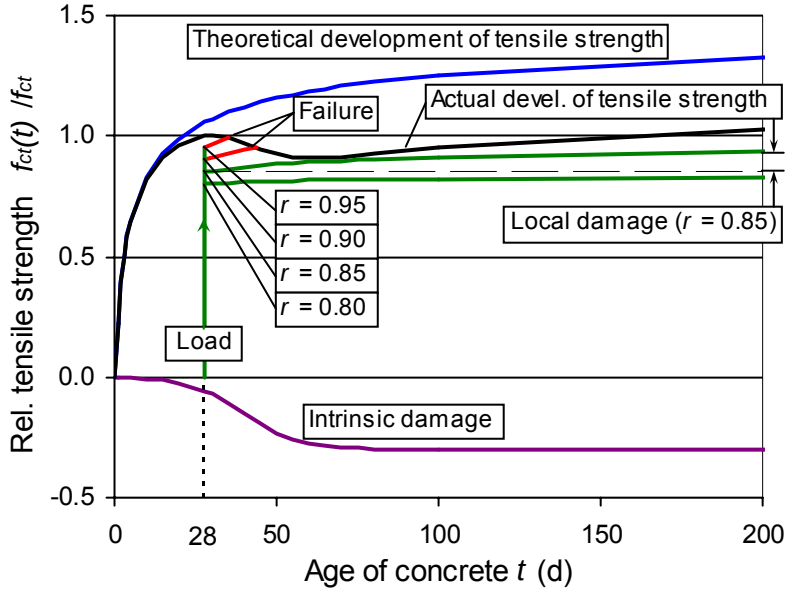

Fig. 6-17: Exemplary schematic representation of the development of tensile strength, the damage process, and the loading [Rinder (2003)]

An uncertainty whether the ultimate long-term tensile strength of high strength concrete is lower due to its high brittleness, than expected after the measurements on normal strength concrete, does exist [Rinder (2003)]. The relation between short-term and ultimate long-term strength is represented in Table 6-3.

	NSC	HSC
f_{cm} (MPa)	40	80
Compression	65 %	80 %[1)]
Tension	60 %	75 %[1)]

[1)] acc. to [Han, Walraven (1993)]

Table 6-3: Mean values of ultimate long-term tensile strength of normal strength and high strength normal concrete

The ultimate long-term tensile strength for specimens wrapped in foil can be as high as 85 % of the average [Rinder (2003)]. That means that in some cases, e.g. large structural elements, a higher ultimate long-term tensile strength than given in Table 6-2 can be assumed.

6.3 Development of the modulus of elasticity with time

At the early concrete age the modulus of elasticity develops more rapidly than the compressive strength, because $E_c(t)$ is to a large extent controlled by the modulus of elasticity of the aggregates which is independent of concrete age. In CEB-FIP Model Code 1990 this is taken into account introducing by Eqs. (6-14) and (6-15) which posses an additional exponent 0.5 in comparison with Eqs. (6-2).

$$E_{ci}(t) = \beta_E(t) \cdot E_{ci} \tag{6-14}$$

with

$$\beta_E = [\beta_{cc}(t)]^{0.5} \tag{6-15}$$

where:

$E_{ci}(t)$	tangent modulus of elasticity of concrete [MPa] at an age t [days]
E_{ci}	tangent modulus of elasticity of concrete [MPa] at an age of 28 days acc. to Eq. (4-1)
$\beta_E(t)$	function to describe the development of modulus of elasticity with time
$\beta_{cc}(t)$	coefficient acc. to Eq. (6-2)
t	concrete age [days].

The British code (BS 8110) provides the following formula for ages of concrete t > 3 days:

$$E_{c,t} = E_{co,28}\left(0.4 + 0.6 \cdot \frac{f_{cm,t}}{f_{cm,28}}\right) \tag{6-16}$$

Figure 6-18 shows the experimental data representing the development of the relative modulus of elasticity of high strength concrete with time. The modulus of elasticity at an age

of 28 days was considered as reference. In order to describe this process besides Eqs. (6-15) and (6-16), a modification of Eq. (6-15) was applied by introducing an additional variable b instead of the exponent 0.5 for the calculation of the term $\beta_{cc}(t)$ according to Eq. (6-2), see Figure 6-18. All three formulas seem to be suitable to describe with sufficient accuracy the tendencies observed experimentally. However, the well established and physically sound Eq. (6-4) should be preferred. The parameter s in the term $\beta_{cc}(t)$ according to Eq. (6-2) was found to be equal to 0.199. This value is practically identical to the value s proposed in CEB-FIP Model Code 1990 for rapid hardening high strength cements (s = 0.2) or to the average of all values s obtained for the compressive strength of high strength concrete without admixtures (see section 6.1).

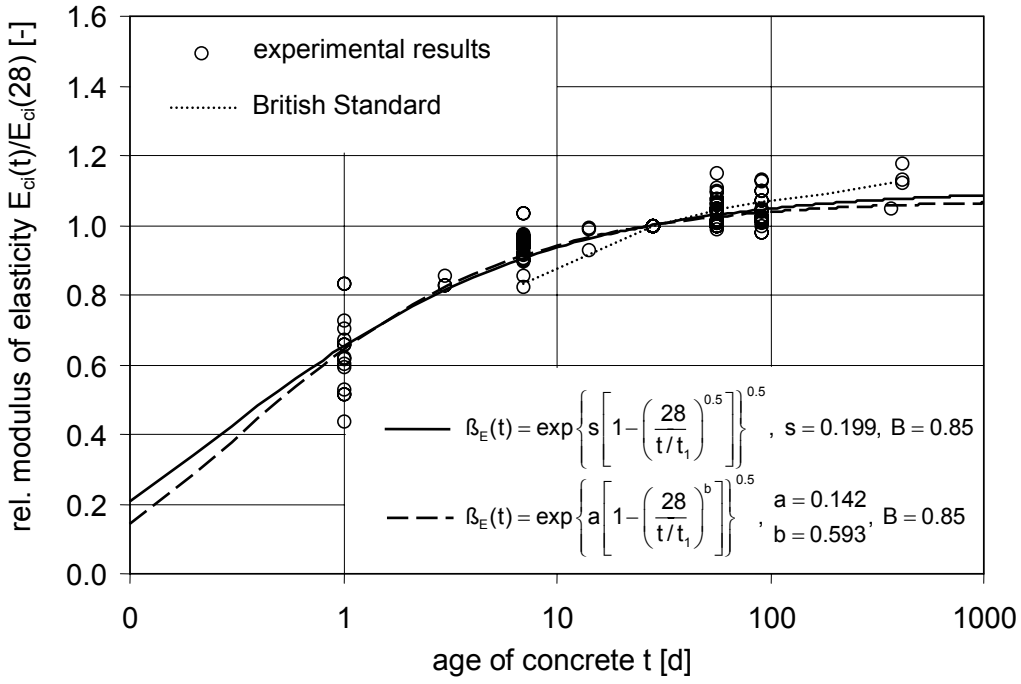

Fig. 6-18: Development of the modulus of elasticity with time

6.4 Creep and shrinkage

6.4.1 Introduction

Practical prediction models for creep and shrinkage of normal strength concrete have been available since various decades. Some of the most widely used actual models were issued by the Committee Euro-International of Concrete [CEB No. 213/214 (1993)]. They cover the time dependent behaviour of ordinary normal strength structural concrete. For high-performance concrete (compressive strength f_{cm} > 60 MPa), which is increasingly used in practice, some particular prediction models have been developed recently, see e.g. [Müller, Küttner (1996), Le Roy, De Larrard, Pons (1996), Han, Walraven (1996)]. One of the deficiencies of these models is that they cover only the behaviour of high-performance concrete and no continuity in combination to the deformation prediction of the models for ordinary concrete is obtained. However, as the fundamental characteristics in the deformation behaviour of normal strength and high-performance concrete are very similar, preference should be given to the development of those approaches which allow for predictions, both for

normal and for high-performance concrete. Such new models for shrinkage and creep will be presented in this chapter.

Based on test data included in the RILEM Data Bank [RILEM TC 107 (1998)], the relevant characteristics of the creep and shrinkage of high-performance concrete are reviewed in comparison to the behaviour of normal strength concrete with respect to the constitutive modelling of the time-dependent material properties. It will be demonstrated that prediction models for normal strength concrete cannot simply be applied and extended to predict the creep and shrinkage of high-performance concrete. However, it will be pointed out that well-established principles and concepts in modelling creep and shrinkage may be kept, and consequently a unified approach to model creep and shrinkage of normal strength and high-performance concrete may be derived on the basis of the relations given in the CEB-FIP Model Code 1990 [CEB No. 213/214 (1993)].

6.4.2 Definitions and general considerations

If thermal strains are neglected, the total strain of concrete $\varepsilon_c(t,t_0)$ occurring at time t in a concrete member exposed to a certain ambient climate and subjected to a sustained uniaxial stress at time t_0 may be expressed by Eq. (6-17):

$$\varepsilon_c(t,t_0,t_s) = \varepsilon_{ci}(t_0) + \varepsilon_{cc}(t,t_0) + \varepsilon_{cs}(t,t_s) \tag{6-17}$$

where $\varepsilon_c(t,t_0,t_s)$ = total strain of concrete;
$\varepsilon_{ci}(t_0)$ = initial strain of concrete at time of stress application t_0;
$\varepsilon_{cc}(t,t_0)$ = creep strain of concrete at a concrete age $t \geq t_0$;
$\varepsilon_{cs}(t,t_s)$ = shrinkage at a concrete age t;
t = time considered or age of concrete, respectively;
t_s = concrete age at the beginning of drying;
t_0 = age of concrete at loading.

The definitions for the individual strain components given above are in accordance with those given in the CEB-FIP Model Code 1990 [CEB No. 213/214 (1993)]. Figure 6-19 indicates graphically the individual strain components. Corresponding equations to predict the individual strain components will be given in sections 6.4.3.2 and 6.4.4.2.

The shrinkage and creep behaviour of concrete is affected both by external factors such as the ambient climate, the size of member and also the age of loading for creep, and by internal factors such as the material properties of the phases of concrete and its composition. Details may be found in [CEB No. 213/214 (1993)]. Some further information are also given in sections 6.4.3.1 and 6.4.4.2, respectively.

Considering the internal factors, the microstructure of the hardened cement paste matrix has a significant effect on the shrinkage and creep characteristics. Hence, microstructural changes which are associated with the transition from normal strength to high-performance concrete result in pronounced changes of the shrinkage and creep characteristics. High-performance concrete (HPC) shows above all a much lower porosity, a more uniform hardened cement paste matrix and a different and denser structure of the aggregate paste interface zone than normal strength concrete (NSC) [Müller, Rübner (1995)]. Primarily due to the low porosity of the hardened cement paste matrix of high-performance concrete, which is associated with a high stiffness, the magnitude of the shrinkage and the creep deformation is reduced in comparison with normal strength concrete. In particular, those shrinkage and creep characteristics which may be linked to diffusion-type processes are markedly different for high-performance concrete.

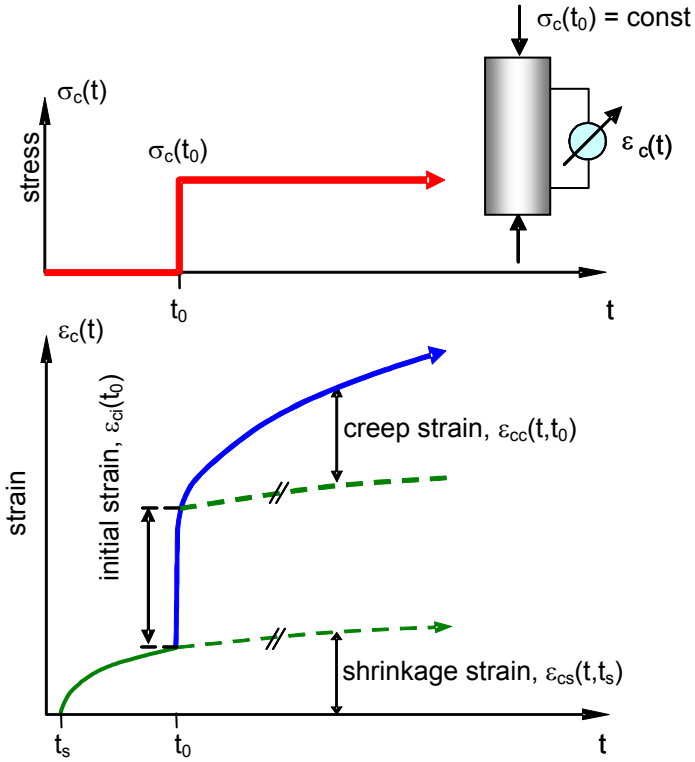

Fig. 6-19: Individual strain components of creep and shrinkage

A decisive question in modeling creep and shrinkage concerns the choice of input parameters, i.e. the type and number of parameters affecting creep and shrinkage. The input parameters of the new prediction models are identical to those of [CEB No. 213/214 (1993)]. There, the compressive strength of concrete at the age of 28 days is used as the only input material parameter which, as a substitute, takes into consideration the effect of the composition of the concrete. Using this concept, parameters such as the water-cement ratio, the aggregate content and the type and amount of additions such as silica fume or fly ash, which are often used for high-performance concrete, are not taken into consideration. The reason is that in most practical situations the engineer only knows the strength at the stage of design but has no information on the mentioned parameters. Nevertheless taking into account only the compressive strength represents a rather crude approach; for high-performance concrete the consideration of the silica fume content as an additional parameter might improve the prediction accuracy. However, in view of the scattering of the data and the lack of systematic investigations, respectively, and considering the general uncertainty associated with the prediction of concrete deformations, such a simplified approach is reasonable and justified, at least for simple code-type prediction models [CEB No. 199 (1990)].

The models for shrinkage and creep presented here are intended to predict the time-dependent mean cross-section behaviour of a concrete member taking into account the average relative humidity and member size. Such types of models imply some strong simplifications and suffer from a number of basic weaknesses [CEB No. 199 (1990)]. However, they are sufficiently accurate and comply with the practical needs in most cases. Nevertheless in very few cases a more accurate point by point analysis of the cross-section e.g. on the basis of a finite element approach, where local stresses and moisture states as well as local cracking are taken into account, has to be carried out. Related material laws may be derived to some extend by means of the models presented below.

6.4.3 Shrinkage

6.4.3.1 Constitutive characteristics of shrinkage

Total shrinkage of concrete may be subdivided into the components

- capillary or plastic shrinkage, occurring in fresh concrete due to an early loss of water;
- chemical shrinkage, caused by the chemical reaction of cement and water;
- autogenous shrinkage, which is mostly understood as the sum of the components chemical shrinkage (see above) and self-desiccation shrinkage resulting from the internal drying due to the hydration process;
- drying shrinkage, caused by the water loss of hardened concrete in a dry environment;
- carbonation shrinkage, which is due to the carbonation of the surface zone of concrete.

Capillary shrinkage may be simply avoided, while the other components of total shrinkage occur under usual ambient conditions to which concrete members are exposed. However, carbonation shrinkage contributes only minor to the total shrinkage and may be neglected. Also chemical shrinkage must not be considered in practice, as it may not be separated from autogenous shrinkage, i.e. the observed autogenous shrinkage of a sealed non-drying specimen includes always a certain amount of chemical shrinkage [Neville (2000)].

While autogenous shrinkage is small for ordinary concretes, it increases significantly for high-performance concrete. Consequently, this component of shrinkage, which occurs irrespective of the ambient climate conditions, has to be considered adequately in a corresponding prediction model. Figure 6-20 indicates schematically the time-development of autogenous and drying shrinkage in normal strength and high-performance concrete.

From Figure 6-20 and further experimental results included in [RILEM TC 107 (1998)] (see Table 1) the following main characteristics for the shrinkage of high-performance concrete in comparison with ordinary concrete may be observed:

- The total shrinkage, i.e. the sum of autogenous shrinkage and drying shrinkage is lower for HPC than for NSC.
- The drying shrinkage component is substantially reduced for HPC, while the autogenous shrinkage component is significantly increased.
- The shape of the time-development function of the total shrinkage for HPC is similar to that of NSC. The autogenous shrinkage component, being independent of external parameters, develops more rapidly with time than the drying shrinkage component which is pronouncedly affected by external parameters such as the ambient humidity and member size.
- The effect of parameters such as e.g. the age at beginning of drying and the type of cement on the development of shrinkage is different for HPC in comparison with NSC.

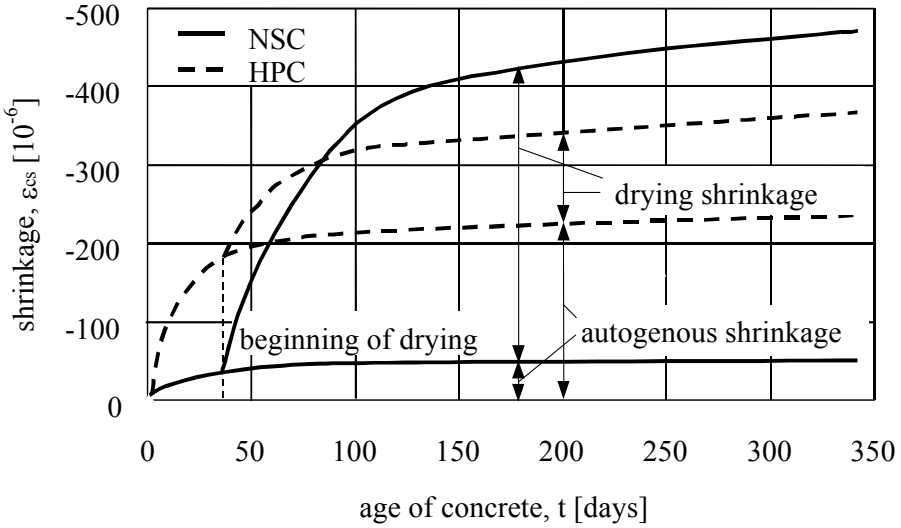

Fig. 6-20: Time-development of autogenous and drying shrinkage in normal strength and high-performance concrete

Experimental investigations give a clear evidence that the autogenous shrinkage component increases with decreasing water-cement ratio, i.e. increasing strength of concrete [Le Roy, De Larrard (1993), Persson (1998)]. This is mainly due to the well-known effect of self-desiccation which leads to an internal relative humidity in a concrete member significantly below 1.0, depending on the water-cement ratio. Consequently, for a high-strength concrete (e.g. $f_{cm} > 100$ MPa) no shrinkage but a swelling effect may occur, if the ambient relative humidity is comparatively high (e.g. RH > 0.90).

An important aspect related to the magnitude and time-development of shrinkage concerns the effect of mineral additions such as e.g. silica fume and fly ash. From various papers [Tazawa (1998)] it is evident that the addition of silica fume increases the autogenous shrinkage component, whereas the addition of fly ash obviously reduces load-independent strains for comparable concretes.

6.4.3.2 Shrinkage prediction formulas

With respect to the findings for high-performance concrete (see section 3.1) the new approach for shrinkage subdivides the total shrinkage into the components autogenous shrinkage and drying shrinkage. While the model for the drying shrinkage component is closely related to the approach given in [CEB No. 213/214 (1993)], for the autogenous shrinkage new relations had to be derived. However, some adjustments have also to be carried out for the drying shrinkage component as the new model should cover both, the shrinkage of normal and high-performance concrete, and consequently the autogenous shrinkage has also to be modelled for normal strength concrete.

The following formulas have been numerically optimized using the data sets on shrinkage included in the RILEM Data Bank (see Table 6-4).

type of deformation	number of references	number of tests	range of f_{cm} [MPa]	max silica fume content [%] *)
autogenous shrinkage	4	33	60 .. 105	8.7
drying shrinkage	11	45	17 .. 111	17.6
*) percentage of the cement content				

Table 6-4: Shrinkage data on high-performance concrete included in [RILEM TC 107 (1998)]

The total shrinkage of concrete $\varepsilon_{cs}(t)$ may be calculated from Eq. (6-18):

$$\varepsilon_{cs}(t,t_s) = \varepsilon_{cas}(t) + \varepsilon_{cds}(t,t_s) \tag{6-18}$$

with

$$\varepsilon_{cas}(t) = \varepsilon_{cas0}(f_{cm}) \cdot \beta_{as}(t) \tag{6-19}$$

and

$$\varepsilon_{cds}(t,t_s) = \varepsilon_{cdso}(f_{cm}) \cdot \beta_{RH}(RH) \cdot \beta_{ds}(t-t_s) \tag{6-20}$$

where
- $\varepsilon_{cs}(t,t_s)$ = total shrinkage at time t;
- $\varepsilon_{cas}(t)$ = autogenous shrinkage at time t;
- $\varepsilon_{cds}(t,t_s)$ = drying shrinkage at time t;
- $\varepsilon_{caso}(f_{cm})$ = notional autogenous shrinkage coefficient from Eq. (6-21);
- $\varepsilon_{cdso}(f_{cm})$ = notional drying shrinkage coefficient from Eq. (6-23);
- $\beta_{as}(t)$ = function to describe the time-development of autogenous shrinkage, from Eq. (6-22);
- $\beta_{RH}(RH)$ = coefficient to take into account the effect of rel. humidity on drying shrinkage, from Eq. (6-24);
- $\beta_{ds}(t-t_s)$ = function to describe the time-development of drying shrinkage, from Eq. (6-25);
- t = concrete age [days];
- t_s = concrete age at the beginning of drying [days];
- $t-t_s$ = duration of drying [days].

The autogenous shrinkage component $\varepsilon_{cas}(t)$ according to Eq. (6-19) may be estimated by means of Eqs. (6-21) and (6-22):

$$\varepsilon_{cas0}(f_{cm}) = -\alpha_{as}\left(\frac{f_{cm}/f_{cm0}}{6 + f_{cm}/f_{cm0}}\right)^{2.5} \cdot 10^{-6} \tag{6-21}$$

and

$$\beta_{as}(t) = 1 - \exp\left(-0.2 \cdot \left(\frac{t}{t_1}\right)^{0.5}\right) \tag{6-22}$$

where f_{cm} = mean compressive strength of concrete at an age of 28 days [MPa];
f_{cm0} = 10 MPa;
t_1 = 1 day;
α_{as} = coefficient which depends on the type of cement, see table 6-5.

The autogenous shrinkage component is independent of the ambient humidity and of the member size and develops more rapidly than the drying shrinkage.

For drying shrinkage $\varepsilon_{cds}(t,t_s)$ according to Eq. (6-20), the subsequent Eqs. (6-23) .. (6-26) may be applied:

$$\varepsilon_{cds0}(f_{cm}) = \left[(220 + 110 \cdot \alpha_{ds1}) \cdot \exp(-\alpha_{ds2} \cdot f_{cm} / f_{cm0}) \right] \cdot 10^{-6} \tag{6-23}$$

$$\beta_{RH} = \begin{cases} -1.55 \cdot \left[1 - \left(\frac{RH}{RH_0} \right)^3 \right] & for\ 40 \le RH < 99\ \% \cdot \beta_{s1} \\ 0.25 & for\ RH \ge 99\ \% \cdot \beta_{s1} \end{cases} \tag{6-24}$$

$$\beta_{ds}(t - t_s) = \left(\frac{(t - t_s)/t_1}{350 \cdot (h/h_0)^2 + (t - t_s)/t_1} \right)^{0.5} \tag{6-25}$$

$$\beta_{s1} = \left(\frac{3.5 f_{cm0}}{f_{cm}} \right)^{0.1} \le 1.0 \tag{6-26}$$

where α_{ds1}, = coefficient which depends on the type of cement, see table 6-5;
α_{ds2} = coefficient which depends on the type of cement, see table 6-5;
β_{s1} = coefficient to take into account the self-desiccation in high-performance concrete;
RH = ambient relative humidity [%];
RH_0 = 100 %;
h = $2A_c/u$ = notional size of member [mm], where A_c is the cross-section [mm^2] and u is the perimeter of the member in contact with the atmosphere [mm];
h_0 = 100 mm;
f_{cm0} = 10 MPa.

According to Eq. (6-24) for normal strength concretes swelling is to be expected if the concrete is exposed to ambient relative humidity near 99 %. For higher strength grades swelling will occur already at lower relative humidities because of the preceding reduction of the internal relative humidity due to self-desiccation of the concrete (see section 6.4.3.1).

type of cement according to EC 2	α_{as}	α_{ds1}	α_{ds2}
SL	800	3	0.13
N, R	700	4	0.12
RS	600	6	0.12

Table 6-5: Coefficient according to Eq. (6-21) and Eq. (6-23)

The model for shrinkage presented above is intended to predict the time-dependent mean cross-section behaviour of a concrete member moist cured at normal temperatures not longer than 14 days and exposed to a mean ambient relative humidity in the range of 40 to 100 % at mean ambient temperatures from 10 °C to 30 °C. It is valid for normal-weight plain structural concrete having an average compressive strength in the range of $15 \leq f_{cm} \leq 120$ MPa.

6.4.3.3 Accuracy of shrinkage prediction

The new model for shrinkage of normal strength and high-performance concrete has been verified in detail on the basis of experimental data included in the available data base [RILEM TC 107 (1998)].

The accuracy of the new prediction model is graphically illustrated in Figure 6-21. It is obvious from this figure that the prediction model agrees reasonably well with experimental data. However, such a comparison of predicted and measured time-dependent strains is somewhat arbitrary due to the selection of the data sets. An unbiased overall accuracy of a prediction model may be estimated by means of the coefficient of variation which can be determined according to a procedure being well documented in the literature [CEB No. 199 (1990)].

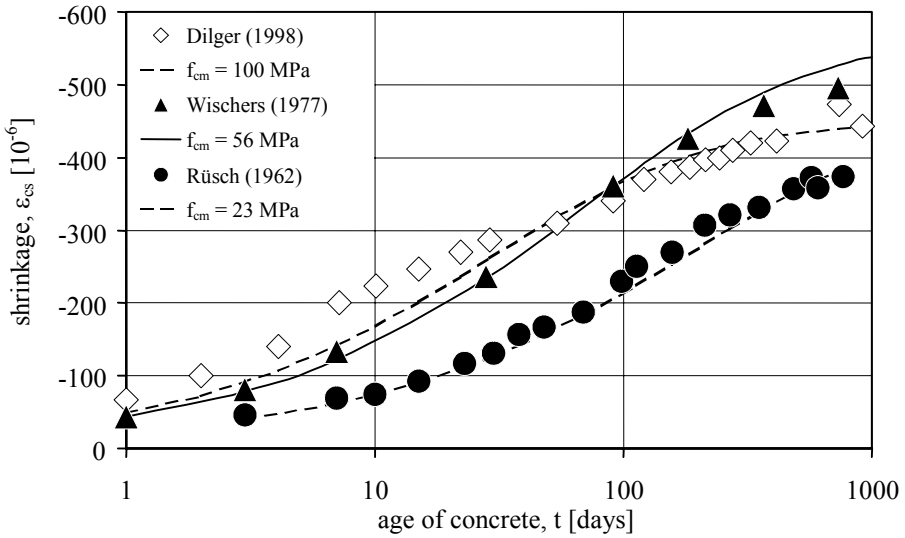

Fig. 6-21: Predicted and observed shrinkage strains

Table 6-6 gives coefficients of variation for the shrinkage strain, for both normal and high-performance concrete. The obtained values indicate that the prediction model is in a reasonably good agreement with measured strain data. Note that the somewhat higher value of V for autogenous shrinkage of HPC is due to the large intrinsic scatter of the respective data sets. If only shrinkage of HPC measured on unsealed specimens is considered a coefficient of variation of V = 33.3 % is obtained.

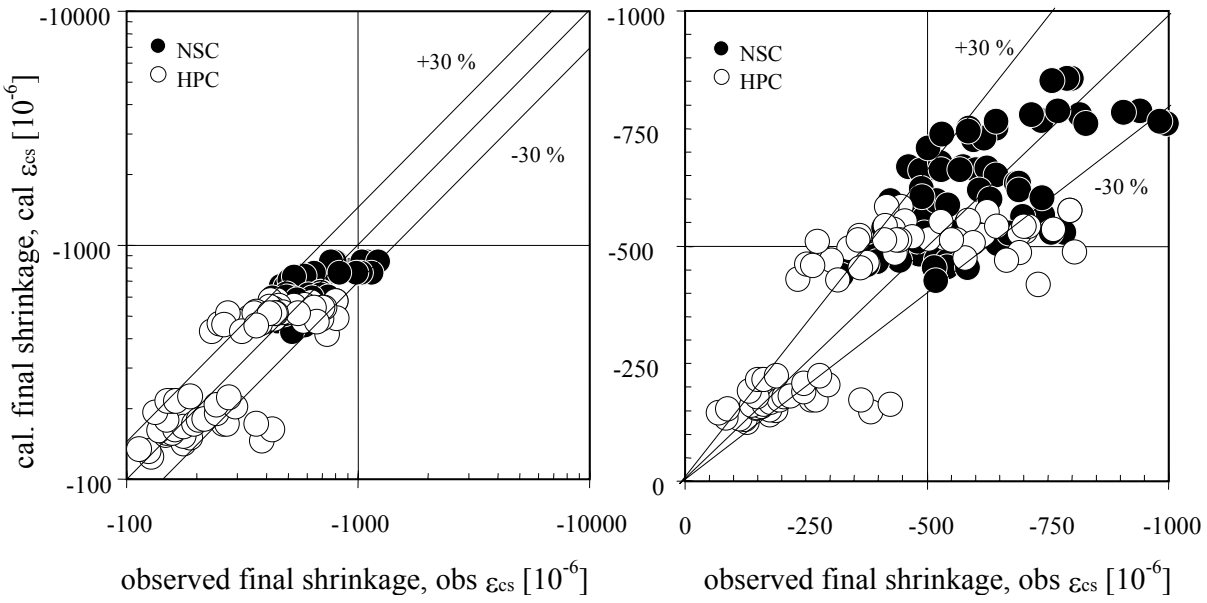

Fig. 6-22: Predicted and observed final shrinkage strains; left: logarithmic scale; right: linear scale

In various practical cases, only the final value of the time-dependent strains, i.e. the final shrinkage is of relevance. Figure 6-22 indicates graphically the accuracy of the new models for the prediction of final deformation values of normal strength and high-performance concrete. It may be seen that in most cases the prediction error is lower than 30 %. The mean prediction error for final shrinkage values, determined according to a procedure given in [CEB No. 199 (1990)], is F = 22.0 %.

type of deformation	type of concrete	number of experiments	V [%]	
shrinkage	HPC sealed	24	43.3	32.4
	HPC unsealed	41	33.3	
	NSC	103	29.0	

Table 6-6: Coefficients of variation for the prediction of shrinkage of concrete

Note that for the prediction model of CEB Model Code 1990, which is only valid for normal strength concrete, a coefficient of Variation of V = 32.9 % was obtained. The mean prediction error of the CEB model was found to be F = 19 %. Hence, it is obvious, that the new shrinkage model results in rather the same prediction accuracy than the corresponding model of CEB which, however, is only applicable for normal strength concrete.

6.4.3.4 Improvement of shrinkage prediction

The prediction of the notional autogenous shrinkage coefficient (Eq. (6-21)) may be improved, if more detailed information on the type of cement beyond the characteristics considered here would be taken into account. Recent experimental studies showed e.g. that the presence of ground blast furnace slag in the cement will increase the autogenous shrinkage considerably [Tazawa (1998)]. As for the time-development function of autogenous

shrinkage (Eq. (6-22)) no significant improvement of the overall prediction accuracy is obtained, if the compressive strength would be introduced as an affecting parameter.

The same aspects as for autogenous shrinkage hold also true for modelling the notional coefficient and the time-development of the drying shrinkage component. Some further improvements of the model might be obtained, if the parameter beginning of drying is introduced in the formulae. This holds true both for normal and high-performance concrete. However, within typical durations of moist curing in practice, no significant effect of this parameter on the magnitude of shrinkage may be observed. The chosen approach regarding the effect of self-desiccation (Eqs. (6-24) and (6-26)) is still very crude and may be refined considering new systematic investigations on structural concretes being under way [Müller, Kvitsel (2001)].

A general problem in finding an optimized prediction accuracy for shrinkage results from an observed characteristic difference in the magnitude of shrinkage depending where the experimental investigation has been carried out. It is clearly evident from the shrinkage data included in the data bank that the concretes investigated in the United States give always a higher shrinkage than comparable concretes of European investigations. This might be traced back e.g. to differences in the types of cements or to some typical differences related to the composition of the concretes. In this context it should be noted, that the given prediction model for shrinkage is unbiased, i.e. the model has been optimized using all data sets included in the data bank.

The prediction accuracy of the model can be improved without modifying the given approaches, if the parameter compressive strength of concrete is replaced by parameters giving the composition of concrete such as the water-cement ratio, the cement content, the content and the type of additions and admixtures etc. Here these parameters have not been introduced for reasons mentioned in section 6.4.2.

The most significant improvement of the shrinkage prediction may be obtained if some short time shrinkage tests on the particular concrete are carried out. By that way, the notional coefficients of autogenous and drying shrinkage, which are the most uncertain parameters of the model, may be determined from the experiment.

6.4.4 Creep

6.4.4.1 Constitutive characteristics and concepts

For practical applications concrete may be considered as an aging linear viscoelastic material. This assumption implies the applicability of the principle of superposition, and the related constitutive behaviour may be expressed as:

$$\varepsilon_\sigma(t,t_0) = J(t,t_0) \cdot \sigma(t_0) + \int_{t_0}^{t} J(t,\tau) \cdot \frac{\partial\sigma(\tau)}{\partial\tau} \cdot d\tau \qquad (6\text{-}27)$$

In Eq. (6-27), $\varepsilon_\sigma(t,t_0)$ is the stress-dependent strain at time t caused by a stress history $\sigma(t)$, which starts at time $t = t_0$. The creep function, or creep compliance, $J(t,t_0)$ represents the total stress-dependent strain by unit stress and may be given by:

$$J(t,t_0) = \frac{1}{E_c(t_0)} + \frac{\varphi(t,t_0)}{E_c} = \frac{1}{E_c}\left[n(t_0) + \varphi(t,t_0)\right] \qquad (6\text{-}28)$$

In Eq. (6-28), $n(t_0) = E_c/E_c(t_0)$, where $E_c(t_0)$ is the modulus of elasticity at the time t_0. Note that $E_c(t_0) = \sigma_c(t_0)/\varepsilon_{ci}(t_0)$, where $\varepsilon_{ci}(t_0)$ is the initial strain at loading (see Eq. (6-17)). The creep coefficient $\varphi(t,t_0)$ gives the ratio of creep strain to elastic strain at the age of 28 days. Hence the creep strain $\varepsilon_{cc}(t,t_0)$ of concrete may be written as:

$$\varepsilon_{cc}(t,t_0) = \varphi(t,t_0) \cdot \frac{\sigma_c(t_0)}{E_c} \tag{6-29}$$

In Eq. (6-29), $\sigma_c(t_0)$ is a constant stress applied at time of loading and E_c is the modulus of elasticity at a concrete age of 28 days.

The creep function, as given in Eq. (6-28), may also be defined different. Consequently attention has to be paid to the definition of the individual strain components: initial elastic strain and creep strain. By using the strain definitions given above, which are identical to the strain definitions in [CEB No. 213/214 (1993)], the individual strain components, given in Eqs. (6-28) and (6-29) are compatible with each other.

It should be noted, that the creep behaviour of concrete, i.e. the creep function $J(t,t_0)$ or the creep coefficient $\varphi(t,t_0)$, respectively, may be modeled by different constitutive approaches. Among them the product-type and the summation type models, which both may include a distinction between the basic creep component and the drying creep component. The most common formulations are given in [CEB No. 199 (1990)]. Depending on the approach and types of aging function and time development function being included in $\varphi(t,t_0)$, different prediction accuracies for creep under constant and in particular under variable stresses are obtained.

If the history of the strain $\varepsilon_\sigma(t,t_0)$ is prescribed (as e.g. in the determination of the stress relaxation function $R(t,t_0)$ under constant unit imposed strain), the constitutive law (6-27) becomes an integral equation which, for realistic forms of the compliance $J(t,t_0)$, requires to be numerically solved [Bažant (1972a), Sassone and Chiorino (2005)]. The same need is experienced in the calculation of creep structural effects [CEB No. 142/142bis (1984), 213/214 (1993), Chiorino (2005), ACI (2007)]. In fact, combining the usual approaches of structural mechanics with Eq. (6-27), and taking into account possible non homogeneities in the creep properties of the different parts of the structure, a system of integral equations of the type of Eq. (6-27) is generally obtained [Mola and Pisani (1993)]. The solution can be facilitated by the transformation of Eq. (6-27) in a differential equation, which requires, however, the adoption of less accurate simplified analytical expressions for the creep function $J(t,t_0)$. In most practical cases sufficient reliable results may be obtained writing Eq. (6-27) in the form of an algebraic incremental elastic law [Bažant (1972b)]:

$$\varepsilon_\sigma(t) - \varepsilon_\sigma(t_0) = \frac{\sigma(t) - \sigma(t_0)}{E_{c,adj}(t,t_0)} + \varepsilon_\sigma(t_0)\varphi(t,t_0) \tag{6-30a}$$

where ε_σ is the stress dependent concrete strain, and having introduced the age-adjusted effective modulus $E_{c,adj}(t,t_0)$ defined as:

$$E_{c,adj}(t,t_0) = \frac{E_c}{n(t_0) + \chi(t,t_0)\varphi(t,t_0)} = \frac{E_c(t_0)}{1 + \chi(t,t_0)\varphi(t,t_0)/n(t_0)} \tag{6-30b}$$

The aging coefficient $\chi(t,t_0)$ – often also termed as relaxation coefficient $\rho(t,t_0)$, in particular for $n(t_0) = 1{,}0$ – is related to the compliance $J(t,t_0)$ and the relaxation $R(t,t_0)$. Information on its magnitude is given in [CEB No. 215 (1993), www.polito.it/creepanalysis/]. In many cases

sufficient accurate results at long term may be obtained when the aging coefficient is assumed to be constant, with typical magnitudes $\chi \cong 0.7 \div 0.9$.

Based on the equations given above, any creep and relaxation problems may be solved if the material parameters E_c, $n(t_0)$ and $\varphi(t,t_0)$ are known or predicted, respectively. Hence, suitable formulas to determine these parameters have to be developed (see section 6.4.4.3).

6.4.4.2 Deformation characteristics and affecting parameters

From many creep tests on structural concrete a rather comprehensive insight in the affecting parameters is available. Summing up, creep at constant ambient temperatures increases

- with increasing stress and duration of loading;
- with increasing cement content, i.e. cement paste volume of the concrete and decreasing stiffness of the aggregates;
- with increasing porosity of the hardened cement paste, i.e. with increasing water-cement-ratio and decreasing degree of hydration (decreasing age at loading);
- with increasing water content of the concrete and increasing rate of water loss during loading (decreasing member size and ambient humidity).

As far as the effect of creep inducing stress is concerned, creep strain increases linearly proportional to the stress up to a limit of a stress/strength ratio of 0.45 at the time of loading. The ambient temperature exerts a rather complex effect on creep which cannot be dealt with here.

The creep characteristics of high-performance concrete have been shown and discussed in [Müller, Küttner (1996)]. The main differences between the creep behaviour of high-performance concrete and normal strength concrete may be summarized as follows:

1. The magnitude of the total creep strains, i.e. the sum of the basic creep component and the drying creep component, is considerably lower for high-performance concrete.
2. While the drying creep component is substantially lower for high-performance concrete, the magnitude of the basic creep component is reduced to a smaller extent. The ratio of the drying creep component to the basic creep component decreases as the strength of concrete increases.
3. The creep rate of the total creep deformation for HPC is significantly lower than for NSC.
4. The shape of the time-development function of the total creep deformation of HPC is similar to that of basic creep of NSC.

The first difference between the creep characteristics of HPC and NSC depends on the attained concrete strength at time of loading and holds particularly true for structural concretes loaded at a concrete age higher than one day. The difference results from the significantly higher strength and stiffness, and the lower porosity of the hardened cement paste matrix of high-performance concrete in comparison with that of normal strength concrete. As a consequence, all effects on the creep of concrete resulting from interactions between the matrix and the aggregates, such as the effects of the aggregate content and the stiffness of the aggregates as well as load-induced microcracking, are reduced for high-performance concrete being made with ordinary aggregates.

The second difference is mainly caused by the low porosity of the hardened high-performance cement paste matrix, and consequently, all related diffusion-type features (see also

section 3.1) such as the effects of ambient humidity, size of member, predrying or curing on the magnitude of creep are reduced for HPC.

From simple material science considerations it becomes clear that also other well-known and relevant effects on the creep of concrete, for instance the effects of age at loading, type of cement, concrete temperature and stress level, must be different to some extent for high-performance concrete. However, the available information from experimental investigations on structural concretes is still very limited, or there is no information available at all to quantify these effects.

6.4.4.3 Prediction formulas

From the available test results on creep of high-performance concrete (see section 4.1) it is evident that the approach for the creep coefficient and the creep function, respectively, must include a separation of the total creep into the components basic creep and drying creep.

Though the approach in [CEB No. 213/214 (1993)] reveals no explicit separation of the total creep into the components basic creep and drying creep, nevertheless this distinction of strain components is existent in a simplified manner, see [CEB No. 199 (1990)]. This fact was decisive for the aptness of the model with regard to its extension towards the prediction of creep of normal and high-performance concrete. For detailed justifications of the new approach for the prediction of creep, see [Müller, Küttner (1996)].

type of deformation	number of references	number of tests	range of f_{cm} [MPa]	max silica fume content [%] *)
basic creep	4	31	62 .. 105	10
drying creep	10	51	60 .. 119	15.8

*) percentage of the cement content

Table 6-7: Creep data on high-performance concrete included in [RILEM TC 107 (1998)]

The subsequent formulas have been numerically optimized using the data sets included in the RILEM Data Bank (see Table 6-7).

Modulus of elasticity

The modulus of elasticity of concrete at the age of 28 days E_c may be estimated from the compressive strength of concrete by means of Eq. (6-31):

$$E_c = 21500 \cdot \sqrt[3]{f_{cm} / f_{cm0}} \tag{6-31}$$

where f_{cm} is the mean compressive strength of concrete [MPa] and f_{cm0} = 10 MPa. The modulus of elasticity at a concrete age $t \neq 28$ days may be obtained from Eq. (6-32), where t_1 = 1 day:

$$E_c(t) = E_c \cdot \exp\left(\frac{s}{2}\left[1 - \sqrt{\frac{28}{t/t_1}}\right]\right) \tag{6-32}$$

f_{cm} [MPa]	type of cement	s
≤ 60	RS N, R SL	0.20 0.25 0.38
> 60	all types	0.20
Legend: RS = rapidly hardening high strength cement; N, R = normal and rapidly hardening cement; SL = slowly hardening cement		

Table 6-8: Coefficient s according to Eq. (6.32)

The coefficient s in Eq. (6.32) depends on the type of cement and the compressive strength of concrete and may be taken from Table 6-8.

Creep coefficient

In accordance with [CEB No. 213/214 (1993)] the creep coefficient $\varphi(t,t_0)$ may be written as follows from Eq. (6-33):

$$\varphi(t,t_0) = \varphi_0 \cdot \beta_c(t,t_0) \tag{6-33}$$

where φ_0 is the notional creep coefficient and $\beta_c(t,t_0)$ is the coefficient to describe the development of creep with time after loading.

The coefficients φ_0 and $\beta_c(t,t_0)$ may be determined from Eqs. (6-34) .. (6-41):

$$\varphi_0 = \varphi_{RH} \cdot \beta(f_{cm}) \cdot \beta(t_0) \tag{6-34}$$

with

$$\varphi_{RH} = \left[1 + \frac{1 - RH/RH_0}{\sqrt[3]{0.1 \cdot h/h_0}} \cdot \alpha_1 \right] \cdot \alpha_2 \tag{6-35}$$

$$\beta(f_{cm}) = \frac{5.3}{\sqrt{f_{cm}/f_{cm0}}} \tag{6-36}$$

$$\beta(t_0) = \frac{1}{0.1 + (t_0/t_1)^{0.2}} \tag{6-37}$$

where

$$t_0 = t_{0,T} \cdot \left[\frac{9}{2 + (t_{0,T}/t_{1,T})^{1.2}} + 1 \right]^{\alpha} \geq 0.5 \text{ days} \tag{6-38}$$

and

$$\beta_c(t,t_0) = \left[\frac{(t-t_0)/t_1}{\beta_H + (t-t_0)/t_1} \right]^{0.3} \tag{6-39}$$

with

$$\beta_H = 150 \cdot \left[1 + \left(1.2 \cdot RH/RH_0 \right)^{18} \right] \cdot h/h_0 + 250 \;\; \alpha_3 \le 1500 \;\; \alpha_3 \tag{6-40}$$

and

$$\alpha_1 = \left[\frac{3.5 f_{cm0}}{f_{cm}} \right]^{0.7} \quad \alpha_2 = \left[\frac{3.5 f_{cm0}}{f_{cm}} \right]^{0.2} \quad \alpha_3 = \left[\frac{3.5 f_{cm0}}{f_{cm}} \right]^{0.5} \tag{6-41}$$

where: t = age of concrete [days] at the moment considered;
t_0 = age of concrete at loading [days];
$t_{0,T}$ = age of concrete at loading adjusted according to the concrete temperature; for T = 20 °C, $t_{0,T}$ corresponds to t_0; for other cases refer to [CEB No. 213/214 (1993)];
$t_{1,T}$ = 1 day;
α = coefficient which depends on the type of cement; α = -1 for slowly hardening cement; α = 0 for normal or rapidly hardening cement; α = 1 for rapidly hardening high strength cement;
α_i = coefficients which depend on the mean compressive strength of concrete according to Eq. (6-41).

All other parameters and variables are defined in the preceding sections.

The model for creep presented above is intended to predict the time-dependent mean cross-section behaviour of a concrete member moist cured at normal temperatures not longer than 14 days and exposed to a mean ambient relative humidity in the range of 40 to 100 percent at mean ambient temperatures from 10 °C to 30 °C. It is valid for normal-weight plain structural concrete having an average compressive strength in the range of $15 \le f_{cm} \le 120$ MPa. The age at loading should be at least one day, and the creep inducing stress should not exceed 40 percent of the concrete strength at the time of loading.

6.4.4.4 Accuracy of creep prediction

Corresponding to the shrinkage model also the new model for creep of normal strength and high-performance concrete has been verified in detail on the basis of experimental data included in the available data base [RILEM TC 107 (1998)].

The accuracy of the new prediction models for creep is graphically illustrated in Figure 6-23. Table 6-9 gives coefficients of variation for the creep function, both for normal and high-performance concrete. The coefficient of variation is an objective and unbiased statistical parameter obtained from a numerical procedure described elsewhere [CEB No. 199 (1990)]. The obtained values indicate that the prediction model is in a reasonably good agreement with measured strain data.

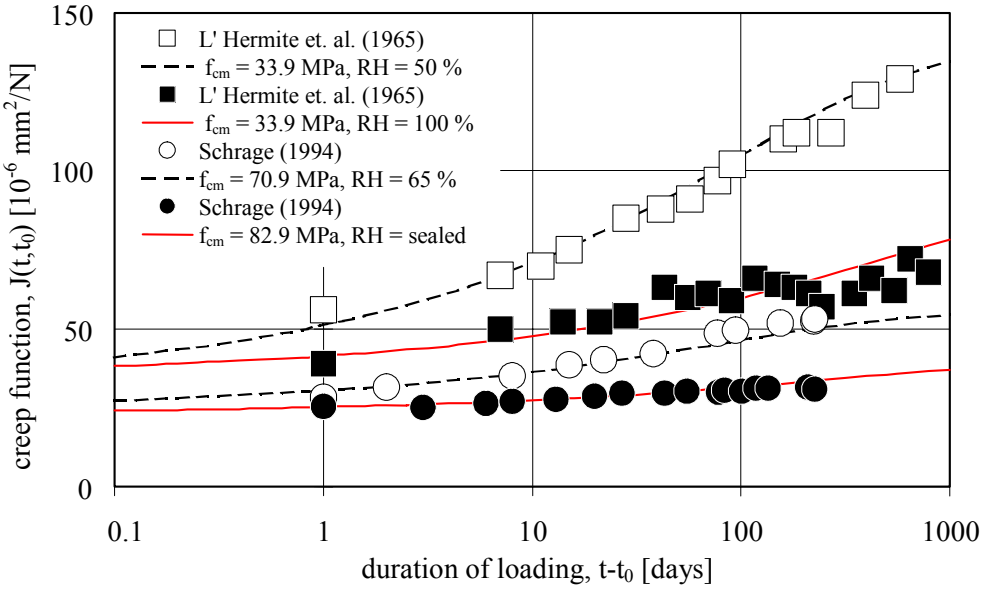

Fig. 6-23: Predicted and observed creep functions

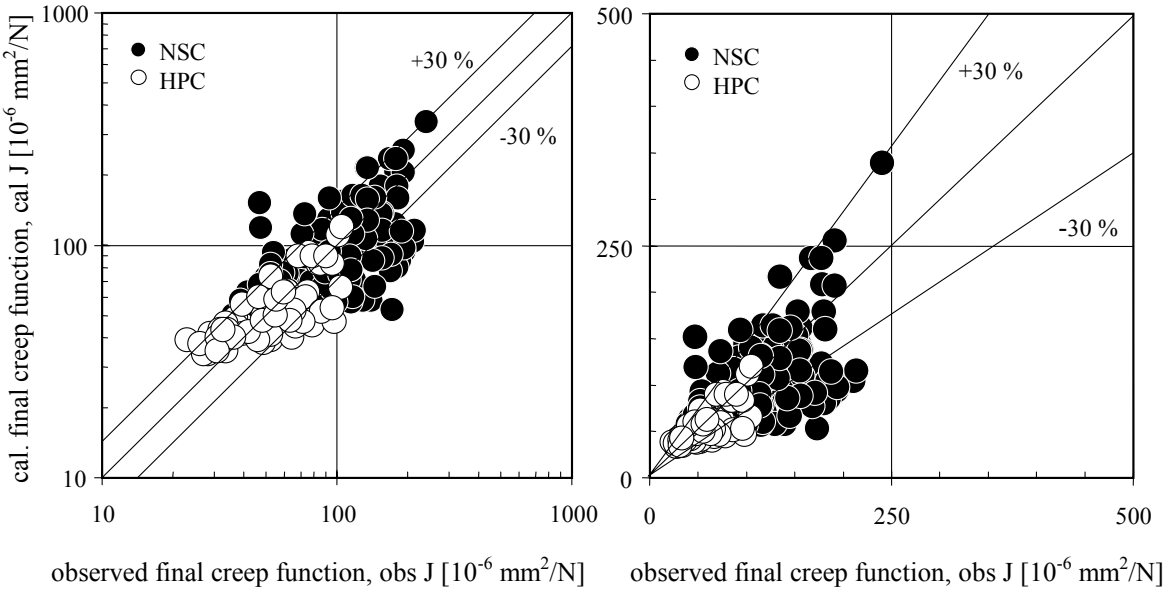

Fig. 6-24: Predicted and observed final creep functions; left hand diagram: logarithmic scale; right hand diagram: linear scale

In various practical cases, only the final value of the creep function or the creep coefficient, i.e. extrapolated values for $(t - t_0) \rightarrow \infty$, is of relevance. Figure 6-24 indicates graphically the accuracy of the new model for the prediction of final deformation values of normal strength and high-performance concrete. It may be seen that in most cases the prediction error is lower than 30 %. The mean prediction error, determined according to a procedure given in [CEB No. 199 (1990)], is F = 23.9 %.

For the prediction model of the CEB Model Code 1990, which is only valid for normal strength concrete, a coefficient of Variation of V = 20.4 % was obtained [CEB No. 199 (1990)]. Hence, the new creep model results in a somewhat higher coefficient of variation. The reason is that the new model represents an approach of the same simplicity as the CEB model while being applicable both for normal strength concrete and high strength concrete. The mean prediction error of the CEB model for extrapolated values (final values) has not been determined.

type of deformation	type of concrete	number of experiments	V [%]	
creep	HPC	71	20.7	26.1
	NSC	187	27.9	

Table 6-9: Coefficients of variation for the prediction of creep of concrete

6.4.4.5 Improvement of creep prediction

It is well known that even for a given strength, the modulus of elasticity depends on the type of aggregate. Eq. (6-29) is valid for concretes made of quartzitic aggregates. In [CEB No. 213/214 (1993)], coefficients are given to take into account the effect of the type of aggregate. As far as no other information is available, these coefficients may be applied. From material science considerations it appears, however, that these coefficients might change slightly for high-performance concrete. This is due to the fact that the ratio of the moduli of elasticity of the cement paste matrix and of normal strength aggregates increases with increasing strength of concrete. Detailed investigations on this subject are not available so far.

Eq. (6-30) does not take into consideration that the time-development of the modulus of elasticity depends also on the composition of concrete, i.e. the water-cement ratio and the amount and type of additions such as silica fume or fly ash. Consequently some modifications of Eq. (6-30) on the basis of suitable experimental data seem to be necessary for high-performance concrete. However, from [Müller, Küttner (1995)] it is apparent, that as a first step a reasonably satisfactory approximation for the aging of the modulus of elasticity of high-performance concrete may be obtained, if in Eq. (6-30) s = 0.2 is taken (see Table 6-8).

One should expect that perhaps additional coefficients have to be introduced to adjust also the aging function given in Eq. (6-35). However, the information on the aging behaviour of high-performance concrete and on the effect of the type of cement is still very scarce. In view of the limited and rather scattering data, Eq. (6-35) has been maintained at the present stage as given in [CEB No. 213/214 (1993)].

The time development function (Eq. (6-39)) gives a rather good approximation of experimental data and represents a reasonable compromise if basic creep and drying creep are described by means of only one time function. However, improvements may be achieved, if the time development of the basic creep component is described by a logarithmic time function while for drying creep the hyperbolic function may be maintained.

Some attention has to be paid to the combination of aging and time development functions (Eqs. (6-37) and (6-39), respectively) in an approach for the creep coefficient, if creep effects are analysed by means of Eq. (6-27). Under certain extreme conditions irrational results for calculated strains or stresses, e.g. relaxation stress may change sign, may be obtained [CEB No. 199 (1990)]. To avoid such problems, e.g. a factor may be introduced in the formulas [Müller, Kvitsel (2001)]. However, as long as Eq. (6-30) is applied, for which the new approach primarily is considered, no problems will be obtained.

It may be generally stated that without modifying the given approaches, the prediction accuracy can be improved if the parameter compressive strength of concrete is replaced by parameters giving the composition of concrete such as water-cement ratio, cement content, content and type of additions and admixtures etc. These parameters have not been introduced here for reasons mentioned in section 6.4.2.

The most significant improvement of the creep prediction may be obtained if the results of some short time tests are included in the prediction. By that way, the notional coefficients of

creep, which are the most uncertain parameters of the model, may be determined from the experiment.

6.4.5 Closing considerations

Though a considerable number of data on high-performance concrete exists, one must admit that in view of the complexity of the time-dependent deformations the data base is actually very limited. For various effects on the shrinkage and creep deformations, suitable data for the derivation of corresponding relations of the models have not yet been available. Hence, the new approaches for shrinkage and creep might be changed or extended in view of newly gained information on the deformation characteristics of high-performance concrete. Corresponding experimental and theoretical investigations are under way [Müller, Kvitsel (2001)]. On the other hand, the approaches should be kept simple as long as no substantial improvements are obtained when more sophisticated relations are introduced.

7 Fatigue

7.1 Introduction

Some concrete structures such as bridges, concrete pavements, offshore structures or rail road ties may be exposed to frequently varying stresses. Under such conditions they are subjected to fatigue. State-of-Art-Reports on fatigue of concrete – mainly addressing normal strength concrete – may be found e.g. in [CEB Bulletin No. 188 (1988)] and [ACI Committee 215 (1993)]. The fatigue behaviour of structures made of high performance concrete (HPC) has rarely been investigated. The two CEB/FIP bulletins 197 and 228 [CEB/FIP bulletin 197 (1990), CEB/FIP bulletin 228 (1995)] and the state-of-the-art-report of the national research council [Zia et al. (1991)] as well are reminding the lack of knowledge on the fatigue behaviour of HPC. As a preliminary conclusion it is stated in [CEB/FIP bulletin 197 (1990)] that the specific values obtained from fatigue tests on HPC are of the same magnitude as obtained from tests on normal strength concrete as long as the specific values are referred to particular values obtained in static tests. Following [CEB/FIP bulletin 228 (1995)] the rules are unnecessarily conservative in some cases, especially for alternative loading conditions. Kim and Kim had observed an increased fatigue crack propagation with increasing concrete quality [Kim and Kim (1999)].

In classical experiments on the fatigue behaviour of a material a specimen is generally subjected to stresses fluctuating around a constant mean stress so that a certain stress history can be characterised either by the mean stress and the stress amplitude or by the minimum and the maximum stress. These load-controlled tests are so called Wöhler tests. Failure occurs after a certain number of load cycles, N. The resistance of concrete against repeated loads is influenced mainly by the same technological parameters which control the strength of concrete subjected to short term static loads. Therefore, it is useful to express the stresses applied in a fatigue test as fractions of the static reference strength, i.e. in terms of the stress levels S_{min} and S_{max}, respectively. Then the fatigue behaviour of a material may be presented in so-called S-N-relationships, where the maximum stress levels S_{max} for a given minimum stress level S_{min} are plotted versus the number of load cycles, N, causing failure.

The fatigue strength of a material is defined as the maximum stress which the material can sustain for a given number of load cycles. It decreases with increasing number of load cycles and is considerably lower than the static strength for most materials. The fatigue limit or endurance limit corresponds to the maximum stress which the material can sustain for an infinite number of load cycles. Whether such a limit exists for concrete – even for normal strength concrete – is still controversial.

Due to the predetermined upper and lower load level these experiments are not capable to detect the softening behaviour of concrete, which might be essential to know with regard to durability of the concrete members. In section 7.2.3 a fracture mechanical approach based on deformation-controlled cyclic tensile tests, which also provides the softening behaviour of concrete is specified.

7.2 Experimental investigations

7.2.1 Plain concrete in compression

In this section the most significant investigations on fatigue of HPC will be summarized. Following [CEB/FIP bulletin 197 (1990)] the effect of the moisture condition is more pronounced for HPC than for normal strength concrete. Therefore this moisture effect is discussed in particular.

Many researches concerning the mechanical behaviour of high performance concrete have been done at SINTEF in Norway [Waagaard et al. (1987), Petkovic et al. (1990)].

Waagaard et al. (1987) investigated the effect of dry and wet moisture conditions on the fatigue behaviour of HPC with normal density and with lightweight aggregates. Specimens were tested in air and with a proper curing in water during fatigue tests. As a main result it could be concluded that the specimens that were dried out and tested in air achieved a longer lifetime for the same relative stress situation. The effect was found to be most evident for the concrete with normal density. This observation is even more remarkable since the increase in lifetime occurred despite of the fact that the stress range of the dried-out specimens was larger than for the submerged ones (see also [CEB/FIP bulletin 197 (1990)].

Hilsdorf and Müller pointed out that in general concretes with a high moisture content and in particular water saturated concretes have a considerably lower fatigue strength than dry concretes. Since thick concrete sections dry out at a much slower rate than thin sections and, therefore, may have a much higher moisture content, there is a size effect on the fatigue resistance of concrete so that thin sections tend to have a higher fatigue strength than very large sections [Hilsdorf and Müller (1999)].

Figure 7-1 shows mean test results of [Petkovic et al. (1990)] which were performed on Ø100*300 mm cylinders to investigate the effect of the minimum stress level on the fatigue life of HPC. Two types of normal density concrete, denoted as ND65 and ND95, and one type of light-weight aggregate concrete, LWA75, were used. The main attention was paid to the ND95 and LWA75 concretes, while the ND65 quality was included as an intermediate strength as a reference concrete.

The mean strengths at 28 days of the Ø150x300 mm cylinders were about 55 and 75 MPa for the ND65 and ND95 concretes and about 80 MPa for the LWA concrete.

All the cylinders of each quality for the fatigue tests were cast from the same batch. During storage and testing the cylinders were sealed by means of a watertight tape on the surface to keep their natural content of water. The loading form in the cyclic tests was sinusoidal with a frequency of 1 Hz.

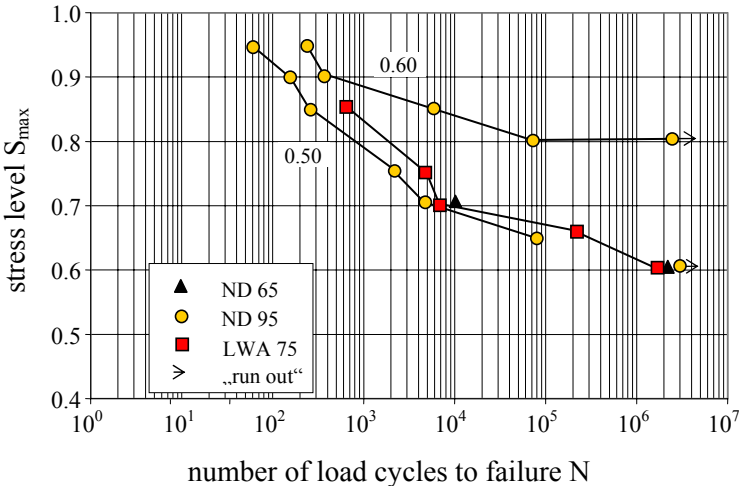

Fig. 7-1: Mean results of ND65, ND95 and LWA75 concrete in fatigue for S_{min}=0.05 and 0.60, respectively [Petkovic et al. (1990)]

As shown in Fig. 7-1 the effect of the minimum stress level is clear in that longer fatigue lives were obtained at higher minimum stresses for the same maximum stress levels. A factor analysis also showed that there was no reason for distinguishing between the three concrete qualities when the results were presented relative to their static strength [Petkovic et al. (1990)].

The behaviour of HPC in biaxial fatigue tests has been investigated by Nelson et al.

(1987). They performed tests on 125·125·12.5 mm³ concrete plates. The compressive strength of the concrete obtained on cylinders after 56 days was about 62 MPa. They observed in pure compression fatigue tests that the increase in concrete strength resulting from the biaxial stresses applied is lost when the concrete is subjected to more than about 50 repeated load cycles at any given stress ratio (in the tests four stress ratios 0, 0.2, 0.5 and 1.0 has been applied). It was concluded that HPC has a lower fatigue limit compared to normal strength concrete mainly due to a lower water-cement ratio.

Kim and Kim (1996) investigated the compressive fatigue behaviour on cylindrical concrete specimens with various strength levels. The strength level was varied from 26 MPa to 103 MPa, the maximum stress applied from 75 % to 95 % of the static compressive strength determined before the fatigue tests. As a main result they found the fatigue life decreasing with increasing the concrete strength. Furthermore, the rate of the fatigue strain increment of HPC was found to be greater than that of lower strength concrete.

Mucha (2003) describes the crack growth in different HPC caused by compressive fatigue loading. He stated that fatigue damage is significantly connected with microcracking he observed with a high solution light microscopy system. This phenomenon is further discussed in section 7.3.

7.2.2 Plain concrete in tension

Since the load bearing capacity of concrete is mostly connected to its compressive strength the tensile behaviour of concrete and in particular HPC under fatigue tensile loading has rarely been investigated.

Most fatigue tensile experiments have been performed as bending tests, e.g. [Waagaard (1982), Lambotte and Taerwe (1987), Ohlsson et al. (1988), Alliche and Francois (1992), Bažant and Schell (1993)].

Lambotte and Taerwe (1987) investigated normal and high strength concrete beams with cylinder strengths of about 40 MPA and 90 MPa, respectively. With the same curing and tests conditions for both concrete grades they found no significant difference between the Wöhler lines obtained for HPC and normal strength concrete. Nevertheless, the Wöhler lines for HPC showed a slightly higher fatigue life for the stress range $0.7 < S_{max} < 0.9$, whereas the inverse is true for the lower stress ranges < 0.7, in other words: the Wöhler line in the case of HPC is more inclined.

Figure 7-2 summarizes different test results obtained from fatigue tensile tests on HPC [Ohlsson et al. (1988), Alliche and Francois (1992), Bažant and Schell (1993)]. Ohlsson et al. (1988) mainly investigated the effect of the temperature, Alliche and Francois (1992) the variation of the stress ratio and Bažant and Schell (1993) the size effect. It can be concluded from the Wöhler lines that in general the effects observed on normal strength concrete hold true for HPC as well. Due to the different test set-ups and the typical scatter of fatigue experiments the inclination of the Wöhler lines varies from steep to shallow.

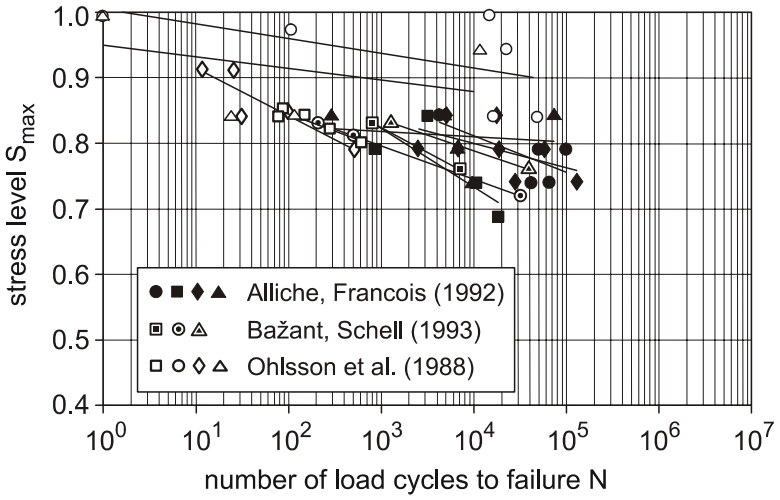

Fig. 7-2: Test results and S-N lines for flexural tensile strength of HPC [Ohlsson et al. (1988), Alliche and Francois (1992), Bažant and Schell (1993)]

The fatigue behaviour of HPC has intensely been studied by Kessler-Kramer et al. (2005) by means of uniaxial tensile tests. Besides the effect of higher concrete strengths the influences of moisture conditions and the frequency have been investigated.

By considering the mean deformation ($\delta_m = ½ \cdot (\delta(F_{upper}) + \delta(F_{lower}))$) measured in Wöhler tests the relations shown in Fig. 7-3, left could be obtained. The increase of the deformation with increasing actual number of load cycles – referred to the number of load cycles at final failure – provide a so-called cyclic creep curve, which can be divided into three parts predominantly representing three phases of cracking, but also creep deformations. The phase of microcrack initiation and primal creep up to a number of cycles of approximately 0.2·N (in Fig. 7-3 denoted as phase I) is characterised by an extensive increase of deformation ($d\delta/dN > 0$; $d2\delta/d2N < 0$). Phase II shows an approximately linear ascent meaning a constant value of $d\delta/dN$ up to about 0.8·N. Above a number of load cycles of about 0.8·N the deformations increase dramatically up to final failure (phase III). The use of high strength concrete instead of normal strength concrete resulted in a shift of the cyclic creep curve to higher values of deformations. This effect can be drawn back mainly to higher absolute values of the upper load level for the same loading degree in the case of high strength concrete, which may lead to larger elastic deformations and a more pronounced primal creep.

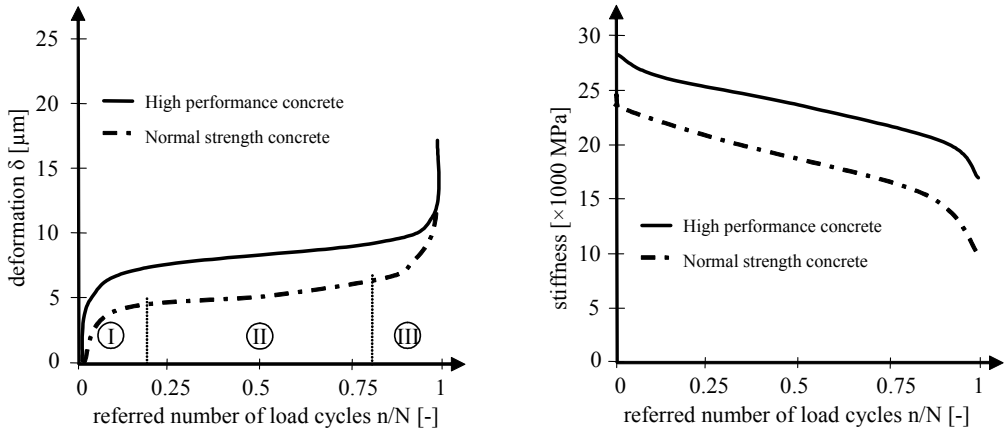

Fig. 7-3: Effect of the increasing number of load cycles on mean deformation (left) and mean stiffness (right) as observed in fatigue tensile tests

The stiffness decrease with an increasing number of load cycles is shown in Fig. 7-3, right. The method used for the calculation of the inclination of mean straight lines within hysteretic loops is leaned on [Holmen (1979)]. Again, there is only a minor effect of the concrete grade with regard to the curve shape. Similar to the curves obtained for the deformations three phases can be identified, however, with the first phase ending already at a number of load cycles of about 0.05·N. The observed stiffness in the last load cycles is up to 60 % less than the initial stiffness, which is proportional to the modulus of elasticity of the undamaged concrete at the first load cycle.

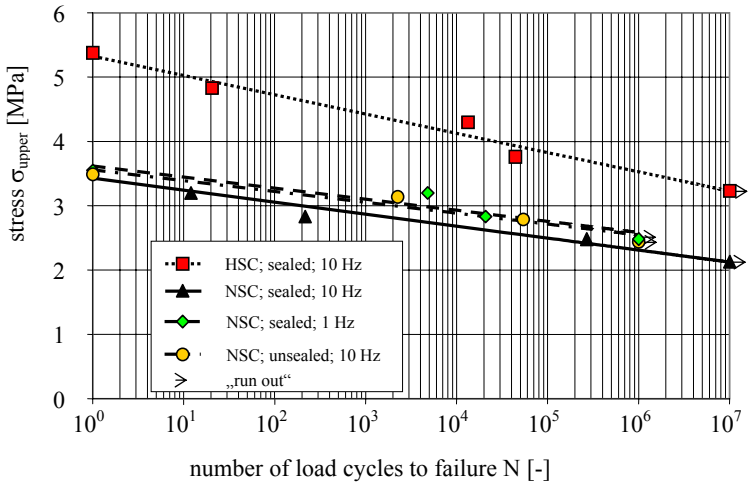

Fig. 7-4: Effect of the upper load level on the attained number of load cycles to failure in load-controlled cyclic tensile tests (Wöhler lines)

If the results of the fatigue tensile tests are plotted in a stress-number of load cycles diagram lines as shown in Fig. 7-4 can be obtained. First, it is worth to be mentioned that for two specimens – one made of normal strength concrete and one of high strength concrete – could bear more than 10 million load cycles without a final failure at a degree of load $S = \sigma_{upper} / f_t = 0.6$. Afterwards these specimens were undertaken a monotonic deformation controlled uniaxial tensile test. The load-deformation relations obtained from these monotonic tests showed similar characteristic mechanical and fracture mechanical values as obtained in deformation controlled fatigue tests with a high number of load cycles (see following section). This supports the assumption of a constant fatigue limit for concrete as it is true e.g. for steel. The effect of the concrete grade is reflected by a line being more inclined in the case of HPC compared to normal strength concrete, which indicates its higher sensibility to fatigue. However, if the results are transferred to a normalized S-N diagram the inclination of the Wöhler lines are mostly coincide [Kessler-Kramer et al. (2005)].

7.2.3 Fracture mechanical fatigue tests

Fracture mechanical tests on HPC concerning its fatigue behaviour have rarely been the subject of concrete research studies [Gopalaratnam and Shah (1985), Hordijk (1991), Kessler-Kramer et al. (2002)]. The fracture mechanical tests have been performed by means of a predetermined number of load cycles. Therefore, usually the total deformation has been taken from preceding monotonic tensile tests and the deformation increment per cycle is calculated as the total deformation divided by the intended number of load cycles.

Gopalaratnam and Shah (1985) analysed classical fracture mechanical parameters such as the energy release rate and the fracture toughness on different concrete grades with maximum compressive strengths however limited to 50 MPa.

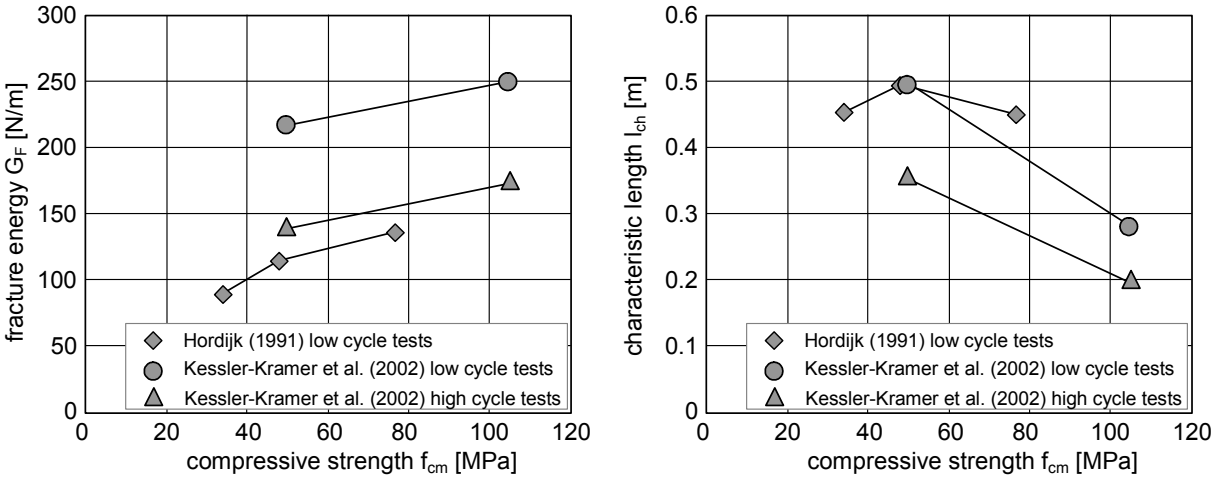

Fig. 7-5: Effect of the compressive strength on the fracture energy (left) and on the characteristic length (right) in uniaxial tensile tests

Fig. 7-5 shows the effect of various compressive strengths on nowadays common fracture mechanical parameters such as the fracture energy G_F or the characteristic length l_{ch} defined as fraction of the fracture energy times Young's Modulus and the net tensile strength squared as a characteristic value for the brittleness [Hordijk (1991) and Kessler-Kramer et al. (2002)]. Thus the fracture energy is increasing with higher concrete grades and the characteristic length is reaching lower values meaning a higher brittleness.

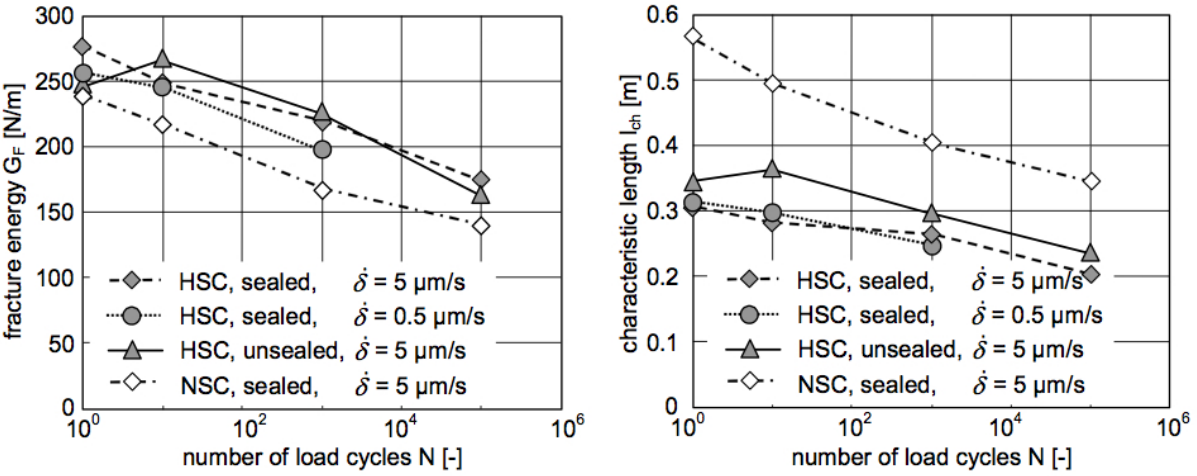

Fig. 7-6: Effect of the number of load cycles to failure on the fracture energy (left) and on the characteristic length (right) in tension tests on normal strength and high strength concrete specimens for different deformation rates and curing conditions [Kessler-Kramer et al. (2002)]

Figure 7-6, left shows a decrease of the fracture energy G_F in the high-cycle fatigue tests with an increasing number of load cycles. The G_F-values were calculated as the area under the measured stress-deformation curves. In the case of cyclic tests the envelope curves of the corresponding stress-deformation relations have been chosen. Therefore, a possible contribution of the area within the hysteretic loops is not considered.

Since the reduction of the investigated parameters, namely the fracture energy and the characteristic length with an increasing number of load cycles is approximately the same for normal strength and high strength concrete, it can be concluded that the effect of the fatigue loading is similar for both types of concrete (HPC and NSC).

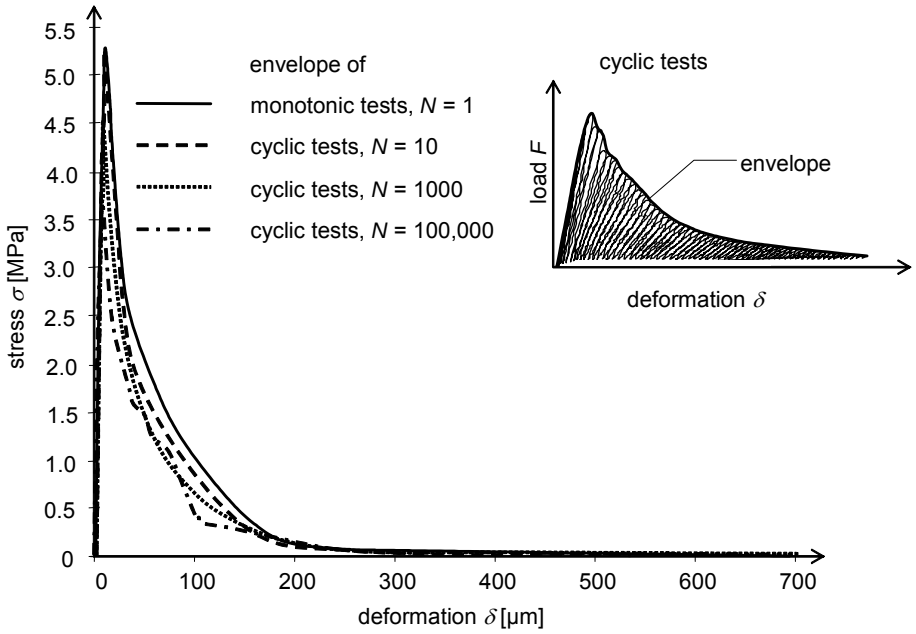

Fig. 7-7: Envelopes of the stress-deformation relations obtained from the monotonic and cyclic uniaxial tensile tests on sealed high performance concrete specimens

The main finding in [Kessler-Kramer et al. (2002)] is that for an increasing number of load cycles the envelope curves of the σ-δ relations differ significantly from the corresponding monotonic curve, see Figure 7-7. The ascending branches show approximately the same shape and the same stiffness for all curves. Because of lower tensile strength-values for the high-cycle fatigue tests these curves are below the curves for the monotonic and the low-cycle fatigue tests in the first, steeper part of the stress-deformation relation. Additionally, the curves from the high-cycle fatigue tests are steeper than the curves for the monotonic and the low-cycle fatigue tests, see Figure 7-7. In the second, shallow part of the softening branch the average curves for the cyclic tests match the monotonic curve beginning at a crack opening of about 200 µm up to the entire separation of the specimens into two parts. In the case of normal strength concrete the shape of the typical stress-deformation curve was found to be similar to that of the corresponding curve obtained for the HPC.

7.2.4 Conclusions from experimental tests

Since the behaviour of HPC under fatigue loading conditions is not required to be known for every construction made of concrete or reinforced concrete it is inevitable that less experimental data is available. Nevertheless, it can be concluded from a critical analysis of the present data especially from the newest studies that a higher concrete grade leads to a significant higher brittleness as to be observed in monotonic loading conditions as well. Looking especially at the results obtained in classical Wöhler tests in different studies a higher sensibility to fatigue can be ascertained for increasing concrete grades even if the Wöhler lines found in some studies are showing the same inclination. This is in contrast to the preliminary conclusion stated in section 7.1 that the specific values obtained from fatigue tests on HPC are of the same magnitude as obtained from tests on normal strength concrete [CEB/FIP bulletin 197 (1990), König and Danielewicz (1994)]. This statement will certainly be updated with deeper knowledge on ultra high strength concretes (UHPC).

7.3 Phenomenological behaviour of HPC under fatigue loading

The controlling structural mechanisms of the fatigue behaviour have not been clarified to an acceptable conclusion, yet. There are basically two hypotheses addressing the crack initiation in concrete under cyclic loading conditions which can be traced back to the results obtained under static loading conditions [Hordijk (1991), RILEM committee 36-RDL (1984)]. The first hypothesis is describing the continuous release of the boundaries between the coarse aggregates and the cementitious matrix as reason for failure under fatigue loading. The second hypothesis is based on the assumption of the existing microcracks before applying the external loads being responsible for the further crack propagation under fatigue loading. The microcracks coincide with increasing deformation and create macro cracks weakening the loaded cross section. Thus the load can not be bore further more. Both hypotheses could not be confirmed or proved wrong in experiments. Supposable both mechanisms are present and interfere each other in normal strength concrete as well as in high performance concrete under fatigue loading conditions with varying proportions.

Looking at concrete on the macro level irreversible deformations can be determined as well as a continuous decrease of the stiffness. In [Schäfli (1999)] these effects are associated with two so called fatigue drives. The first fatigue drive is the viscoelastic deformation proportion [Guénot-Delahaie (1997)]. The short term deformations hereof can be traced back to capillary flow due to a thermodynamic disequilibrium. For the long term deformations it is assumed that calcium silicate hydrate may dislocate within the nanopores. If these viscoelastic deformations are locally higher than the deformation capacity of the concrete cracks will occur and propagate. The second fatigue drive can be attributed to the effect that loosened or pulled out aggregates or hardened cement paste particles may dislocate while the crack is open and lead to local tensile as well as compressive stresses in the case of unloading.

Following the microscopic investigations of Toumi et al. (1998) the observations on static tests such as crack propagation along the interfacial crack zone can be found in fatigue tests as well. However they detected a more diffuse microcracking on the concrete members' surface near the crack tip. Compared to monotonic tests no distributed microcracking in front of the macro crack could be obtained inside the concrete members. According to König and Danielewicz (1994) the crack compactness is higher for concrete subjected to fatigue loading than to monotonic loading.

Remmel (1994) observed the crack initiation in notched concrete members made of HPC by means of acoustic emissions. When about 90 % of the maximum load is reached the cumulative impulses, i.e. the amount of impulses within a specific time interval above a certain trigger threshold, show a first increase due to increasing microcracking which is more significant after the peak. In the second, shallow part of the softening curve the impulse rate is less due to transmitting lower tensile stresses by means of friction between the crack banks and the material bridges.

Acoustic emission analyses to clarify the mechanisms of the crack formation and propagation processes in high performance concrete under cyclic loading have also been performed by Kessler-Kramer et al. (2002).

Fig. 7-8, left shows that the curves for the cumulative impulses obtained from uniaxial tensile tests on HPC are well above the curves received from tests on normal strength concrete. Fig. 7-8, right shows the effect of cyclic tensile loading on the shape of the curve of the cumulative impulses for HPC. Additionally, curves are shown for the case of cyclic tests considering just the deformation increments $\Delta\delta$, i.e. neglecting the deformations within the hysteretic loops (as marked with dotted lines in Fig. 7-8, right).

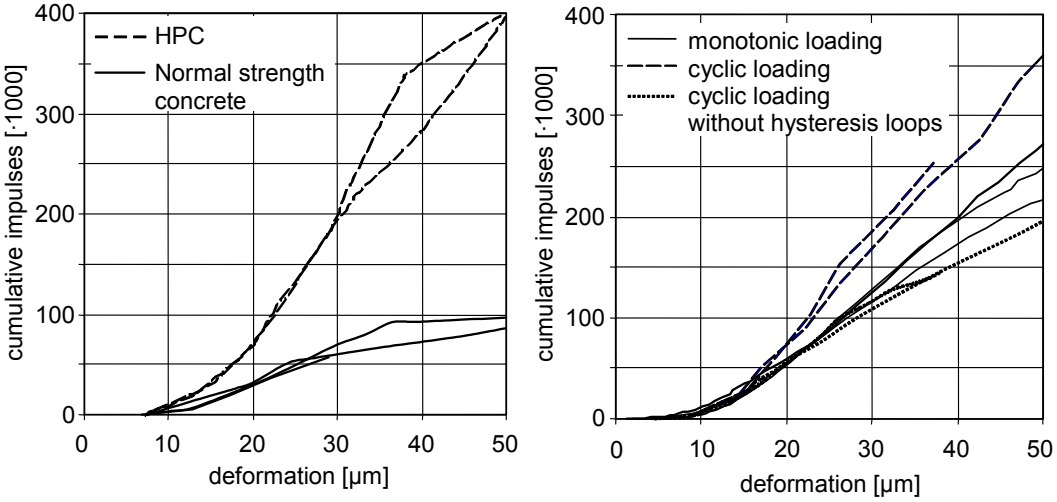

Fig. 7-8: Effect of the concrete grade on the shape of the cumulative impulses for low-cycle fatigue tests (left); effect of loading cycles on the shape of the cumulative impulses for HPC (right)

Up to a deformation of around 30 µm the curve for the monotonic loading matches the curve for the cyclic loading without hysteretic loops quite well. With further increasing crack propagation the cyclic tests provided lower acoustic emissions. However, in the case of cyclic tests with the consideration of the hysteretic loops higher values of the cumulative impulses could be obtained. For high-cycle fatigue tests this detailed consideration of the individual deformation parts was not suitable due to the extremely low deformation increments per cycle. Nevertheless, it could be observed that the curves for the cumulative impulses in the case of high-cycle fatigue tests are far above the corresponding curves obtained from monotonic and low-cycle fatigue tests.

A further method to analyse failure mechanisms of different types of concrete is the measuring of the fractures surfaces using the projected fringes technique [Kessler-Kramer et al. (2002), Mechtcherine and Müller (2002)].

concrete	strain rate $\dot{\varepsilon}$ [1/s]	roughness R_S [-]	fractal dimension D_{GS} [-]
HPC, sealed	$1 \cdot 10^{-4}$	1.245 (0.027)	2.041 (0.003)
HPC, unsealed	$1 \cdot 10^{-4}$	1.243 (0.005)	2.041 (0.001)
HPC, sealed	$1 \cdot 10^{-5}$	1.243 (0.010)	2.042 (0.005)
NSC, sealed	$1 \cdot 10^{-4}$	1.281 (0.003)	2.043 (0.005)

Standard deviations are given in parentheses.

Table 7-1: Roughness and fractal dimension of concrete fracture surfaces for different curing conditions, strain rates and concrete grades

From the optical measurement data the roughness R_S and the fractal dimension of the surfaces D_{GS} were calculated. The roughness R_S of the fractured surface was calculated using the surface area with 0.16 mm mesh size divided by the projected area. The fractal dimension defined by the grid scaling method is a measure almost independent of the refinement of the grid pattern. Tab. 7-1 gives the results of the calculations.

The roughness and the fractal dimension of the fracture surfaces increase with decreasing strength of concrete. In contrast to the results for normal strength concrete no pronounced effect of the curing conditions as well as the strain rate on the condition of the fracture surfaces could be found for HPC (Tab. 7-1).

7.4 Modelling the fatigue behaviour of HPC

7.4.1 Models for compressive fatigue behaviour

For the modelling of fatigue failure with compressive loading plenty of models are available. In the following only models for plain concrete modelling the envelope curve for cyclic loading conditions are presented.

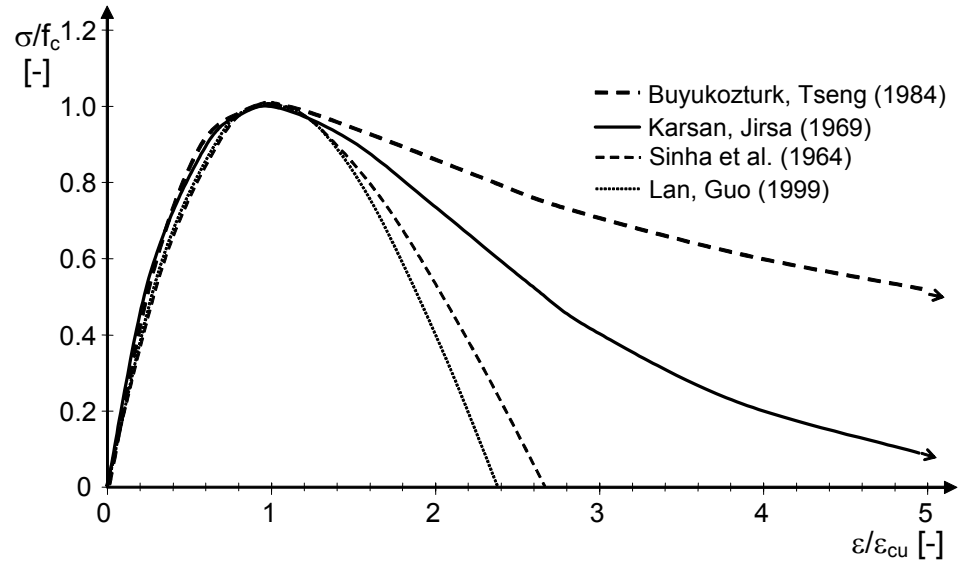

Fig. 7-9: Referred stress-strain relations of envelope curves for concrete under compressive cyclic loading

Fig. 7-9 shows a comparison of various envelope curves from models to describe the behaviour of concrete under compressive cyclic loading in a referred stress-strain diagram. As reference the stress when bearing the maximum load and the related strain has been taken. The figure clearly shows the different description of the softening behaviour. While two curves show distinctive brittle post peak behaviour [Sinha et al. (1964) and Lan, Guo (1999)], the rest two curves exhibit a more or less ductile softening. This rough comparison already proofs that the modelling of the compressive fatigue behaviour has not bee solved to complete satisfaction, yet.

Further restrictions are the missing consideration of the loading history [Karsan, Jirsa (1969), Sinha et al. (1964), Lan, Guo (1999)] and the effect of the strain rate [Buyukozturk, Tseng (1984)]. The models of Lan, Guo (1999) and Buyukozturk, Tseng (1984) are both capable to describe the biaxial fatigue stress behaviour as well as the decrease of stiffness with increasing number of load cycles. Due to the above mentioned constraints all models are only suitable for low cyclic loading conditions but rarely applicable for high cycle fatigue.

7.4.2 Models for tensile fatigue behaviour

In the field of tensile fatigue behaviour several models have been developed, mostly restricted to low cycle fatigue as will be discussed subsequently. The first important model for the tensile fatigue behaviour of concrete was given by Gylltoft (1984) using an energy

based criterion for modelling the failure. Due to load cycles the monotonic stress-strain relation can not be reached again. Unfortunately Gylltoft overestimates the energy release and does not give a new constitutive relation for the following envelope curve.

The model by Reinhardt et al. (1986) is using parameters for the constitutive relations which are unknown at that moment they are used for modelling. Therefore, this model is a pure description rather than a prognosis. The well-known focal-point model by Yankelevsky and Reinhardt (1989) is using several auxiliary construction points and is thus rather complex. Furthermore it is not reflecting the effect of the lower stress limit.

The continuous function model by Hordijk (1991) is restricted to low cycle fatigue likewise since it is a closed analytic relation based on curve fitting of fatigue experiments with a limited number of load cycles. Contrary to the empiric approach of Hordijk Duda (1991) is using simple rheological elements such as springs and friction blocks. Remmel (1994) is extending the Duda model for the application on high performance concrete. Since it is still neglecting the effect of time effects by not applying dashpots as rheological elements it remains limited for the modelling of low cycle fatigue behaviour.

Based on new experimental results, Kessler-Kramer (2002) developed a new constitutive law on the basis of a rheological statistical model considering in particular the number of load cycles, time effects and the heterogeneity of concrete, see Fig. 7-10.

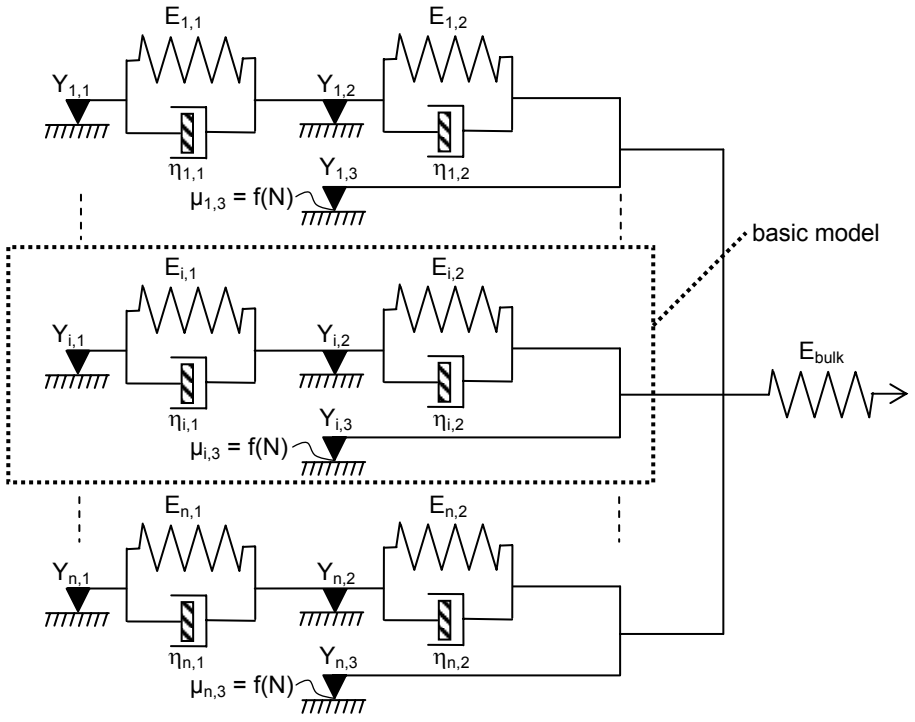

Fig. 7-10: Rheological statistical model for the description of the fatigue behaviour of concrete under tensile loading [Kessler-Kramer (2002)]

The model consists of simple rheological elements like springs, friction blocks and dashpots representing the elastic, frictional and viscous deformation components of concrete.

The hysteretic loops are described by a serial arrangement of two friction blocks and two Kelvin-Voigt elements. The dashpots $\eta_{i,1}$ and $\eta_{i,2}$ arranged parallel to the spring elements $E_{i,1}$ and $E_{i,2}$ enable to consider the rate dependency of concrete and to include effects like e.g. the load history. The parallel arrangement of a further friction block $Y_{i,3}$ allows for the modelling of the effect that loosened or pulled out aggregates or hardened cement paste particles may dislocate while the crack is open and lead to local tensile as well as compressive stresses in

the case of unloading. Since this phenomenon just appears within the hysteretic loops the associated friction coefficient $\mu_{i,3}$ is given as a function of the number of load cycles N.

The complete model consists of n basic models arranged parallel with the parameters Y, E and η being statistically distributed and following an exponential function after Weibull. This approach considers the heterogeneity of concrete. The bulk behaviour of the undamaged concrete is taken into account by an additional spring element E_{bulk}.

7.5 Constitutive relations and fatigue treatment in codes

As specified in the preceding section the models are underlined with constitutive relations. In the following only the latest model will be taken up for a further consideration.

The complete rheological-statistical model [Kessler-Kramer (2002)] can transfer the stress σ given with Eq. (7-1) as a function of the actual crack opening w under the condition of both serial arranged friction blocks $Y_{i,1}$ and $Y_{i,2}$ being in motion and transferring the full friction load. Thus Eq. (7-1) is valid for monotonic loading as well as for the deformation increments $\Delta\delta$ outside the hysteretic loops in the case of cyclic loading (in other words the envelope curve):

$$\sigma(w) = c_1 \cdot (\sigma_{Y1,0} + \sigma_{Y2,0}) \cdot f_{H1}(w) + c_2 \cdot (\sigma_{Y1,0} + \sigma_{Y2,0}) \cdot f_{H2}(w) \tag{7-1}$$

In Eq. (7-1) $\sigma_{Y1,0}$ and $\sigma_{Y2,0}$ denote the transferable stresses of the first and the second friction elements, respectively and c_1 and c_2 are correlation coefficients. The functions $f_{H1}(w)$ and $f_{H2}(w)$ are the statistical distributions according to the theory of Weibull with different coefficients α, β and γ .

The transferable stress within the hysteretic loops can be calculated by adding the load carrying capacities of the second spring elements $E_{i,2}$, the second dash pots $\eta_{i,2}$ and the parallel arranged third friction elements $Y_{i,3}$ according to Eq. (7-2:

$$\sigma(w) = c_1 \cdot \left[(w - w_2) \cdot k_2 + \frac{\eta_2}{l_{meas}} \cdot (\dot{w} - \dot{w}_2) \right] \cdot f_{H1}(w)$$
$$+ c_2 \cdot \left[(w - w_2) \cdot k_2 + \frac{\eta_2}{l_{meas}} \cdot (\dot{w} - \dot{w}_2) \right] \cdot f_{H2}(w) + \sigma_{Y3,0} \cdot f_{Y3}(w) \tag{7-2}$$

The displacement $w_2 = f(\eta_1, \eta_2, k_2)$ as well as the corresponding velocity $\dot{w}_2$ of the second friction elements $Y_{i,2}$ in Eq. (7-2) are dependent whether the material is actually un- or reloaded. The parameter k_2 denotes the stiffness of the second spring elements, η_2 the viscosity of the second dash pots and l_{meas} the measuring length used in the experiments. $\sigma_{Y3,0}$ denotes the stresses transferable by the third friction elements and $f_{Y3}(w)$ the corresponding statistical distribution of a hyperbolic type.

To proceed from the developed material model to a constitutive material law the unknown model parameters in Eqs. (7-1) and (7-2) have to be determined by means of an appropriate inverse analysis. Thereby it could be concluded that the parameters β_2, c_1 and c_2 are most suitable to reflect the relevant effects of the concrete grade, the strain rate, the curing conditions and the number of load cycles on the stress-crack opening relation in Eq. (7-1). Eq. (7-3) summarizes the coefficients from Eq. (7-1) defined as constants and Eq. (7-4) gives the corresponding values of the parameters for describing the hysteretic loops using Eq. (7-2).

$$\alpha_1 = \alpha_2 = 0 \;\; ; \qquad \beta_1 = 0.02 \;\; ;$$
$$\gamma_1 = 2.0 \qquad and \qquad \gamma_2 = 1.2 \tag{7-3}$$

$$\sigma_{Y1,0} = 2/3 \cdot f_t \quad ; \qquad \sigma_{Y2,0} = 1/3 \cdot f_t \quad ; \qquad \sigma_{Y3,0} = 0.05 \cdot f_t \quad ;$$
$$k_2 = (167 - 5 \cdot \log N) \cdot f_t \tag{7-4}$$

Further details concerning the determination of the model parameters and an additional simplification of the constitutive law by replacing the description of the hysteretic loops with a single relation for the actual compliance as a function of the crack opening may be found in Kessler-Kramer (2002).

As a last step for the modelling the functional dependences of the f_t-, E_0-,ε_{tu}- and G_F-values from the investigated parameters had to be formulated. For this purpose the functional expressions were chosen similar to those proposed by the CEB-FIP Model Code 1990 (1993).

The effect of the concrete grade on the uniaxial tensile strength f_t as well as on the Young's Modulus E_0 has been experimentally determined well according to the formulas given in MC 90 (1993). Therefore, these functional dependencies could be adopted directly as given by the Eqs. (7-5) and (7-6):

$$f_t = 1.40 \cdot (f_c / 10)^{2/3} \tag{7-5}$$

$$E_0 = 2.15 \cdot 10^4 \cdot (f_c / 10)^{1/3} \tag{7-6}$$

where f_c = characteristic compressive strength (all parameters in [MPa]).

In contrast thereto the formulation for the fracture energy G_F is deviating from the formula given in MC 90 (1993):

$$G_F = 157 \cdot (f_c / 10)^{0.215} \tag{7-7}$$

The derived Eq. (7-7) is resulting in higher values for the fracture energy G_F than the formula given in MC 90 (1993) – though more pronounced for normal strength concrete. This can be traced back mostly to an optimized test set-up and the use of non-rotatable boundary conditions in the tensile tests by Kessler-Kramer (2002) which is assumed to be the standard of nowadays laboratory equipments.

According to Hooke's law the strain at the peak stress ε_{tu} is given by the Eqs. (7-5) and (7-6):

$$\varepsilon_{tu} = 65 \cdot 10^{-6} \cdot (f_c / 10)^{1/3} \tag{7-8}$$

In contrast to Eq. (7-8) MC 90 (1993) provides a constant value for ε_{tu} of about $150 \cdot 10^{-6}$. This constant value for the strain at the peak stress in tensile tests could already be disproved in experiments by many researchers [Mechtcherine (2000)].

The verification of the new constitutive law by means of a finite element simulation of three-point bend tests that were not considered for the derivation of the constitutive relations as described above, provided a rather good prediction of the concrete behaviour observed experimentally [Kessler-Kramer (2002)].

Further to constitutive relations most codes are dealing with fatigue in the sense of classical analytical expressions to estimate the number of cycles to failure for given boundary conditions.

In the CEB-FIP MC 90 analytical expressions are given to estimate the number of load cycles to failure for pure compression, compression-tension and pure tension, respectively for a constant minimum and maximum stress level. In these relations the maximum and minimum stress levels for compression $S_{c,max}$ and $S_{c,min}$ are defined as given in Eqs. (7-9a) and (7-9b). There, the maximum and minimum stress levels are expressed as a fraction of the fatigue reference compressive strength $f_{ck,fat}$ which follows from Eq. (7-9c). In this equation the coefficient $\beta_{c,sus}(t, t_o)$ takes into account the effect of high sustained loads in cases where the mean stress during fatigue loading is high. Relations for $\beta_{c,sus}(t, t_o)$ are given in CEB-FIP MC 90. Eq. (7-9c) also considers the increased sensitivity to fatigue loads with increasing

concrete compressive strength. For an age at loading of 28 days $f_{ck,fat}$ decreases from about $0.82 \cdot f_{ck}$ for a low strength grade to about $0.75 \cdot f_{ck}$ for a high strength grade.

$$S_{c,\max} = |\sigma_{c,\max}| / f_{ck,fat} \quad (7\text{-}9a)$$

$$S_{c,\min} = |\sigma_{c,\min}| / f_{ck,fat} \quad (7\text{-}9b)$$

with

$$f_{ck,fat} = \beta_{cc}(t) \cdot \beta_{c,sus}(t,t_o) \cdot f_{ck} \cdot (1 - f_{ck} / 25 f_{cko}) \quad (7\text{-}9c)$$

where:

$S_{c,max}$	maximum stress level
$S_{c,min}$	minimum stress level
$\sigma_{c,max}$	maximum compressive stress [MPa]
$\sigma_{c,min}$	minimum compressive stress [MPa]
f_{ck}	characteristic compressive strength [MPa]
$f_{ck,fat}$	fatigue reference compressive strength [MPa]
f_{cko}	= 10 MPa
$\beta_{cc(t)}$	coefficient to take into account the effect of age at the beginning of fatigue loading on the compressive strength of concrete
$\beta_{c,sus(t, to)}$	coefficient to take into account the effect of high mean stresses during fatigue loading.

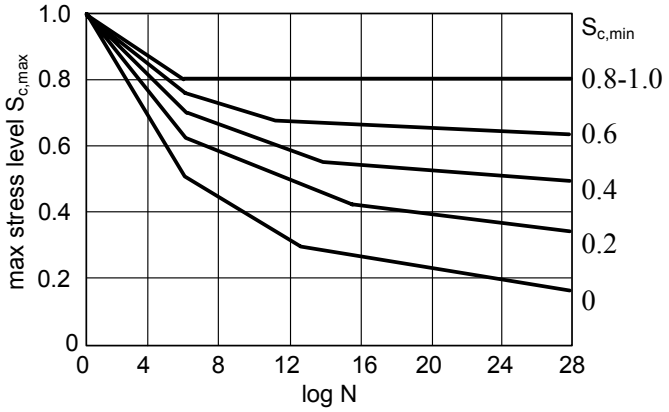

Fig. 7-11: S-N relations for concrete subjected to pure compressive fatigue loading as obtained from the analytical expressions given in CEB-FIP MC 90 (1993)

In Fig. 7-11 S-N relations for concrete subjected to pure compressive stresses are shown which have been obtained from the relations given in CEB-FIP MC 90. They are generally considered as rather conservative giving lower bound limits for severe loading conditions.

As mentioned above this design formulation does not distinguish between different moisture conditions. For normal dimensions of structural elements the effect of drying and water penetration at the surface will not be the same as for laboratory size specimens. Especially for HPC, drying and absorption will particularly be a surface phenomenon due to the relatively small porosity of this concrete.

If small tensile stresses are occurring ($\sigma_{ct,max} \leq 0.026 \ |\sigma_{c,max}|$) Eq. (7-10) has to be applied:

$$log\ N = 9\ (1 - S_{c,max}) \quad (7\text{-}10)$$

In this case it is assumed that concrete is always failing in compression.

For concrete in tension the fatigue life is defined as

$$\log N = 12\,(1 - S_{ct,max}) \tag{7-11}$$

with $S_{ct,max} = (\sigma_{ct,max}) / f_{ctk,min}$ where

$\sigma_{ct,max}$ maximum tensile stress [MPa]

$f_{ctk.min}$ minimum characteristic tensile strength [MPa].

Thus, in this case the effect of different minimum stress levels is not included. Moreover, autogenous shrinkage may result in early cracking on the surface of HPC specimens. However, it is a necessary condition for fatigue calculations in tension that the concrete is uncracked.

Generally, structural elements are subjected to a spectrum of load levels which deviate considerably from the constant stress level-amplitude conditions applied in laboratory experiments. To estimate the fatigue life of concrete subjected to realistic stress histories CEB-FIP MC 90 recommends the application of the so called Palmgren-Miner summation rule as expressed by Eq. (7-12).

$$D = \sum_i \frac{n_{Si}}{N_{Ri}} \tag{7-12}$$

where:

D fatigue damage

n_{Si} number of cycles applied at a given stress level and stress range

N_{Ri} number of cycles causing failure at the same stress level and stress range.

Failure occurs, if D = 1. According to [Siemes (1988)] the value of the Miner sum indicating failure is varying in various codes from 0.2 to 1.0. Consequently, the Palmgren-Miner rule is only a very rough approximation of the actual concrete behaviour. It may over- or underestimate the actual fatigue strength of concrete subjected to varying repeated loads.

7.6 Conclusions

In spite of enhanced research activity in the field of high performance concrete one has not yet succeeded in finding adequate design rules for fatigue behaviour taking into consideration the special properties of HPC. On the experimental level further progress has taken place especially concerning the fracture mechanical behaviour and the underlying phenomenological mechanisms. Unfortunately it is not possible to convert these results reciprocally by just a simple transformation formula in design rules based on the classical Wöhler approach. For that reason the existing design rules can be applied to HPC as well due to its unnecessarily conservative formulation.

7.7 Acknowledgment

The valuable contribution of Mr. Hammer, SINTEF, Norway is gratefully acknowledged.

8 Temperature effects

8.1 Range of application

In this chapter the effect of substantial deviations from a mean concrete temperature of 20 °C in the range of approximately 0 °C to +80 °C is dealt with.

8.2 Maturity

The rate of hydration of cement increases with increasing temperature. Consequently, the mechanical properties of concrete and their development with time are also influenced by the temperature of the concrete and of the surrounding environment. In order to quantify the effect of temperature on concrete properties the maturity concepts are generally applied.

As an alternative to maturity also the concrete age may be adjusted in order to take temperature effects into account: If the concrete temperature deviates from 20 °C then the *effective* or the *equivalent concrete age* corresponds to the time interval at a temperature T after which the concrete has reached the maturity it would have at a temperature of 20 °C.

The modern maturity concepts are based on thermodynamics. If the well known Arrhenius relation is applied, than a maturity function should have a general form as expressed by Eq. (8-1), refer to e.g. Carino and Tank (1990). This approach holds true for both, normal strength and high strength concrete.

$$M = const \cdot \int_{t_o}^{t_i} e^{-Q/RT} dt \tag{8-1}$$

where: T temperature at a concrete age t [K]
Q activation energy for cement hydration [kJ/mol]
R universal gas constant [kJ/mol · K].

According to CEB-FIP MC 90 the effective concrete age can be estimated from Eq. (8-2) which is based on the maturity function according to Eq. (8-1) and an activation energy for cement hydration of 33 kJ/mol (Müller and Hilsdorf [1993]).

$$t_T = \sum_{i=1}^{n} \Delta t_i \cdot exp\left[13.65 - \frac{4000}{273 + T(\Delta t_i)/T_o} \right] \tag{8-2}$$

where: t_T effective concrete age [days]
$T(\Delta t_i)$ temperature [°C] during the time interval Δt_i [days]
T_o = 1 °C.

The activation energy for cement hydration Q is in the range of 30 < Q < 65 kJ/mol. Since for the derivation of Eq. (8-2) a low bound of the activation energy was chosen it is valid for concretes made of Portland cements or cements containing only low amounts of components other than Portland cement clinker.

According to Carino and Tank (1990) the activation energy not only depends on the type and strength class of cement, but also on the water/cement ratio, additions and admixtures. Since for the production of high strength concrete both additions and admixtures are often used, their effects on the maturity of concrete should be considered. Presently there is no data

basis available, which would enable to propose a modification of Eq. (8-2) in order to consider these influences. Therefore, whenever accurate estimates of temperature effects are required, the activation energy Q should be determined experimentally.

Another approach for the evaluation of the data for high strength concrete was applied by Bergner (1997). He investigated the temperature effect by curing concrete specimens (w/c = 0.33) for 7 days in a climatic chamber at temperatures of 4 °C, 7 °C, 23 °C, 36 °C, 42 °C and 60 °C, respectively (see also section 8.4). For the calculation of the so-called weighed maturity the CEMIJ-method (Weigler and Karl [1989]) was used. According to Eq. (8-3) the weighed maturity R_g is a function of time, temperature and the type of cement.

$$R_g = \sum \left(10 \cdot (C^{(0.1 \cdot T - 1.245)} - C^{-2.245}) / \ln C \right) \cdot \Delta t_i \tag{8-3}$$

where: C a factor, dependent on the cement type, and which can be experimentally determined; $C = 1.3$ for an ordinary Portland cement

T average concrete temperature within Δt_i intervals.

Figure 8-1 shows the compressive strength of concrete as a function of the weighted maturity. Since the symbols for different curing temperatures follow approximately a steadily increasing curve, the proposed relation (Eq. (8-3)) seems to work well also for high strength concrete.

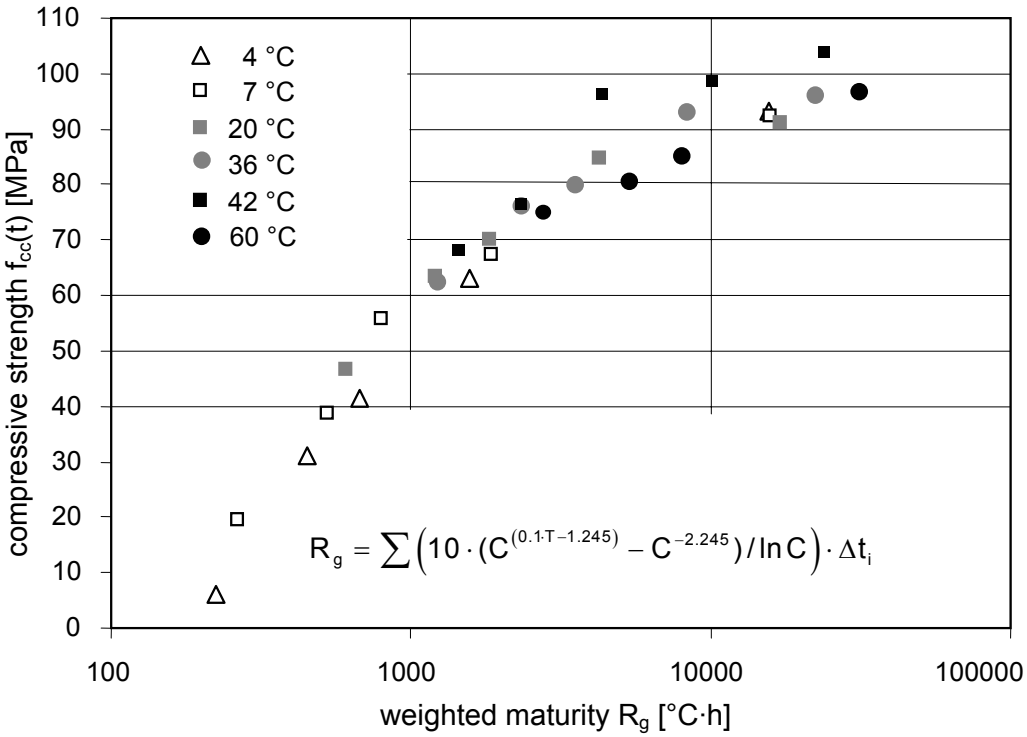

Fig. 8-1: Development of the compressive strength as a function of the weighted maturity

8.3 Thermal expansion

The coefficient of thermal expansion α_{cT} of concrete depends on the coefficients of thermal expansion of the aggregates α_{gT} and of the hydrated cement paste α_{hpT}, on the volume fraction of the aggregates v_g and of the paste v_{hp}, as well as on the moisture state of the concrete. For both, normal strength concrete and high strength concrete, it may be estimated from Eq. (8-4), refer to e.g. Ziegeldorf et al. (1979).

$$\alpha_{cT} = \alpha_{gT} \cdot v_g + \alpha_{hpT} \cdot v_{hp} \tag{8-4}$$

The coefficient of thermal expansion of hydrated cement paste, α_{hpT} primarily depends on the moisture content of the paste and amounts to about $10 \cdot 10^{-6}$ 1/K for water saturated and for very dry paste to a maximum value around $20 \cdot 10^{-6}$ 1/K at a relative humidity of about 70 %.

For the production of high strength concrete various types of aggregates, partly given in Table 8-1, can be used. Generally, the coefficient of thermal expansion of the aggregates increases with an increasing quartz content.

Coefficients of thermal expansion of normal weight concrete, including high strength concrete, range from about $5.5 \cdot 10^{-6}$ 1/K to about $14 \cdot 10^{-6}$ 1/K. Typical values for such concretes in an air-dry state made of different types of aggregates are listed in Table 8-1. They are somewhat lower for water-saturated concrete.

Type of aggregate	Coefficient of thermal expansion $\alpha_{cT} \cdot 10^{-6}$ [1/K]
Quartzitic rock, sand or gravel	12 – 14
Granite, gneiss	9 – 12
Syenite, diorite, gabro, diabase, basalt	8.5 – 11
Dense limestone	6.5 – 9

Table 8-1: Effect of the type of aggregate on the coefficient of thermal expansion of concrete, acc. to Dettling (1962)

For the purpose of structural analysis the same coefficient of thermal expansion as proposed by CEB-FIP MC 1990, i.e. $\alpha_{cT} = 10 \cdot 10^{-6}$ 1/K, may be used also for high strength concrete.

The linear relationship between thermal strain and temperature change, expressed by the coefficient of thermal expansion, holds true only for temperatures in the range of about 0 °C to 60 °C. The coefficient of thermal expansion increases with increasing temperature, in particular for higher temperatures.

8.4 Mechanical properties

The effect of the temperature at the time of testing on the mechanical properties of high strength concrete has not been investigated so far. From the investigations on normal strength concrete without exchange of moisture it is known that for concrete with a higher content of cement paste, which is often the case for high strength concrete, a more pronounced decrease of the strength and stiffness can be observed (Mechtcherine [2000]).

In the cases where a moisture exchange takes place, the effect of temperature on the mechanical properties depends on the size and shape of the member. According to CEB-FIP MC 1990, as a first approximation for the *compressive strength* the effect of the temperature

can be neglected since the reduction in strength due to a temperature increase is offset by an increase in strength due to drying. The effect of drying might however be less pronounced in the case of high strength concrete, which has only a small content of capillary water. So the reduction of the compressive strength with increasing temperature should be higher.

According to CEB-FIP MC 1990 the uniaxial *tensile strength* and the tensile splitting strength are not significantly affected by the temperature at the time of testing. However, newer research results by Mechtcherine et al. (1995) and Slowik (1995) show, that for normal strength concrete a considerable decrease of the uniaxial tensile strength can be observed with increasing temperature. Further, the moisture gradients due to drying cause a significant decrease of the tensile strength, in particular of the uniaxial tensile strength and the flexural strength. The temperature gradients may influence the obtained values of the tensile strength as well.

According to the formula by CEB-FIP MC 1990 the *fracture energy* of concrete decreases significantly with increasing temperature. Though, Mechtcherine et al. (1995) and Slowik (1995) found no effect of the temperature on this material parameter.

In the following sections mainly the data concerning the effect of curing temperature on the mechanical properties will be presented, i.e. the maturity of concrete is the main parameter.

8.4.1 Compressive strength

Bergner (1997) investigated the temperature effect by curing concrete specimens (w/c = 0.33) for 7 days in a climatic chamber at temperatures of 4 °C, 7 °C, 23 °C, 36 °C, 42 °C and 60 °C. Specimens cured at higher temperatures possessed, after 2 days and 7 days, already 80 % and 95 % of the 28 days strength, respectively. Those cured at low temperatures exhibited after 7 days just 70 % of the 28 days strength, cf. Figure 8-2.

Marzouk and Hussein (1990) studied the behaviour of a high strength concrete containing 12 percent of fly ash and 8 percent of silica fume by mass of Portland cement. Cast specimens were cured for 24 hours at a temperature of 20 °C in a climatic chamber and then exposed to ocean water in pre-prepared tanks at 20 °C, 10 °C, 0 °C, -5 °C and -10 °C, respectively, for a time period of 1 to 91 days (the study was carried out with regard to the utilization of the high strength concrete for offshore structures in ocean cold regions).

Figure 8-3 shows a considerably slower strength development at lower temperatures of the applied ocean water compared with the corresponding values for the concrete kept in ocean water at a temperature of 20 °C. With decreasing temperature this tendency becomes more and more pronounced. This effect might be traced back to both, a slower cement hydration and to a low reactivity of the calcium hydroxide, a byproduct of the hydration process. Its reaction with silica fume and fly ash, which is referred to as the secondary hydration process forming a tobermorite gel, can only slowly proceed at low temperatures.

Marzouk and Hussein (1990) found that a logarithmic function according to Eq. (8-5) is in good agreement with their experimental results.

$$f_{cc} = a + b \cdot \log t \tag{8-5}$$

where: f_{cc} compressive strength in MPa
t time in days
a, b constants.

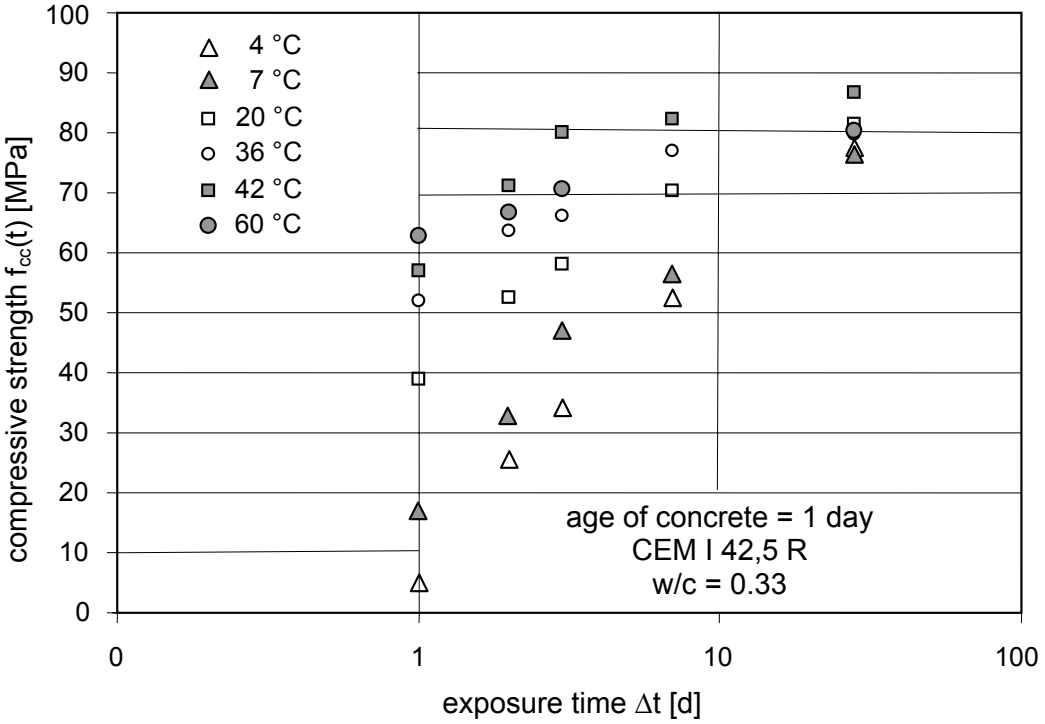

Fig. 8-2: Development of the compressive strength – effect of temperature, acc. to Bergner (1997)

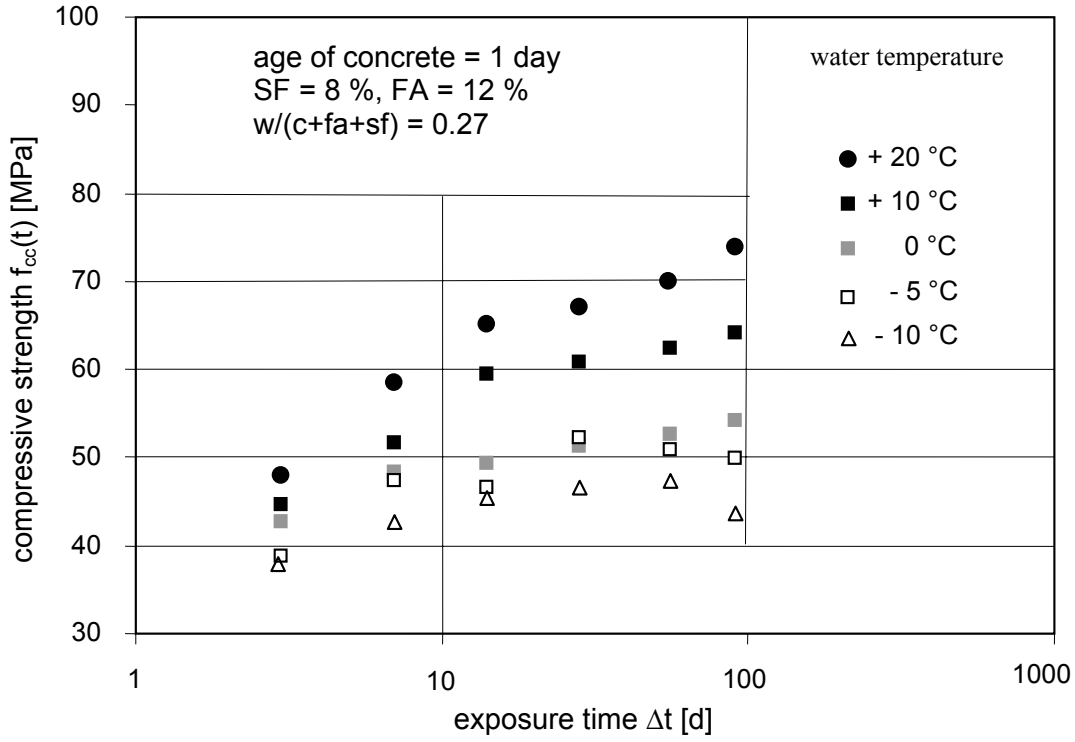

Fig. 8-3: Development of the compressive strength – effect of storage in ocean water at different temperatures, acc. to Marzouk and Hussein (1990)

In a further study Marzouk and Hussein (1995) found out for the same composition of concrete that a prolongation of curing at room temperature of 20 °C from 1 day to 14 or 28 days before placing the specimens into the tanks with cold ocean water very positively affects the strength development, see Figure 8-4.

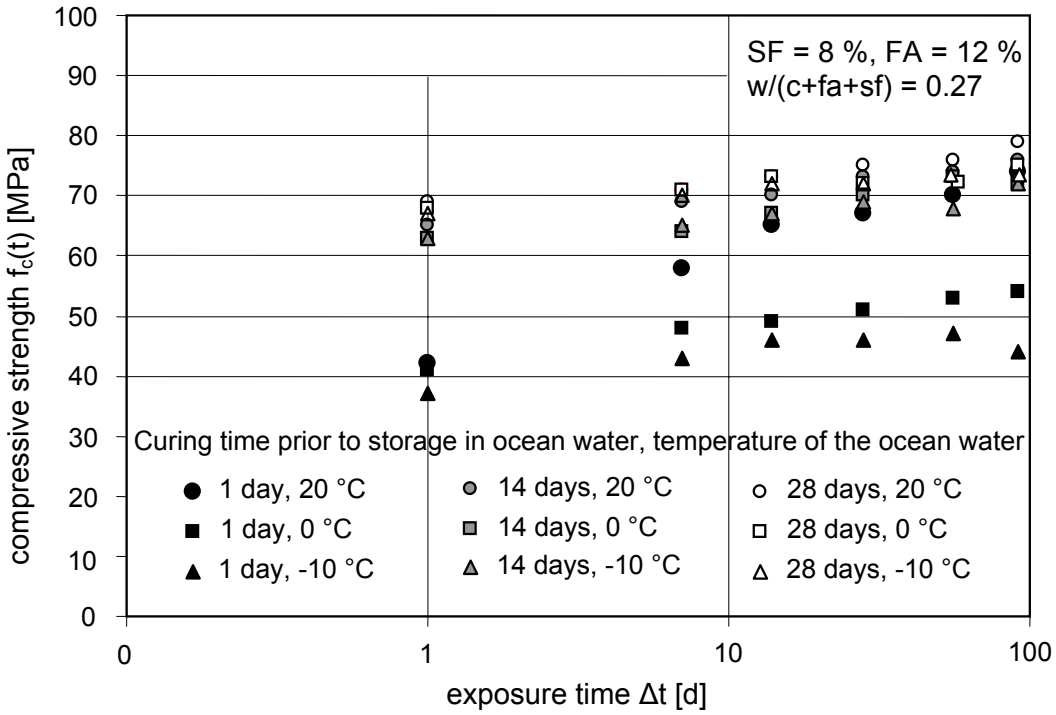

Fig. 8-4: Development of the compressive strength – effect of curing period prior to storage in ocean water, acc. to Marzouk and Hussein (1995)

Wild et al. (1995) investigated the effect of the temperature, storage in water at 20 °C and 50 °C, respectively, on the strength development of a high strength concrete, which contained different amounts of silica fume (SF), between 0 and 24 % by cement weight. The results are presented in Figure 8-5.

At higher concrete ages an apparent increase of the compressive strength of concrete with increasing amounts of silica fume was observed for both series, whereas the effect of silica fume on the strength of concrete stored at the temperature of 50 °C was more pronounced. However, the development of the compressive strength with time was strongly affected by the storage temperature.

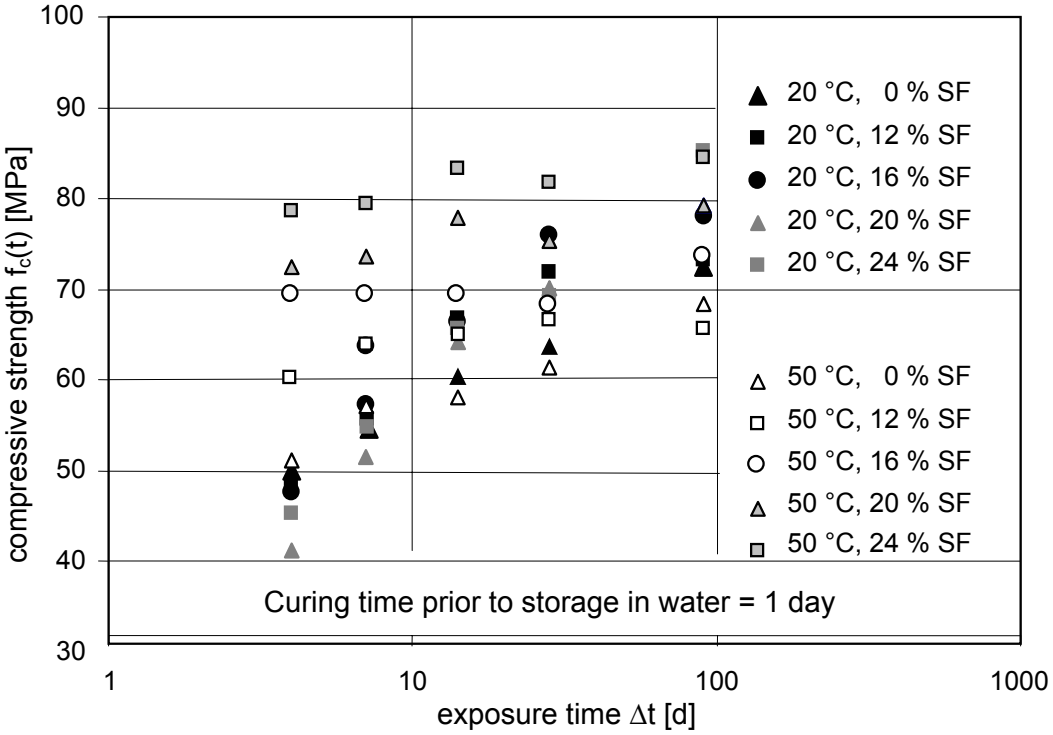

Fig. 8-5: Development of the compressive strength – effect of the content of silica fume and temperature; storage in water, acc. to Wild et al. (1995)

For the storage at the temperature of 20 °C the addition of silica fume causes a decrease of the compressive strength at early concrete age. The explanation might be an increase of the formation of Portlandite due to the presence of silica. Pozzolanic reactions are at this temperature rather slow. With increasing age of concrete the contribution of the reactions between silica fume and Portlandite crystals and as a result the formation of additional C-S-H gel at the interfacial zone between the cement paste and aggregate becomes more and more pronounced. For concretes containing a higher amount of silica fume a higher increase of strength in time could be observed.

At the temperature of 50 °C not only the hydration process of alite and other cement components are faster, but also the pozzolanic reactions proceed at a much higher rate. This results in very high values of the compressive strength for concrete containing a high amount of silica fume, already at an age of 3 days. On the other hand the further increase of the strength is much less pronounced in comparison with concretes stored at the room temperature. This is especially true for concretes with a very high content of silica fume.

8.4.2 Tensile strength and modulus of elasticity

Marzouk and Hussein (1990, 1995) studied the effect of curing in ocean water at different temperatures on the tensile splitting strength and the modulus of elasticity of high strength concrete containing 12 percent of fly ash and 8 percent of silica fume by mass of Portland cement. The results are presented in Figure 8-6 and Figure 8-7, respectively. The same tendencies as for the corresponding compression tests could be observed (see section 8.4.1).

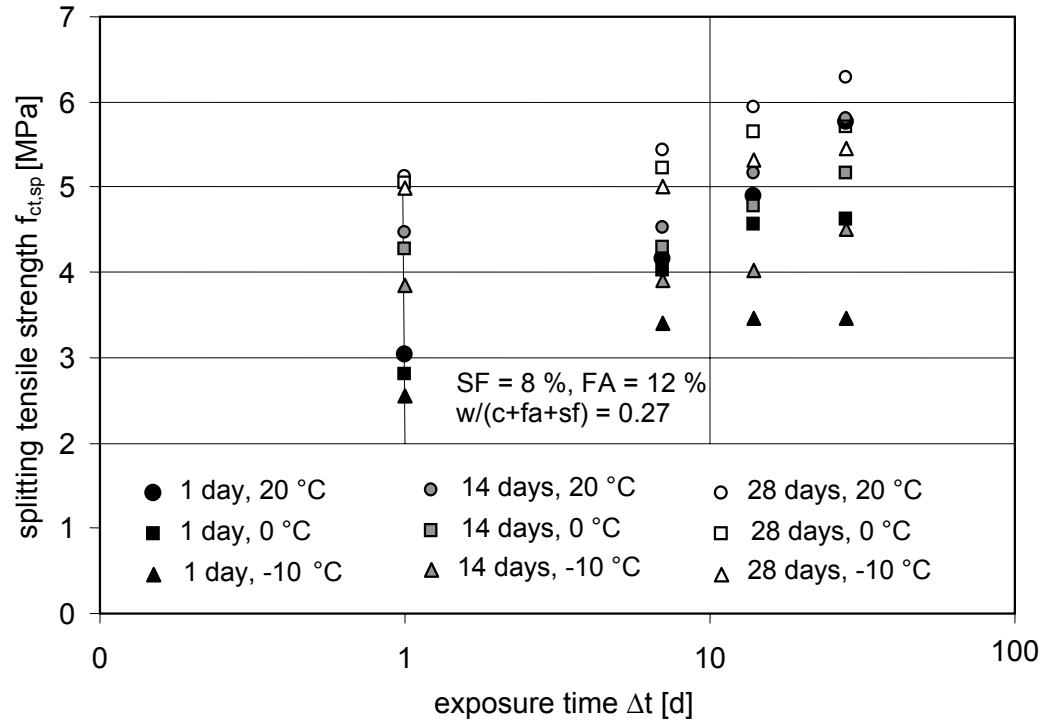

Fig. 8-6: Development of the splitting tensile strength – effect of curing time prior to storage in ocean water, acc. to Marzouk and Hussein (1995)

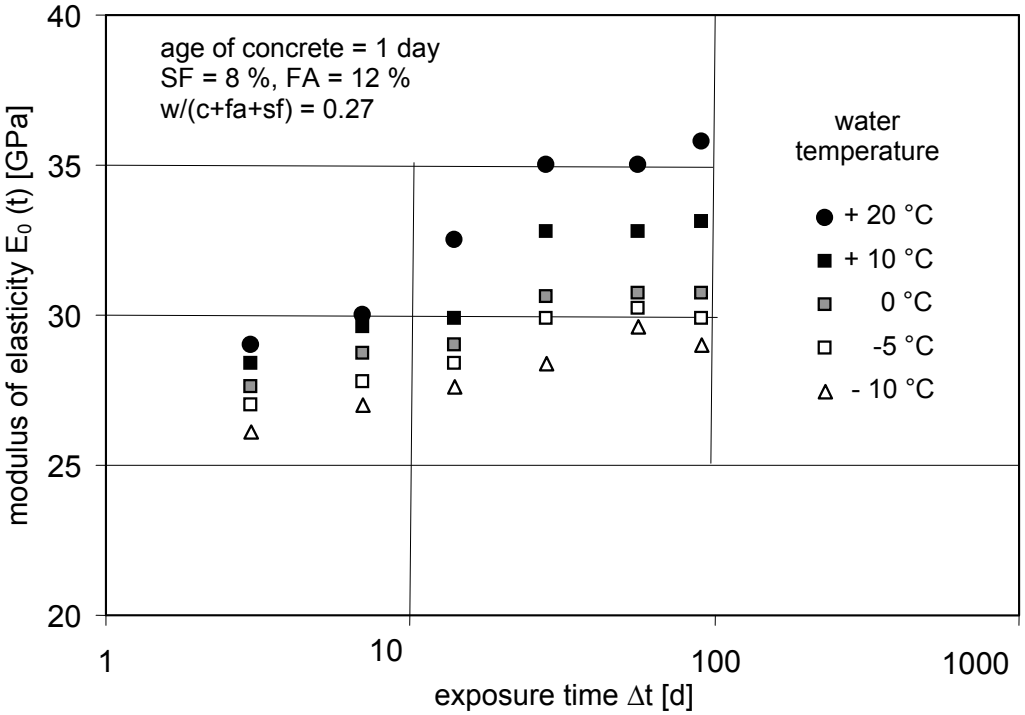

Fig. 8-7: Development of the modulus of elasticity – effect of storage in ocean water at different temperatures, acc. to Marzouk and Hussein (1990)

9 Transport of water, vapour and chloride in hardened concrete

9.1 Introduction

Constitutive laws for estimating the transport of water, vapour and chloride in Portland cement based systems are outlined. The diffusivity, permeability and capillary conditions of concrete are modelled. Normal concrete is regarded as a porous material affected by the ambient climate. A low water-cement ratio, *w/c*, may affect several characteristics of concrete, first of all degree of hydration, α, and curing. The corrosion of reinforcement and the freeze-thaw resistance are factors affected entirely by the lower $w/c \leq 0.40$ of High Performance Concrete, HPC. The chloride diffusion is dependent on w/c of the concrete as well as the diffusion of gas [Tuutti (1982)]. Above a certain degree of pore saturation a substantial amount of surface concrete will spall due to ice lenses created in freeze-thaw periods [Fagerlund (1976, 1994)]. A freeze-thaw resistant concrete must be either air-entrained or contain a sufficient air-filled pore volume developed due to the chemical shrinkage that takes place during the hydration. In this case knowledge of the state of moisture in the concrete is of the utmost importance, too. It was observed that concretes with low *w/c-ratios* show an internal relative humidity, *RH*, substantially lower than 1 even when they were stored under water. It was then of general interest to investigate the diffusivity, permeability and the capillarity of HPC to explain the properties of the material. Mechanisms of moisture transfer may be explained by modelling the diffusivity and the capillary conditions of HPC. Figure 9-1 shows the water diffusivity of cement mortar with *w/c* varying between 0.40 and 0.80 as a function of *RH* [(Nilsson (1977)]. The diffusivity of HP cement mortar ($w/c = 0.40$) was less dependent on *RH* than that of normal cement mortar. Also the resistance to capillary suction, $m = t/h^2$, where *t* is time and *h* is penetration depth, is clearly dependent on *w/c*, Figure 9-2 [Ahlgren et al (1972), Persson (1992)]. Figure 9-2 shows *m* versus the capillary porosity of the paste of cement mortar, $P(cap)_p = (w/c - 0.39\cdot\alpha)/(0.317+w/c)$. Also the coefficient of chloride migration, *D*, is related to *w/c* but also to the cement content and the content of mineral additives of the concrete, Figures 9-3 and 9-4. High efficiency of blast furnace slag on the chloride migration coefficient was observed. On the other hand, slag content in HPC may decrease the frost resistance [Persson (2001)]. The vapour permeability of mature HPC (dependent on *w/c* and *RH*) was substantially lower than that of normal concrete, Figure 9-5 [Persson (1992)].

9.2 Parameters affecting water, vapour and chloride transport in HPC

The main factors affecting water and chloride transport in HPC are *w/c*, α, *RH* and the content of silica fume and other mineral additives. Concrete, which is regarded as a fine porous material, has a great ability to bind moisture and chlorides. The higher *RH*, the more water can be bound. The higher the cement gel content, the more chlorides may be bound. The ability to bind moisture, hygroscopicity, depends on either adsorption, at $RH < 0.45$, or capillary condensation, at $RH \geq 0.45$. HPC possesses less mixing water than necessary to reach the maximum degree of hydration, $\alpha_{max} = 1$. Due to chemical shrinkage, self-desiccation takes place, which lowers *RH* in the concrete until the reaction ceases, at about $RH \approx 0.70$. Silica fume is more or less necessary to use in order to obtain acceptable fresh HPC properties but also for the purpose of the high strength of HPC. The content of silica

fume in HPC affects the moisture properties of HPC as well as the chloride ingress, especially at early ages.

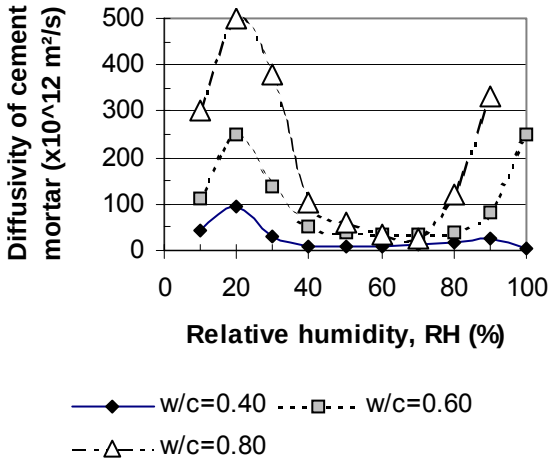

Fig. 9-1: Water diffusivity of cement mortar with different w/c as a function of RH

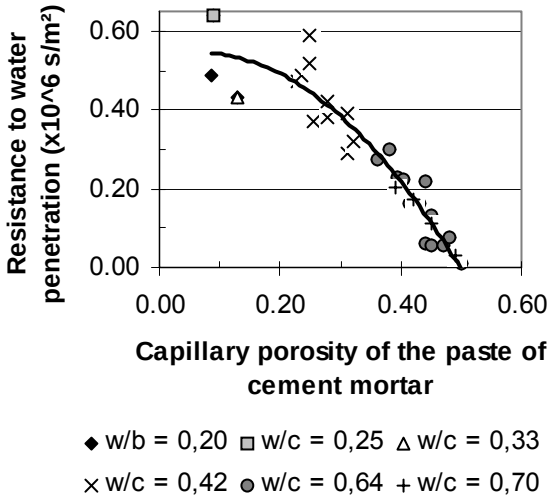

Fig. 9-2: m versus the capillary porosity of the paste of cement mortar, $P(cap)_p$.

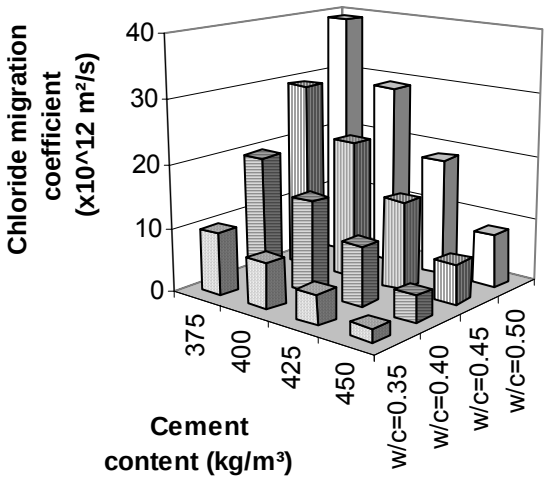

Fig. 9-3: Influence of w/c and cement content on the chloride migration coefficient

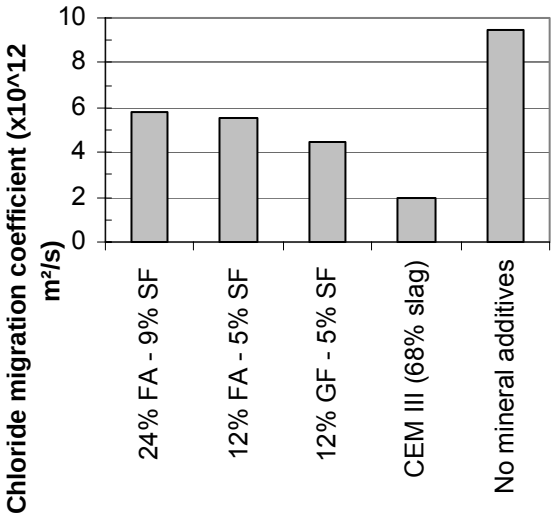

Fig. 9-4: Influence of mineral additives on the chloride migration coefficient. FA = fly ash, GF = glass filler, SF = silica fume

9.3 Constitutive laws for transport of water, vapour and chloride

A general relationship for transport of water in concrete exists [Persson 1992)]:

$$m = -2.911 \cdot P(cap)_p^2 + 0.3783 \cdot P(cap)_p + 0.533 \qquad \{R^2 = 0.91\} \qquad (9\text{-}1)$$

where

m = t/h^2 the resistance to capillary suction (s/m²)
t time (s)
h penetration depth ($0.005 < h < 0.03$ m)

For vapour transport of mature HPC the following correlation was found [Persson (1992)]:

$$\delta_c = (97.4 \cdot (RH) - 59) \cdot (w/c)^2 - (66.6 \cdot (RH) - 41.5) \cdot w/c + 14.2 \cdot (RH) - 9.7 \qquad (9\text{-}2)$$

where

w/c denotes the water-cement ratio ($0.25 < w/c < 0.50$)
RH denotes the relative humidity ($0.90 < RH < 0.95$)
δ_c denotes the vapour permeability of HPC ($x10^6$ m²/s)

The vapour permeability of mature HPC seems to have a minimum at w/c ≈ 0.30. The reason for this may be compaction problems at w/c < ≈ 0.30. At larger depth of the concrete, especially of HPC, the water transport is more or less prohibited by internal forces mainly due to autogenous shrinkage [Persson (1997, 1997a)]. Even after 13 years of water curing concrete did not obtain saturation, Figure 9-6. Long-term RH in 1 m diameter concrete columns was correlated in the following way [Persson (1996)]:

$$RH_A = 0.91 \cdot (w/c)^{0.2322} \qquad \{R^2 = 0.93\} \qquad (9\text{-}3)$$
$$RH_S = 0.96 \cdot (w/c)^{0.1989} \qquad \{R^2 = 0.82\} \qquad (9\text{-}4)$$
$$RH_W = 0.84 \cdot (w/c)^{-0.0152} \qquad \{R^2 = 0.52\} \qquad (9\text{-}5)$$

where

A denotes air curing
RH denotes long-term RH in 1 m diameter columns after 13 years
S denotes sealed curing
W denotes water curing

The following equation for the chloride migration coefficient, D, is based on studies on concretes with a low-alkali CEM I 42.5 BV/SR/LA cement (C_3A = 1.7 % and C_4AF = 13 %), typical for HPC production [Persson (2001)]:

$$D = \{[(0.0055 \cdot ln(t) - 0.2122) \cdot c - 3.5 \cdot ln(t) + 104] \cdot (4 \cdot w/b - 1.2)/0.4\} \cdot (10^{-12}) \ \{R^2 = 0.88\} \qquad (9\text{-}6)$$

where

c denotes the cement content ($375 < c < 450$ kg/m³)
D denotes D ($\cdot 10^{-12}$ m²/s)
$ln(t)$ denotes the natural logarithm of concrete age ($1 < t < 36$ months)
w/b denotes the water-binder ratio, 1:1 ($0.35 < w/b < 0.50$)

The following equation was obtained for the Pozzolan interaction between Portland cement and additions of silica fume, fly ash and slag as regards *D* [Boubitsas (2000), CTH Nordtest 492, Tang (2000), Persson (2001, 2001a)]:

$$c_{eq.} = c + 0.2 \cdot fl + 1.6 \cdot sf + 1.0 \cdot sl \qquad \{R^2 = 0,81\} \qquad (9\text{-}7)$$

where

$c_{eq.}$ denotes the equivalent amount of cement to be used in equation (9-6)
fl denotes the amount of fly ash ($0.1 < (fl/c) < 0.25$)
sf denotes the amount of silica fume ($0.05 < (sf/c) < 0.12$)
sl denotes the amount of slag ($0 < (sl/c) < 0.70$)

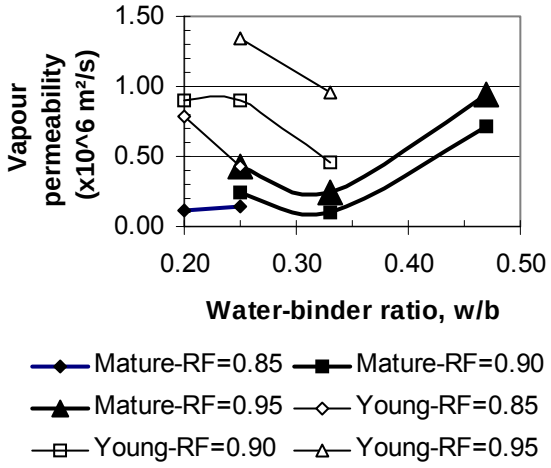

Fig. 9-5: The vapour permeability of mature and young HPC at varying w/c and RH

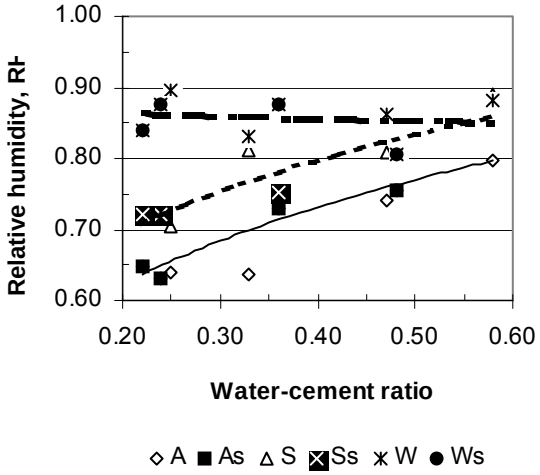

Fig. 9-6: Long-term RH in 1 m concrete columns versus w/c. s = 10% silica fume, A = air curing, S = sealed, W = water

9.4 Conclusions

Constitutive laws for estimating the transport of water, vapour and chloride in Portland cement based systems were outlined. The diffusivity, permeability and capillary conditions of concrete were modelled. HPC generally exhibited lower water and chloride transport coefficients than normal concrete. For vapour transport a minimum transport coefficient seems to exist at w/c ≈ 0.30 (thus increasing at lower and larger w/c than 0.30).

References

ACI - American Concrete Institute: ACI 03.95 – R8860, State-of-the-Art Report on Dynamic Fracture, ACI Committee 446, 1995.

ACI - American Concrete Institute: ACI 209.3R-XX, Time Dependent Effects in Concrete Structures, Reported by ACI Committee 209, M. A. Chiorino and W. Dilger Editors, Draft November 2007

Ahlgren, L., Bergström, S. G., Fagerlund, G., Nilsson, L.-O.: Moisture binding in Porous Building Materials, Report 36, Div. of Building Physics, Lund Institute of Technology, Lund, 1972.

Al-Kubaisy, M.A., Young A.G.: Failure of concrete under sustained tension. Magazine of Concrete Research, Vol. 27, 1975, 171-178.

Alliche, A., Francois, D.: Damage of Concrete in Fatigue. ASCE Journal of Engineering Mechanics, Vol. 118, No. 11, 1992.

Alonso Junghanns, M.T.: Zur Risssicherheit zementgebundener dehnungsbehinderter Schichten unter Berücksichtigung von Dauereinflüssen. Dissertation, TU Hamburg-Harburg, Shaker Verlag, Aachen 1998.

Altoubat, S.A., Lange, D.A.: Tensile basic creep: Measurements and behaviour at early age. ACI Materials Journal Vol. 98 No. 5, September-October 2001, pp. 386-393.

Altoubat, S.A., Lange, D.A.: The Pickett effect at early age and experiment separating its mechanisms in tension. Materials and Structures / Matériaux et Constructions, Vol. 35, May 2002, 211-218.

ASTM E 104-85: Standard Practice for Maintaining Constant RH by Means of Aqueous Solutions. ASTM. Philadelphia, 1985, pp. 33-34, 637.

Bache, H.H.: Densified Cement/Ultra-fine Particle-Based Materials. 2. International Conference on Superplasticizers in Concrete, Ottawa, 1981; also published by Aalborg Portland-Cement-Fabrik, DK-9100 Aalborg Denmark, pp. 1-35.

Barpi, F., Ferrara, G., Imperato, L., Valente, S.: Lifetime of concrete dam models under constant loads. Materials and Structures / Matériaux et Constructions, Vol. 32, March 1999, 103-111.

Bažant Z.P. (1972a): "Numerical Determination of Long-range Stress History from Strain History in Concrete", Materials and Structures, Vol. 5, 1972, pp. 135-141.

Bažant, Z.P. (1972b): "Prediction of Concrete Creep Effects Using Age-adjusted Effective Modulus Method", Journal of the American Concrete Institute, V. 69, 1972, pp. 212-217.

Bazant, Z.P., Kazemi, M. T., Hasegawa, T., Mazars, J.: Size effect in Brazilian split-cylinder test: measurements and fracture analysis. ACI Materials Journal, Vol. 88, No. 3, 1991, pp. 325-332.

Bažant, Z.P., Schell, W.F.: Fatigue Fracture of High-Strength Concrete and Size-Effect. ACI Materials Journal, Vol. 90, No. 5, 1993.

Bergner, H.: Rissbreitenbeschränkung zwangbeanspruchter Bauteile aus hochfestem Normalbeton. Deutscher Ausschuss für Stahlbeton, Heft 482, Beuth Verlag GmbH, Berlin, Wien, Zürich, 1997.

Bissonnette, B., Pigeon, M.: Tensile creep at the early ages of ordinary, silica fume and fiber reinforced concretes. Cement and Concrete Research Vol. 25, No. 5, 1995, pp. 1075-1085.

Bissonnette, B., Pigeon, M.: Viscoelastic behaviour of concrete in tension and dimensional compatibility of concrete repairs. Materials and Structures / Matériaux et Constructions, Vol. 33, March 2000, 108-118.

Blaschke, F., Losekamp, Ch., Mehlhorn, G.: Zugtragvermögen nach lang andauernder statischer sowie schwellender Zugvorbelastung von Beton. Forschungsbericht Nr. 20 aus dem Fachgebiet Massivbau der Gesamthochschule Kassel, 1993.

Boubitsas, D., Paulou, K.: SCC for Marine Environment, TVBM-5048, Lund Institute of Technology, Lund, 2000, 55 pp.

Buyukozturk, O., Tseng, T.-M.: Concrete in Biaxial Cyclic Compression. ASCE Journal of Structural Engineering, Vol. 110, Nr. 3, 1984.

Carino, N. J., Tank, R. C.: Maturity functions for concrete made with various cements and admixtures. In: Testing During Construction, Proceedings o f an International RILEM Workshop, Chapman and Hall, 1990, pp. 192-206.

Carpinteri, A., Valente, S., Zhou, F.P., Ferrara, G., Melchiorri, G.: Tensile and flexural creep rupture tests on partially damaged concrete specimens. RILEM Materials and Structures, Vol. 30, 1997, 269-276.

Carrasquillo, P. M., Carrasquillo, R. L.: Evaluation of the use of current concrete practice in the production of high strength concrete. ACI Materials Journal, Vol. 78, No. 14, 1981, pp. 171-178.

Carrasquillo, R. L., Nilson, A. H., Slate, F. O.: Properties of high strength concrete subjected to short-term loads. ACI Journal, May-June 1981, pp. 171-178.

CEB – Comité Euro-international du Béton: CEB Design Manual on Structural Effects of Time-dependent Behaviour of Concrete, M. A. Chiorino Chairman of Editorial Team, CEB Bulletin d'Information No. 142-142 Bis, March 1984.

CEB – Comité Euro-international du Béton: State of the Art Report, Fatigue of Concrete Structures. CEB Bulletin D'Information, No. 188, 1988.

CEB – Comité Euro-international du Béton: State of the Art Report, High Strength Concrete. CEB Bulletin d'Information, No. 197, 1990.

CEB – Comité Euro-international du Béton: Evaluation of the time dependent behavior of concrete. CEB Bulletin d'Information, No. 199, 1990.

CEB – Comité Euro-international du Béton: Revision of the design aids of the CEB Design Manual Structural Effects of Time-dependent Behaviour of Concrete in accordance with the CEB-FIP Model Code 1990, (principal authors M. A. Chiorino and G. Lacidogna), CEB Bulletin d'Information, No. 215, 1993.

CEB – Comité Euro-international du Béton: CEB-FIP Model Code 1990, Bulletin d'Information, No. 213/214, Thomas Telford Ltd., London, 1993.

CEB – Comité Euro-international du Béton: State of the Art Report, High Performance Concrete, Recommended Extensions to the Model Code 90, Research Needs. CEB Bulletin d'Information, No. 228, 1995.

Cetin, A., Carrasquillo, R. L.: High-performance concrete: Influence of coarse aggregates on mechanical properties, ACI Materials Journal, technical paper, title No. 95-M24, May-June 1998, pp. 252-261.

Chiorino M.A.: A Rational Approach to the Analysis of Creep Structural Effects, in: J. Gardner and J. Weiss Editors, Shrinkage and Creep of Concrete, ACI American Concrete Institute SP-227, 2005, pp. 107-141.

Cook, J. E.: 10,000 psi concrete. Concrete International, Vol. 11, No. 10, 1989, pp. 67-75.

CTH Rapid Test for Determination of D in Concrete, NT BUILD 492, 2000.

Dahl, K.: A Constitutive Model for Normal and High Strength Concrete. Dissertation, Danmarks Tekniske Højskole, Lynhby, 1992.

Dargel, H. J.: Zur rechnerischen Analyse von Stahlbetontragwerken unter stoßartiger Beanspruchung. Dissertation, Darmstadt, 1985.

de Larrard, F., Acker, P.: Creep in high and very high performance concrete. High Performance Concrete - From material to structure, edited by Y. Malier, E & FN Spon, Paris, 1992, pp. 115-126.

Dettling, H.: Die Wärmedehnung des Zementsteins, der Gesteine und der Betone. Schriftenreihe des Otto-Graf-Instituts der Technischen Hochschule Stuttgart, No. 3, Stuttgart, 1962.

Dilger, W. (1998): Private communication, 1998.

Dilger, W. H. et al.: Shrinkage and creep of high-performance concrete (HPC). Proceedings Adam Neville Symposium on Concrete Technology, Las Vegas Nev. USA, V. M. Malhotra (ed.), CANMET, June 1995, pp. 59-84.

DIN 1048-5: Prüfverfahren für Beton, Festbeton, gesondert hergestellte Probekörper, Juni 1991.

Dipartimento di Ingegneria Strutturale e Geotecnica, Politecnico di Torino: www.polito.it/creepanalysis, 2004-2007

Duda, H.: Fracture Mechanical Behaviour of Concrete under Monotonic and Cyclic Tensile Loading (in German). Deutscher Ausschuss für Stahlbeton, Heft 419, Beuth Verlag, Berlin, 1991.

EN 12394 [1996]: Testing Concrete - Determination of Compressive Strength of Test Sprecimen. 1996.

ENV 1992-1 (1991), European Committee for Standardization (CEN), ENV 1992-1, Design of Concrete Structures. Part 1: General rules and rules for buildings, 1991.

Fagerlund, G.: Influence of Environmental Factors on the Frost Resistance of Concrete, TVBM-3059, Lund Institute of Technology, Lund, 1994, pp. 19-22.

Fagerlund, G.: The Critical Degree of Saturation Procedure - A General Procedure of Estimating the Frost Resistance of Materials and Structures, Report Fo 12:76, The Cement and Concrete Research Institute, Stockholm, 1976.

Franke, L.: Schadensakkumulation und Restfestigkeit im Licht der Bruchmechanik. Fortschritte im konstruktiven Ingenieurbau, Gallus Rehm zum 60. Geburtstag, Ernst & Sohn, Berlin 1984, pp. 187-197.

Frénaij, J.: Time dependent shear transfer in cracked reinforced concrete. Dissertation, TU Delft 1989.

Gardner, N. J., Zhao, J. W.: Creep and shrinkage revisited. ACI Materials Journal, Vol. 90, No. 3, 1993, pp. 236-246.

Giaccio, G., Rocco, C., Zerbino, R.: The fracture energy (G_F) of high-strength concretes. Materials and Structures, Vol. 26, 1993, pp. 381-386.

Gopalaratnam, V.S., Shah, S.P.: Softening Response of Plain Concrete in Direct Tension. ACI Journal, Vol. 82, No. 27, 1985.

Grimm, R.: Einfluss bruchmechanischer Kenngrößen auf das Biege- und Schubtragverhalten hochfester Betone. Doctoral thesis, Technical University of Darmstadt, Civil Engineering, 1996.

Guénot-Delahaie, I.: Contribution à l'analyse physique et à la modélisation du fluage propre du béton. Laboratoire Central des Ponts et Chaussées, Série Ouvrages d'Art OA25, Paris, 1997.

Guse U., Hilsdorf, H.K.: Surface Cracking of High Strength Concrete. Proc. of the 4th Weimar Workshop on High Performance Concrete, High Performance Concrete: Material Properties and Design, eds. F. H. Wittmann and P. Schwesinger, AEDIFICATIO Verlag, Freiburg und Unterengstringen, p. 69-89, 1995.

Guse, U., Hilsdorf, H.K.: Dauerhaftigkeit hochfester Betone. DAfStb Heft 487, Beuth Verlag GmbH, Berlin 1998.

Gutierrez, P. A., Canovas, M. F.: The modulus of elasticity of high performance concrete. Materials and Structures, Vol. 28, 1995, pp. 559-568.

Gylltoft, K.: A Fracture Mechanics Model for Fatigue in Concrete. Materials and Structures, Vol. 17, No. 97, 1984.

Hampel, T., Scheerer, S., Speck, K., Curbach, M.: High Strength Concrete under Biaxial and Triaxial Loading. Proceedings of the 6th International Symposium on Utilization of High Strength/High Performance Concrete, Vol. 2, Leipzig, Germany, 2002, pp. 1027-1036.

Han, N., Walraven, J. C.: Creep and Shrinkage of Young High Strength Concrete. Proc. of the 4th International Symposium on Utilization of High-Strength/High-Performance Concrete, Paris, France, pp. 339-348, 1996.

Han, N., Walraven, J.C.: Creep and shrinkage of high strength concrete. Progress in Concrete Research Vol. 5, Delft University of Technology, 1997, pp. 3-12.

Han, N., Walraven, J.C.: Sustained loading effects in high strength concrete. Proceedings High-Strength Concrete 1993, I. Holand and E. Sellevold eds., Vol. 2, Lillehammer, 1993, pp. 1076-1083.

Hansen, E. A., Leive, M., Rodriguez, J., Cather, R.: Mechanical Properties of High Strength Concrete - Influence of test Conditions, Specimens and Constituents. Proceedings of Fourth International Symposium on the Utilization of High Strength / High Performance Concrete, I. Holand and E.J. Sellevold (eds.), Vol. 2, Paris, France, 1996, pp. 187-196.

Hansen, E. J., Hansen, K. K., Persson, B.: Concrete, hardened: Self-desiccation. Nordtest Procedure NT Build 490, NORDTEST OY, Espoo, Finland, 1999, 8 pp.

Haque, M. N., Kayali, O.: Properties of high-strength concrete using a fine fly ash. Cement and Concrete Research, Vol. 28, No. 10, 1998, pp. 1445-1452.

Hashin, Z.: Analysis of composite materials: A survey. Journal of Applied Mechanics, Vol. 16, 1983, pp. 481/505.

Heinrich, U., Seyfarth, K., Stark, J.: Dauerhaftigkeit von Hochleistungsbeton. DAfStb, 37. Forschungskolloquium, Bauhaus-Universität Weimar, 1999, pp. 145-155.

Held, M.: Ein Beitrag zur Herstellung und Bemessung von Druckgliedern aus hochfestem Normalbeton (B 60 – B 125). Dissertation, Darmstadt, 1994.

Hillerborg, A.: Analysis of one Single Crack. in: Fracture Mechanics of Concrete. F. H. Wittmann, Elsevier Science Publishers, Amsterdam, 1983.

Hilsdorf, H. K: Concrete. In: Concrete Structures Euro-Design Handbook. Ernst & Sohn Verlag, Berlin, 1995.

Hilsdorf, H.K., Müller, H.S.: Concrete. In: Structural Concrete, CEB/FIB Manual Textbook: Textbook on Behaviour, Design and Performance, Volume 1, 1999.

Holmen, J.O.: Fatigue of Concrete by Constant and Variable Amplitude Loading. Division of Concrete Structures, Norwegian Institute of Technology, University of Trondheim, 1979.

Hordijk, D.A.: Local Approach to Fatigue of Concrete. Doctoral Thesis, Delft University of Technology, Delft, 1991.

Hu, X.-Z., Wittmann, F. H.: Experimental method to determine extension of fracture process zone. Journal of Materials in Civil Engineering, Vol. 2, 1990, pp. 15-23.

Hussein, A., Marzouk, H.: Behavior of High-Strength Concrete under Biaxial Loading. Applied Science Technical Report Series, East Report No. 98003, Memorial University of Newfoundland, St. John's, Canada, 1998.

Igarashi, S., Bentur, A., Kovler, K.: Autogenous shrinkage and induced restraining stresses in high-strength concretes. Cement and Concrete Research Vol. 30 (2000), pp. 1701-1707.

Immam, M., Vandewalle, L., Mortelmans, F.: Are current concrete strength tests suitable for high strength concrete? Materials and Structures, Vol. 28, 1995, pp. 384-391.

Ipatti, A.: Effect of size, shape and end conditions of test specimens on compressive strength of HSC. Helsinki, 1992.

Iravani, S.: Mechanical properties of high-performance concrete. ACI Materials Journal, title No. 93-M47, September-October 1996, pp. 416-426.

Jaccoud, J. P., Farra, B., Leclercq, A.: Tensile Strength - Modulus of Elasticity - Bond - Tension Stiffening - Limit State of Cracking. Report to the Joint CEB/FIP Working Group on HSC/HPC. IBAP, EPF Lausanne, March 1995.

Jensen, J. J.: Ductility of High Strength Concrete at High Rate Loading. 3rd International Symposium on Utilization of High Strength Concrete/High Performance Concrete, Lillehammer, 1993, pp. 241-250.

Jianyong, L., Pei, T.: Effect of slag and silica fume on mechanical properties of high strength concrete. Cement and Concrete Research, Vol. 27, No. 6, 1997, pp. 833-837.

Karsan, I.D., Jirsa, J.O.: Behaviour of Concrete under Compressive Loads. Journal of the Structural Division, Vol. 95, Nr. ST12, 1969.

Kessler-Kramer, C., Diehl, K., Mechtcherine, V., Müller, H.S.: High Strength Concrete under Cyclic Tensile Loading. Proceedings of the 6th Int. Symposium on Utilization of High Strength/High Performance Concrete, Leipzig, 2002.

Kessler-Kramer, C., Mechtcherine, V., Müller, H.S.: Fracture Mechanical Assessment of Railway Superstructures made of Concrete. 11th International Conference on Fracture, Turin, Italy, 2005.

Kessler-Kramer, C.: Tensile Structural Behaviour of Concrete under Fatigue Loading (in German). Series of the Institute of Concrete Structures and Building Materials, University of Karlsruhe, Vol. 49, 2002.

Khatri, R. P., Sirivivatnanon, V., Gross, W.: Effect of different supplementary cementitious materials on mechanical properties of high performance concrete. Cement and Concrete Research, Vol. 25, No. 1, 1995, pp. 209-220.

Khayat, H. K., Bickley, J. A., Hooton, R. D.: High-strength concrete properties derived from compressive strength values. Cement, Concrete and aggregates, ASTM, Vol. 17, No. 1, June 1995, pp. 126-133.

Khedr, S. A., Abou-Zeid, M. N.: Characteristics of silica-fume concrete. Journal of Materials in Civil Engineering, Vol. 6, No. 3, Aug. 1994, pp. 356-375.

Kim, J.-K., Kim, Y.-Y.: Experimental Study of the Fatigue Behavior of High Strength Concrete. Cement and Concrete Research, Vol. 26, No. 10, 1996.

Kim, J.-K., Kim, Y.-Y.: Fatigue Crack Growth of High-Strength Concrete in Wedge-Splitting Test. Cement and Concrete Research, Vol. 29, 1999.

König, G., Danielewicz, I.: Fatigue Strength of Reinforced and Prestressed Concrete Members with Comments on the Design Calculations According CEB-FIP Model Code 1990 (in German). Deutscher Ausschuss für Stahlbeton, Nr. 439, Beuth Verlag, Berlin, 1994.

König, G., Remmel, G.: Tensile behaviour of high-strength concrete (HSC). Darmstadt Concrete, Vol. 7, pp. 247-256, 1992.

Kovler, K., Igarashi, S., Bentur, A.: Tensile creep behavior of high strength concretes at early ages. Materials and Structures / Matériaux et Constructions, Vol. 32, June 1999, pp. 383-387.

Kupfer, H., Hilsdorf, H. K., Rüsch, H.: Behavior of concrete under biaxial stresses. ACI Journal, Vol. 66, No. 8, 1969.

L'Hermite R.G., Mamillan, M., Lefèvre C.: Nouveaux résultats de recherches sur la déformation et la rupture du béton. Annales de l'Institut Technique du Bâtiment et des Travaux Publics, Vol. 18, No. 207-208, p. 323-360; see also International Conference on the Structure of Concrete, Cement and Concrete Association, London, p. 423-433, 1965.

Lambotte, H., Taerwe L.: Fatigue of Plain High Strength Concrete subjected to Flexural Tensile Stresses. Proceedings, Utilization of High Strength Concrete, Stavanger, 1987.

Lan, S., Guo, Z.: Biaxial Compression Behaviour of Concrete under Repeated Loading. ASCE Journal of Materials in Civil Engineering, Vol. 11, No. 2, 1999.

Le Roy, R., De Larrard, F.: Creep and Shrinkage of High-Performance Concrete: The LCPC Experience. Proc. of the 5th RILEM Symposium, Creep and Shrinkage of Concrete, eds. Z. P. Bažant and I. Carrol, E & FN Spon, London, pp. 499-504, 1993.

Le Roy, R., De Larrard, F., Pons, G.: The AFREM Code Type Model for Creep and Shrinkage of High Performance Concrete. Proc. of the 4th International Symposium on Utilization of High-Strength/High-Performance Concrete, Paris, France, pp. 387-396, 1996.

Lerner, A.: Zeit- und Temperatureinflüsse auf die mechanischen Eigenschaften von hochfestem Beton. Vertieferarbeit, Institut für Massivbau und Baustofftechnologie, Universität Karlsruhe, 2000.

Maage, M., Smeplass, S., Johansen, R.: Long term strength of high strength silica fume concrete. High-Strength Concrete, Second International Symposium, ACI, Weston T. Hester ed., 1990, pp. 399-408.

Maage, M.: Strength and heat development in concrete: Influence of fly ash and condensed silica fume. American Concrete Institute Special Publication SP-91, 1986, pp. 923-940.

Malhotra, V. M, Carette, G. G., Sivasundaram, V.: Role of silica fume in concrete: a review. In: Advances in Concrete Technology, V. M. Malhotra (ed.), 1994, pp. 915-990.

Malvar, L., Crawford, E.: Dynamic increase factors for concrete. 28. DDESB seminar Orlando, Florida, 1998.

Markeset, G.: Failure of Concrete under Compressive Strain Gradients. Doktor Ingeniøraforhandling 1993:110, Institutt for Konstruksjonsteknikk, Norsge Tekniske Høgskole Trondheim. 1993.

Marzouk, H., Hussein, A.: Effect of curing age on high-strength concrete at low temperatures. Journal of Materials in Civil Engineering, August 1995, pp. 161-167.

Marzouk, H., Hussein, A.: Properties of high-strength concrete at low temperatures. ACI Materials Journal, technical paper, title No. 87-M19, March-April 1990, pp. 167-171.

Masuda, Y., Nakamura, S.: Experimental study on mix proportion and properties of high-strength concrete using high-blaine fly-ash. Conference on Utilization of HSC/HPC, 1999, pp. 1237-1243.

Mattock, A.: Shear transfer in concrete having reinforcement at an angle to the shear plane. ASCE Special Publication 42, "Shear in reinforced concrete", Michigan 1974, pp. 17-42.

Mau, S.T., Hsu, T.C., PCI Journal, Vol. 33, No. 1, Jan/Feb. 1988, pp. 166-170.

Mechtcherine, V., Garrecht, H., Hilsdorf, H. K.: Effect of temperature and loading rate on fracture behaviour of concrete subjected to uniaxial tension. Fracture Mechanics of Concrete Structures, F. H. Wittmann (ed.), Aedificatio Publishers, 1995, pp. 719-728.

Mechtcherine, V., Müller, H. S.: Effect of the test set-up on fracture mechanical parameters of concrete. Fracture Mechanics of Concrete Structures, H. Mihashi and K. Rokugo (eds.), Aedificatio Publishers, 1998, pp. 377-386.

Mechtcherine, V., Müller, H. S.: Fracture mechanical and fractological investigations on normal and high strength concrete. Proceedings of the Fifth International Symposium on Brittle Matrix Composites, A. M. Brand, V. C. Li and I. H. Marshall (eds.), Woodhead Publishing Ltd./Cambridge - Bigraf/Warshaw, 1997, pp. 231-240.

Mechtcherine, V., Müller, H.S.: Fracture Mechanical, Fractological and Numerical Investigations on the Failure Mechanisms of HPC. Proceedings of the 6th Int. Symposium on Utilization of High Strength/High Performance Concrete, Leipzig, 2002.

Mechtcherine, V.: Fracture Mechanical and Fractological Investigation on the Crack Propagation in Concrete (in German). Series of the Institute of Concrete Structures and Building Materials, University of Karlsruhe, Vol. 40, 2000.

Meyer, J.: Ein Beitrag zur Untersuchung der Verformungsfähigkeit von Bauteilen aus Beton unter Biegedruckbeanspruchung. Doctoral thesis. Institut für Massivbau und Baustofftechnologie. Universität Leipzig, 1998.

Mindess, S.: Relationships between Strength and Microstructure for Cement-Based Materials: An Overview. Materials Research Society Symposia, Proceedings, Vol. 42, 1984 pp. 54-68.

Mola, F., Pisani, M.A.: Creep Analysis of Non-Homogeneous Concrete, Proceedings of the Fifth International RILEM Symposium on Creep and Shrinkage of Concrete, Z. P. Bazant and I. Carol ed., E & FN Spon, London, 1993, pp. 597-602.

Mucha, S.: Determination of Crack Growth in Different High Strength Concretes caused by Fatigue Loading. LACER 8, University of Leipzig, 2003.

Müller, H. S., Küttner C. H.: Characteristics and Prediction of Creep of High Performance Concrete. Proc. of the 4th Weimar Workshop on High Performance Concrete, High Performance Concrete: Material Properties and Design, eds. F. H. Wittmann and P. Schwesinger , AEDIFICATIO Verlag, Freiburg und Unterengstringen, p. 145-162, 1995.

Müller, H. S., Küttner C. H.: Creep of High-Performance Concrete - Characteristics and Code-Type Prediction Model. Proc. of the 4th International Symposium on Utilization of High-Strength/High-Performance Concrete, Paris, France, p. 377-385, 1996.

Müller, H. S., Kvitsel, V.: Kriechen und Schwinden von Beton, Grundlagen der neuen DIN 1045 und Ansätze für die Praxis. In: Beton- und Stahlbetonbau 97, No. 1, pp. 8-19, 2002.

Müller, H.S., Rübner K.: High-Strength Concrete - Microstructural Characteristics and Related Durability Aspects. In: Durability of High-Performance Concrete, ed. H. Sommer, RILEM, Cachan, France, p. 23-37, 1995.

Müller, H. S., Hilsdorf, H. K.: Constitutive relations for structural concrete. CEB Bulletin d'Information No. 217, April 1993, pp. 17-65.

Nelson, E.L., Carrasquillo, R.L., Fowler, D.W.: Fatigue of High Strength Concrete subjected to Biaxial Compression. Proceedings, Utilization of High Strength Concrete, Stavanger, 1987.

Neville, A.: Water and concrete: a love-hate relationship. ACI Concrete-International, Vol. 22, No. 12, pp. 34-38, December 2000.

Nilsen, U.A., Monteiro, P.J.M.: Concrete: a three phase material. Cement and Concrete Research, Vol. 23, 1993, pp. 147-151.

Nilsson, L.-O.: Moisture Problems in Concrete Flooring. Report TVBM-3002. Lund Institute of Technology, Lund, 1977.

Nordisk Industrifysik AB, www.industrifysik.se.

Norwegian Standard NS 3473: Concrete Structures, Design Rules, 1989.

Ohlsson, U., Daerga, P.A., Elfgren, L.: Fracture Energy and Fatigue Strength of unreinforced Concrete Beams at normal and low Temperatures. International Conference on Fracture and Damage of Concrete and Rock, Vienna, Austria, 1988.

Ottosen, N.S.: Constitutive Model for Short-Time Loading of Concrete. Journal of the Engineering Mechanics Division, Feb. 1979, Vol. 105, EM1, pp. 127-141.

Persson, B.: Quasi-instantaneous and Long-term Deformations of High-Performance Concrete. Doctoral Dissertation, Report TVBM-1016, Lund University, Lund, Sweden, 1998.

Persson, B.: Drying of Concrete subjected to different Kinds of Curing. Materials and Structures. 30, 1997, pp. 533-544.

Persson, B.: Chloride Diffusion Coefficient and Salt Frost Scaling of Self-compacting Concrete and Normal Concrete, Prediction Models of Chloride Ingress and Corrosion Initiation in Concrete Structures, Nordic Seminar - fib Meeting, Report P01:6, Chalmers University of Technology, Gothenburg, Ed. by Nilsson, L.-O, 2001A, 13 pp.

Persson, B.: Chloride Migration Coefficient of Self-Compacting Concrete, Nordic Seminar on Durability of Exposed Concrete Containing Secondary Cementitious Materials, Hirtshals, Ed.: D. Bager, The Nordic Concrete Federation, Oslo, 2001, 187-207.

Persson, B.: Compatibility between Flooring Materials and Concrete. Materials and Structures. 35, 2002, pp. 170-182.

Persson, B.: Hydration, Structure and Strength of HPC, TVBM-1009, Lund Institute of Technology, Lund, 225-254, 1992, pp. 317-335.

Persson, B.: Moisture in Concrete Subjected to Different Kinds of Curing. Materials and Structures 30, 203, 1997A, pp. 533-544.

Persson, B.: Quality assurance of the Measurements of Moisture on Levels 14 and 15 of the Children Clinic, University Hospital, Lund Report U00.16, Division of Building Materials, Lund Institute of Technology, Lund, 2000A, 11 pp.

Persson, B.: Self-Desiccation and its Importance in Concrete Technology. Materials and Structures 30, 199, 1997A, pp. 293-305.

Pesch, A.: Ein Beitrag zum zeitabhängigen Verhalten von hochfestem Beton und hochfestem Mörtel. Dissertation, Technische Hochschule Darmstadt, 1997.

Petkovic, G., Lenchow, R., Stemland H., Rosseland, S.: Fatigue of High Strength Concrete. Proceedings of the Second International Symposium on Application of High Strength Concrete, Berkeley, 1990.

Popovic, S.: A Numerical Approach to the complete Stress-Strain Curve of Concrete. Cement and Concrete Research. Vol. 3. S. 583-599. Pergamon Press. Inc.. 1973.

Popovics, S.: Effect of curing method and final moisture condition on compressive strength of concrete. Proceedings, American Concrete Institute Vol. 83, No. 4, 1986, pp. 650-657.

Powers, T.C., L.E. Copeland, Mann, H.M.: Capillary Continuity or Discontinuity in Cement Pastes. PCA Research Bulletin No. 110, Skokie, Illinois USA, 1959.

prEN 1992-2 (Draft 1.2): Eurocode 2 – Design of concrete structures. European Committee for Standardization, July 2002.

RBK: Measurement of Moisture in Concrete. The Swedish Council for Construction Competency, RBK. Stockholm, 2000.

Reinhardt, H. W.: Simple Relations for the Strain Rate Influence of Concrete. Darmstadt Concrete, Annual Journal on Concrete and Concrete Structures, Volume 2, 1987.

Reinhardt, H.-W., Cornelissen, H.A.W., Hordijk, D.A.: Tensile Tests and Failure Analysis of Concrete. ASCE Journal of Structural Engineering, Vol. 112, No. 11, 1986.

Reinhardt, H.-W., Cornelissen, H.A.W.: Zeitstandzugversuche an Beton. Baustoffe 1985, Bauverlag Wiesbaden 1985, pp. 162-167.

Reinhardt, H.-W., Hilsdorf, H. K.: Beton. In: Betonkalender 2001, Verlag Ernst & Sohn, Berlin, 2001.

Reinhardt, H.-W.: Structural behaviour of high performance concrete. Otto Graf Journal 11 2000, pp. 9-17.

Remmel, G.: On the Tensile and Shear Behaviour of High Strength Concrete Members (in German). Deutscher Ausschuss für Stahlbeton, Nr. 444, Beuth Verlag, Berlin, 1994.

RILEM Committee 36-RDL: Long Term Random Dynamic Loading of Concrete Structures. Materials and Structures, Vol. 17, Nr. 97, 1984.

RILEM TC 69: "Material Models for Structural Creep Analysis" (principal author Z.P. Bažant), Chapter 2 in "Mathematical Modeling of Creep and Shrinkage of Concrete", Z.P. Bažant, ed., J. Wiley, Chichester & New York, 1988, pp. 99-215.

RILEM TC 107, Subcommittee 5: "Data Base on Creep and Shrinkage", RILEM Draft Report, principal authors: H.S. Müller, Z.P. Bažant and C.H. Küttner, to be published, 1998.

Rinder, T., Reinhardt, H.-W.: High strength concrete under sustained tensile loading. Concrete under Severe Conditions 3, eds. N. Banthia, K. Sakai, O.E. Gjørv, The University of British Columbia, Vancouver, Canada 2001, pp. 1514-1521.

Rinder, T.: Hochfester Beton unter Dauerzuglast. DAfStb Heft 544, Beuth Verlag GmbH, Berlin 2003.

Rocco, C., Guinea, G. V., Planas, J., Elices, M.: Size effect and boundary conditions in the Brazilian test: Experimental verification. Materials and Structures, Vol. 32, April 1999, pp. 210-217.

Rocco, C., Guinea, G. V., Planas, J., Elices, M.: Size effect and boundary conditions in the brazilian test: Theoretical analysis. Materials and Structures, Vol. 32, July 1999, pp. 437-444.

Rogge, A.: Materialverhalten von Beton unter mehrachsiger Beanspruchung. Dissertation, München, Germany, 2002.

Rossi, P., Wu, X., Le Maou, F., Belloc, A.: Scale effect on concrete in tension. Materials and Structures, Vol. 27, 1994, pp. 437-444.

Rüsch H., Kordina K., Hilsdorf H. K.: Versuche über das Kriechen des Betons. Deutscher Ausschuss für Stahlbeton, Heft 146, Berlin, Germany, 1962.

Sassone, M., Chiorino, M.A.: Design Aids for the Evaluation of Creep Induced Structural Effects, in: J. Gardner and J. Weiss eds., Shrinkage and Creep of Concrete, ACI American Concrete Institute SP-227, 2005, pp. 239-259.

Schläfli, M.: Fatigue of Bridge Decks made of Reinforced Concrete (in German). Dissertation, École Polytechnique Fédérale de Lausanne, Lausanne, 1999.

Sellovoid, E. J., Radjy, F. F.: Condensed silica (microsilica) in concrete: Water demand and strength development. American concrete institute special publication SP-91 (Ed. V. M. Malhotra), Detroit, 1983, pp. 677-694.

Setunge, S.: Short-term and long-term behaviour of high performance concrete. Proceedings of the USA-Australia Workshop on High Performance Concrete (HPC), School of Civil Engineering, Sydney, Australia, August 1997, pp. 201-208.

Setzer, M. J.: Einfluss des Wassergehaltes auf die Eigenschaften des erhärteten Betons. Schriftenreihe des Deutschen Ausschusses für Stahlbeton, Heft 280, Verlag Ernst & Sohn, Berlin, 1977, pp. 43-117.

Shrage, I.: Versuche über das Kriechen hochfesten Betons. Abschlussbericht zum Forschungsvorhaben AIF-Nr. 8798, DBV-Nr. 148. Technical University of Munich, Germany, 1994.

Siemes, A.J.M.: Fatigue Evaluation of Concrete Structures – Preliminary Studies, Procedure and Examples. Heron, Vol. 33, No. 3, 1988.

Sinha, B.P., Gerstle, K.H., Tulin, L.G.: Stress-Strain Relations for Concrete under Cyclic Loading. ACI Journal, Vol. 61, No. 2, 1964.

Skalny, J. P.: Materials science of concrete. The American Ceramic Society, Inc., Westerville, OH, 1989.

Slowik, V., Wittmann, F. H.: Influence of strain gradient on fracture energy. Fracture Mechanics of Concrete Structures, Z. P. Bazant (ed.), Elsevier Applied Science, London/New York, 1992, pp. 424-429.

Slowik, V.: Beiträge zur experimentellen Bestimmung bruchmechanischer Materialparameter von Betonen. Building Materials Reports, No. 3, ETH Zürich, Aedificatio Publishers, Freiburg, 1995.

Smadi, M.M., Slate, F.O.: Microcracking of high and normal strength concretes under short- and long-term loadings. ACI Materials Journal Vol. 86 No. 2, March-April 1989, pp. 117-127.

Swamy, R. N.: Properties of high-strength concrete, Cement, Concrete and Aggregates, ASTM, Vol. 8, 1986, pp. 33-41.

Tang, L., Nilsson, L.-O.: Modelling of Chloride Penetration into Concrete – Tracing Five Years' Field Exposure, Concrete Science Engineering, 2 (2000) 170-175.

Tazawa, E. (1998): Proceedings of the International Workshop on Autogenous Shrinkage of Concrete, ed. E. Tazawa, Japan Concrete Institute, Hiroshima, Japan, 1998.

Torii, K., Kawamura, M.: Mechanical and durability-related properties of high-strength concrete containing silica fume. High-performance concrete: Proceedings ACI international conference, V. M. Malhotra (ed.), Singapore, 1994, pp. 461-474.

Toumi, A., Bascoul, A., Turatsinze, A.: Crack Propagation in Concrete Subjected to Flexural-Cyclic Loading. Materials and Structures, Vol. 31, 1998.

Tuutti, K.: Corrosion of Steel in Concrete, Report Fo 4:82, The Cement and Concrete Research Institute, Stockholm, 277-286, 1982, pp. 302-303.

Waagaard, K., Keep, B., Stemland, H.: Fatigue of High Strength Lightweight Aggregate Concrete. Proceedings, Utilization of High Strength Concrete, Stavanger, 1987.

Waagaard, K.: Fatigue Strength Evaluation of Offshore Concrete Structures. IABSE, Proceedings, 1982.

Walraven, J.C.: Fundamental analysis of aggregate interlock. Journal of the Structural Division, ASCE, V11, Nov. 1981, pp. 2245-2270.

Walraven, J.C., Reinhardt, H.W.: Theory and experiments on the mechanical behaviour of cracks in plain and reinforced concrete subjected to shear loading. Heron, V. 26, No. 1, 1981.

Walraven, J.C., Frenay, J., Pruijssers, A.: Influence of concrete strength and load history on the shear friction capacity of concrete members. Journal of the PCI, VOl. 32, No. 1, Jan/Feb. 1987, pp. 166-170.

Weerheijm, J.: Concrete under Impact Tensile Loading and lateral Compression. Dissertation, Prins Maurits Laboratorium TNO, Rijswijk, 1992.

Weigler, H., Karl, S.: Beton; Arten – Herstellung – Eigenschaften. Ernst & Sohn, Berlin, 1989.

Wild, S., Sabir, B. B., Khatib, J. M.: Factors influencing strength development of concrete containing silica fume. Cement and Concrete Research, Vol. 25, No. 7, 1995, pp. 1567-1580.

Wischers, G., Dahms, J.: Kriechen von frühbelastetem Beton mit hoher Anfangsfestigkeit. Beton, Vol. 27, Heft 2, p. 69-74 und Heft 3, p. 104-108, 1977.

Wittmann, F.H., Roelfstra, P.E., Mihashi, H., Huang, Y.-Y., Zhang, X., Nomura, K.: Influence of age at loading, water-cement ratio and rate of loading on fracture energy of concrete. Materials and Structures, Vol. 20, Paris, 1987, pp. 103-110.

Wittmann, F.H., Zaitsev, Y.B.: Verformung und Bruchvorgang poröser Baustoffe bei kurzzeitiger Belastung und Dauerlast. DAfStb Heft 232, Ernst & Sohn, Berlin 1974, pp. 66-145.

Wright, P. J. F.: The effect of the method of test on the flexural strength of concrete. Magazine of Concrete Research, Vol. 4, No. 11, 1952, pp. 67-76.

Yang, Y., Xu, M., Sato, R., Tezuka, M.: Experimental Investigation on Shrinkage and Creep of High Strength Concrete at early ages. Proceedings of Fourth International Conference Tokushima, Japan 1998, ACI International SP-179, pp. 201-215.

Yankelevsky, D.Z., Reinhardt, H.-W.: Uniaxial Behavior of Concrete in Cyclic Tension. ASCE Journal of Structural Engineering, Vol. 115, No. 1, 1989.

Zhang, Y., Sun, W., Shang, L.: Mechanical properties of high performance concrete made with high calcium high sulphate fly ash. Cement and Concrete Research, Vol. 27, No. 7, 1997, pp. 1093-1098.

Zia, P., Leming, M.L., Ahmad, S.H.: High Performance Concretes. Strategic Highway Research Program, National Research Council, Washington, D.C., 1991.

Ziegeldorf, S., Kleiser, K., Hilsdorf, H. K.: Vorherbestimmung und Kontrolle des thermischen Ausdehnungskoeffizienten von Beton. Schriftenreihe Deutscher Ausschuss für Stahlbeton, No. 305. Verlag Wilh. Ernst & Sohn, Berlin, 1979.

Zink, M.: Diagonal Shear Cracking in Slender Concrete Beams. LACER No. 5, Institut für Massivbau und Baustofftechnologie, University of Leipzig 2000.

fib Bulletins published since 1998

Nº	Title
1	Structural Concrete – Textbook on Behaviour, Design and Performance; Vol. 1: Introduction - Design Process – Materials Manual - textbook (244 pages, ISBN 978-2-88394-041-3, July 1999)
2	Structural Concrete – Textbook on Behaviour, Design and Performance Vol. 2: Basis of Design Manual - textbook (324 pages, ISBN 978-2-88394-042-0, July 1999)
3	Structural Concrete – Textbook on Behaviour, Design and Performance Vol. 3: Durability - Design for Fire Resistance - Member Design - Maintenance, Assessment and Repair - Practical aspects Manual - textbook (292 pages, ISBN 978-2-88394-043-7, December 1999)
4	Lightweight aggregate concrete: Extracts from codes and standards State-of-the-art report (46 pages, ISBN 978-2-88394-044-4, August 1999)
5	Protective systems against hazards: Nature and extent of the problem Technical report (64 pages, ISBN 978-2-88394-045-1, October 1999)
6	Special design considerations for precast prestressed hollow core floors Guide to good practice (180 pages, ISBN 978-2-88394-046-8, January 2000)
7	Corrugated plastic ducts for internal bonded post-tensioning Technical report (50 pages, ISBN 978-2-88394-047-5, January 2000)
8	Lightweight aggregate concrete: Part 1 (guide) – Recommended extensions to Model Code 90; Part 2 (technical report) – Identification of research needs; Part 3 (state-of-art report) – Application of lightweight aggregate concrete (118 pages, ISBN 978-2-88394-048-2, May 2000)
9	Guidance for good bridge design: Part 1 – Introduction, Part 2 – Design and construction aspects. Guide to good practice (190 pages, ISBN 978-2-88394-049-9, July 2000)
10	Bond of reinforcement in concrete State-of-art report (434 pages, ISBN 978-2-88394-050-5, August 2000)
11	Factory applied corrosion protection of prestressing steel State-of-art report (20 pages, ISBN 978-2-88394-051-2, January 2001)
12	Punching of structural concrete slabs Technical report (314 pages, ISBN 978-2-88394-052-9, August 2001)
13	Nuclear containments State-of-art report (130 pages, 1 CD, ISBN 978-2-88394-053-6, September 2001)
14	Externally bonded FRP reinforcement for RC structures Technical report (138 pages, ISBN 978-2-88394-054-3, October 2001)
15	Durability of post-tensioning tendons Technical report (284 pages, ISBN 978-2-88394-055-0, November 2001)
16	Design Examples for the 1996 FIP recommendations *Practical design of structural concrete* Technical report (198 pages, ISBN 978-2-88394-056-7, January 2002)
17	Management, maintenance and strengthening of concrete structures Technical report (180 pages, ISBN 978-2-88394-057-4, April 2002)
18	Recycling of offshore concrete structures State-of-art report (33 pages, ISBN 978-2-88394-058-1, April 2002)
19	Precast concrete in mixed construction State-of-art report (68 pages, ISBN 978-2-88394-059-8, April 2002)
20	Grouting of tendons in prestressed concrete Guide to good practice (52 pages, ISBN 978-2-88394-060-4, July 2002)
21	Environmental issues in prefabrication State-of-art report (56 pages, ISBN 978-2-88394-061-1, March 2003)

Nº	Title
22	Monitoring and safety evaluation of existing concrete structures State-of-art report (304 pages, ISBN 978-2-88394-062-8, May 2003)
23	Environmental effects of concrete State-of-art report (68 pages, ISBN 978-2-88394-063-5, June 2003)
24	Seismic assessment and retrofit of reinforced concrete buildings State-of-art report (312 pages, ISBN 978-2-88394-064-2, August 2003)
25	Displacement-based seismic design of reinforced concrete buildings State-of-art report (196 pages, ISBN 978-2-88394-065-9, August 2003)
26	Influence of material and processing on stress corrosion cracking of prestressing steel - case studies. Technical report (44 pages, ISBN 978-2-88394-066-6, October 2003)
27	Seismic design of precast concrete building structures State-of-art report (262 pages, ISBN 978-2-88394-067-3, January 2004)
28	Environmental design State-of-art report (86 pages, ISBN 978-2-88394-068-0, February 2004)
29	Precast concrete bridges State-of-art report (83 pages, ISBN 978-2-88394-069-7, November 2004)
30	Acceptance of stay cable systems using prestressing steels Recommendation (80 pages, ISBN 978-2-88394-070-3, January 2005)
31	Post-tensioning in buildings Technical report (116 pages, ISBN 978-2-88394-071-0, February 2005)
32	Guidelines for the design of footbridges Guide to good practice (160 pages, ISBN 978-2-88394-072-7, November 2005)
33	Durability of post-tensioning tendons Recommendation (74 pages, ISBN 978-2-88394-073-4, December 2005)
34	Model Code for Service Life Design Model Code (116 pages, ISBN 978-2-88394-074-1, February 2006)
35	Retrofitting of concrete structures by externally bonded FRPs. Technical Report (224 pages, ISBN 978-2-88394-075-8, April 2006)
36	2006 *fib* Awards for Outstanding Concrete Structures Bulletin (40 pages, ISBN 978-2-88394-076-5, May 2006)
37	Precast concrete railway track systems State-of-art report (38 pages, ISBN 978-2-88394-077-2, September 2006)
	Directory 2006 (130 pages, December 2006)
38	Fire design of concrete structures – materials, structures and modelling State-of-art report (106 pages, ISBN 978-2-88394-078-9, April 2007)
39	Seismic bridge design and retrofit – structural solutions State-of-art report (300 pages, ISBN 978-2-88394-079-6, May 2007)
40	FRP reinforcement in RC structures Technical report (160 pages, ISBN 978-2-88394-080-2, September 2007)
41	Treatment of imperfections in precast structural elements State-of-art report (74 pages, ISBN 978-2-88394-081-9, November 2007)
42	Constitutive modelling of high strength / high performance concrete State-of-art report (130 pages, ISBN 978-2-88394-081-9, January 2008)

Abstracts for *fib* Bulletins, lists of available CEB Bulletins and FIP Reports, and an order form are given on the *fib* website at www.fib-international.org/publications.